NASA TECHNICAL NOTE

NASA TN D-4427

C. 1

TECH LIBRARY KAFB, NM
0131186

NASA TN D-4427

LOAN COPY: RETURN TO
AFWL (WLIL-2)
KIRTLAND AFB, N MEX

A MODIFIED MULTHOPP APPROACH FOR PREDICTING LIFTING PRESSURES AND CAMBER SHAPE FOR COMPOSITE PLANFORMS IN SUBSONIC FLOW

by John E. Lamar

Langley Research Center
Langley Station, Hampton, Va.

NATIONAL AERONAUTICS AND SPACE ADMINISTRATION • WASHINGTON, D. C. • JULY 1968

TECH LIBRARY KAFB, NM
0131186

A MODIFIED MULTHOPP APPROACH FOR PREDICTING LIFTING PRESSURES AND CAMBER SHAPE FOR COMPOSITE PLANFORMS IN SUBSONIC FLOW

By John E. Lamar

Langley Research Center
Langley Station, Hampton, Va.

NATIONAL AERONAUTICS AND SPACE ADMINISTRATION

For sale by the Clearinghouse for Federal Scientific and Technical Information
Springfield, Virginia 22151 – CFSTI price $3.00

A MODIFIED MULTHOPP APPROACH FOR PREDICTING LIFTING PRESSURES AND CAMBER SHAPE FOR COMPOSITE PLANFORMS IN SUBSONIC FLOW

By John E. Lamar
Langley Research Center

SUMMARY

This report presents a modified version of Multhopp's subsonic lifting-surface theory which has been programed in two parts for the IBM 7094 electronic data processing system or Control Data 6400 computer system along with a discussion of the character of its results. The first part is used to find both basic and additional loadings over a given planform with known mean camber surface and the second part is used to determine the required mean camber surface for a given planform and set of loadings.

For the loading program, various aerodynamic characteristics are determined on both simple and composite planforms when the spanwise loading is symmetrical. Studies are conducted to determine when these answers are most valid, and some results for delta, sweptback and tapered, double delta, and variable-sweep wings are compared with other theories and experiments to determine the accuracy of this method.

Application of this method is then made in predicting the aerodynamic effects of changing the outer-panel sweep of a variable-sweep wing, of increasing the Mach number in the subsonic regime, and of incorporating twist and camber in a wing. The first two applications also have experimental data presented for comparison.

A study is also undertaken for the mean camber surface program to determine when its best results are obtained. Subsequently, comparisons between the present and other methods are made for a two- and three-dimensional case to aid in the evaluation of the present method. One application is made for a highly sweptback and tapered planform.

INTRODUCTION

In the process of wing design, one is required to determine either the load distribution from a given planform and mean camber surface or the mean camber surface from a prescribed planform and loading. From previous investigations a considerable amount of information of both a theoretical and experimental nature is available to aid the designer if the wings have delta or simple sweptback planforms. However, planforms now being

considered (which in many cases have the divergent requirements of supersonic or hypersonic cruise and subsonic loiter or ferry capability) are much more complex, involving, in many instances, cranked leading and trailing edges. Planforms of this type are classified as being of a composite arrangement.

For these planforms not as much general information is available, due both to their newness and to the large number of planform variables. First-order solutions to these problems have been found in recent years for the sonic (refs. 1 and 2) and supersonic (refs. 3 and 4) speed regimes which are applicable to arbitrary wing planforms. References 3 and 4 have been programed for the high-speed electronic computer so that the designer does not have to perform the lengthy mathematical manipulations required to obtain a solution for each wing considered.

In the subsonic speed regime, the basic theoretical method of Multhopp (ref. 5) has received wide acceptance as one of the most accurate methods for predicting aerodynamic loading data; consequently, it has been selected as the approach to use in solving these two design problems for composite planforms. Some reasons for this selection are

(1) The chordwise pressure distributions (and other section data) as well as overall aerodynamic characteristics are determined

(2) The spanwise locations of the lift-producing singularities and control points are more concentrated along chordwise rows near the tip to insure an adequate representation of the spanwise load distribution

(3) The method can as Multhopp mentioned in reference 5 be used for wings with planform kinks at locations other than just at the plane of symmetry

A computerized solution of the loading determination problem for arbitrary wings has been developed from the basic Multhopp method by Van Spiegel and Wouters in reference 6 and is referred to as the modified Multhopp method. Certain changes in and extensions to their work have been made in the present report to increase the accuracy in representing the actual chordwise pressure distribution and finding the influence of each of these distributions on each point where the boundary conditions are to be met. These modifications resulted from adding additional pressure modes (up to 10 may be used) and by replacing the polynomial approximation technique used in the chordwise integration with the Gaussian quadrature method.

In addition, the formulation procedure and all the modifications made to the basic Multhopp approach are described as well as the techniques used in its solution for both the load and mean camber surface determination problems. After this a study of the resulting answers is made to determine their sensitivity to the number and location of the points where the boundary conditions are met or calculated. Then applications of the programs are made to an assortment of wings, including composite wings and the results

are compared with other theories and, where possible, experiment. All the predictions made from this modified Multhopp method have been obtained with the aid of the IBM 7094 electronic data processing system and Control Data 6000 series electronic computers.

A listing of the computer programs used to find the surface loadings (Langley program A0313) and to find the mean camber surface (Langley program A0457) is presented along with a description of the input data required, sample input and output data, and pertinent comments in a "Supplement to NASA TN D-4427." A large portion of these two programs is given over to the computation of the geometric representation required by later parts of the program from the input quantities supplied. Two additional programs (Langley programs A1590 and A1591) which are useful in obtaining geometric input data for either program A0313 or A0457 are also presented in the supplement along with brief descriptions and sample cases of each. A request form is included at the back of this paper.

SYMBOLS

Any convenient system of measure can be used as long as the linear dimensions of the planform are based on a semispan of unity.

A aspect ratio, b^2/S

a.c. aerodynamic center, in fractions of c_{ref}, referenced to leading edge of reference chord (positive aft), $\frac{-\partial C_m}{\partial C_L} + \frac{1}{4}$

b wing span, set equal to 2

$b_{\nu n}, b_{\nu\nu}$ Multhopp's integrating coefficients

C_A axial-force coefficient, $\frac{\text{Axial force}}{q_\infty S_{ref}}$

$C_{B,o}$ root bending-moment coefficient, $\frac{b}{S_{ref}} \int_0^1 (c_l c)_{basic} \eta \, d\eta$

$C_{D,i}$ induced drag based on the spanwise distribution of circulation

$C_{D,ii}$ induced drag based on axial force, $\alpha C_L - C_A$

C_L lift coefficient, $\frac{\text{Wing lift}}{q_\infty S_{ref}}$

C_{L_α} overall lift-curve slope

C_m pitching-moment coefficient, $\frac{\text{Wing pitching moment}}{q_\infty S_{ref} c_{ref}}$ about $\frac{c_{ref}}{4}$

C_{m_α} overall pitching-moment-curve slope about $\frac{c_{ref}}{4}$

ΔC_p incremental pressure coefficient, $\frac{p_{upper} - p_{lower}}{q_\infty} = \frac{\Delta p}{q_\infty}$

C_s leading-edge-suction coefficient for zero degrees of leading-edge sweep, $\frac{\beta \pi b}{8 S_{ref}} \int_{-1}^{1} \frac{1}{c(\eta)} \left[\frac{q_0(\eta)}{q_\infty}\right]^2 d\eta$

c streamwise chord at y,η

$\bar{c}$ mean geometric chord, $\frac{\int_{-b/2}^{b/2} c^2 dy}{\int_{-b/2}^{b/2} c\, dy}$

$c(\eta), c(y)$ streamwise half-chord at n,y

c_{av} average chord, S/b

c_l local lift coefficient, $\frac{\text{Local chord load}}{q_\infty c}$

c_{m_α} local pitching-moment-curve slope about local leading edge

c_{n_α} local slope of normal-force coefficient

c_r root chord

c_{ref} reference chord, may be mean geometric chord of total wing $\bar{c}$ except when the planform has an inboard trailing-edge chord-extension or may be mean geometric chord of only wing outer panel extended to plane of symmetry in streamwise tip position

$d(\eta)$ x-location of midchord at η

f_j jth chordal loading function

$K(\phi,y;\vartheta,\eta)$ subsonic kernel function

$K_j(\phi,y;\eta)$ subsonic kernel function integrated with jth loading across the chord

$L^j_{\nu n}(\phi_s)$ influence of jth loading function at η_n on control point at y_ν and $x = (c/2)(1 - \cos \phi_s)$

$\overline{L}^j_{\nu n}(\phi_s)$ elements of influence matrix when $n \neq \nu$

M Mach number

m number of span stations where the pressure modes are defined

N number of chordal control points at each of m span stations

Δp lifting pressure, $p_{upper} - p_{lower}$

$q_j(\eta)$ coefficient of jth chordal loading function for additional load

$qt_j(\eta)$ coefficient of jth chordal loading function for twist and/or camber load

q_∞ dynamic pressure

S total wing area

S_{ref} reference area, may be either total wing area or wing area of wing outer panels extended to plane of symmetry in streamwise tip position

s used to locate chordal control points and ranges from 1 to N

U free-stream velocity

w perturbation velocity in z-direction

x,y,z rectangular Cartesian coordinates nondimensionalized with respect to b/2 where origin is in plane of symmetry at half root chord (fig. 1) (they are associated with control points)

$x_{\bar{c}}$ x-location of leading edge of $\bar{c}$

$x_{c_{ref}}$ x-location of leading edge of c_{ref}

y_{cp}, x_{cp} centers of pressure

α angle of attack, deg

α_i induced angle of attack, radians

α_l local angle of attack, $\frac{-dz}{dx} = \frac{-w}{U}$, radians

β Prandtl-Glauert compressibility factor, $\sqrt{1 - M^2}$

γ local nondimensional lift coefficient, $c_l c/2b$

Δ wing tip skew angle, deg

θ angle for locating control points along span (see fig. 2(a))

ϑ angle used to locate pressure doublets chordwise, 0 at leading edge and π at trailing edge

κ ratio of distance of leading-edge break from plane of symmetry to b/2

Λ outboard leading-edge sweep angle, deg

λ taper ratio, $\frac{\text{Tip chord}}{\text{Overall root chord}}$

μ ratio of distance of trailing-edge break from plane of symmetry to b/2

ξ,η rectangular Cartesian coordinates nondimensionalized with respect to b/2 along X- and Y-axes, respectively, and associated with pressure doublet locations

ϕ angle used to locate chordwise rows of control points (see fig. 2(b))

χ inboard leading-edge sweep angle, deg

ψ inboard trailing-edge sweep angle, deg

Ω outboard trailing-edge sweep angle, deg

Subscripts:

cp center of pressure

d distributed

ℓe leading edge

n,ν suffixes numerating spanwise stations, ν station being influenced and n station doing the influencing; n,ν range from $-\frac{m-1}{2}, \ldots 0, \ldots \frac{m-1}{2}$

o value taken at $C_L = 0$

p pivot

te trailing edge

x x-direction

y y-direction

1 result due to twist and/or cambered wing at zero root chord angle of attack

BASIC FORMULATION

The determination of surface loadings on both plane and warped wings and the determination of the mean camber surface can be made from a number of theories already in use. All the theories share a common feature in that the wing is replaced by a mathematical model which produces a similar downwash field to that of the wing. However, the methods differ mainly in the potential used to produce the representative perturbations of the flow field around the wing. These potentials are either of the velocity or acceleration type (ref. 7). The original Multhopp method and its present modified version use the acceleration potential approach in conjunction with the linearized Euler equations to relate the pressure difference across the wing to the downwash field on the wing surface. This results in the following equation which is derived in detail in reference 6 for the incompressible case:

$$\left(\frac{w}{U}\right)_{z=0} = \frac{1}{8\pi q_\infty}\int_{-1}^{1}\int_{\xi_{le}}^{\xi_{te}} \frac{\Delta p(\xi,\eta)}{(y-\eta)^2}\left[1 + \frac{(x-\xi)/\beta}{\sqrt{\frac{(x-\xi)^2}{\beta^2} + (y-\eta)^2}}\right] d\xi\, d\eta \tag{1}$$

Reduction of Basic Equation to Matrix Form

Equation (1) is difficult to solve for the local pressures $\Delta p(\xi,\eta)$ since they appear as part of the integrand and because of the integration across the second-order singularity. The term w/U and its resulting mean camber surface is also difficult to determine because of this same required integration. A solution to either problem can, however, be made by

(1) Replacing $\Delta p(\xi,\eta)$ with as many of the 10 pressure modes of unknown or known amplitude as are needed

$$\Delta p(\vartheta,\eta) = \frac{q_0(\eta)}{c(\eta)} \cot\frac{\vartheta}{2} + \sum_{j=1}^{9} \frac{q_j(\eta)}{c(\eta)} \sin j\vartheta \tag{2}$$

where

$$\xi = -c(\eta)\cos\vartheta + d(\eta) \tag{3}$$

(2) Employing the Multhopp quadrature formula to approximate the spanwise integration of the pressure doublets; this approximating procedure has another feature in that every spanwise station need not be represented but only those stations where information is required

(3) Using a logarithmic singularity correction term (appendix A) to account for the integration across the second-order singularity (this amounts to finding the finite part)

(4) Setting up equation (1) with these approximations in a matrix equation of the form

$$\left\{\frac{-4w(\phi_s, y_\nu)}{U}\right\} = \left[\bar{L}^j_{\nu n}(\phi_s)\right]\left\{\frac{q_j(\eta_n)}{q_\infty}\right\} \tag{4}$$

The details of formulating the matrix of influence coefficients are given in appendix A where they have been taken for the most part directly from reference 6 and presented here for the reader's convenience.

The points (determined from ϕ_s and y_ν) which are selected either to specify the tangential flow boundary condition or to find the downwash ratio are called control points and are located in both the spanwise and chordwise directions by the use of semicircles which are laid along the span from tip to tip and along the local chord from leading to

trailing edge. The spanwise positions, which result from an equiarc angular displacement about the plane of symmetry, can be represented by the following equation:

$$y_\nu = \sin \frac{\nu\pi}{m + 1} \tag{5}$$

where m is the total number of spanwise stations from tip to tip and ν ranges from $-\frac{m - 1}{2}$ to $\frac{m - 1}{2}$ in increments of 1. (See fig. 2(a).) These positions are those required by the Multhopp quadrature formula for the integrand evaluation when approximating the value of the spanwise integral (ref. 5).

At each spanwise location, the control points are also located for equiarc angular displacements defined by

$$\phi_s = \frac{2\pi s}{2N + 1} \tag{6}$$

where N is the total number of chordwise control points and ranges from 1 to N. (See fig. 2(b).) Note that the control points never reach the leading or trailing edge. From this, the control-point locations are found to be determinable by the following equation:

$$\frac{x}{c} = \frac{1}{2}(1 - \cos \phi_s) \tag{7}$$

which locates them aft of the local leading edge. (See fig. 3.)

In order to solve for either the loading (inverse problem) or mean camber surface (direct problem), equation (4) is used. The loadings are found by (1) inverting the matrix in equation (4) and thus solving for the $\frac{q_j(\eta_n)}{q_\infty}$ array and then (2) using these values in the equations given in appendix B to determine the local and overall aerodynamic loading description. The mean camber surface is found by the direct matrix multiplication of equation (4) along with the procedure described in the mean camber surface determination section of this report.

Modification Made to the Original Multhopp Method

From a study of Multhopp's original method, several features are seen to need modification in order that a computerized solution of it could be made to the best advantage. Aside from the logarithmic singularity correction term whose best form is discussed in appendix A they are as follows:

1. The method for solving for the coefficients of the loading terms in the inverse problem. In Multhopp's report, a scheme of iteration on the downwash is used, this is improved in reference 8 with a scheme of submatrix inversion and in reference 6 with a scheme of whole matrix inversion which is also used herein.

2. The chordal integration that sums the influence of the pressure doublets on control points not at the same span station. In Multhopp's report, it is developed from a MacLaurin series then graphed for use. Van Spiegel and Wouters (ref. 6) follow the scheme developed by Van de Vooren (ref. 9) with which the value of the integral is determined, by (a) approximating the loading functions with polynomials, (b) evaluating them at discrete locations, and (c) multiplying the results of part (b) with predetermined coefficients. In this report, the polynomial approximation of reference 6 is replaced with a Gaussian 20- to 30-point numerical integration scheme.

3. The number of chordal loading functions and, therefore, control points. In Multhopp's report they are limited to two, $\cot \frac{\vartheta}{2}$ which gives lift with no pitching moment about $c/4$ and $\cot \frac{\vartheta}{2} - 2 \sin \vartheta$ which yields no lift but a pitching moment about $c/4$. From these, the known downwash and the matrix of influence coefficients, one is able to solve for the coefficients of the loading terms which are the local circulation and pitching moment about local $c/4$. Garner and Lehrian (ref. 10) have extended to four the number of chordal loadings (and consequently, control points) that may be used but employ combinations of terms rather than separate loading modes. Van Spiegel and Wouters also extend the number of chordal loadings and control points to four but separate the loadings into $\cot \frac{\vartheta}{2}$, $\sin \vartheta$, $\sin 2\vartheta$, and $\sin 3\vartheta$, whose coefficients are the strength of the local pressure doublets supporting that loading contribution over the chord. In this report they have been extended to 10 with the addition of $\sin 4\vartheta$, $\sin 5\vartheta$, $\sin 6\vartheta$, $\sin 7\vartheta$, $\sin 8\vartheta$, and $\sin 9\vartheta$ for additional flexibility.

Multhopp's method with the aforementioned modifications is hereafter referred to as the present method and has been programed to handle a wide variety of composite planforms, with a break in the leading and trailing edges as well as the variable-sweep wings. The program at present is capable of handling sets of chordwise and total spanwise stations of 1 by 41, 2 by 41, 3 by 41, 4 by 41, 5 by 39, 6 by 31, 7 by 27, 8 by 23, 9 by 21, or 10 by 19, with the number of chord stations given first. This is not a theoretical limitation but is near the upper limit of machine storage presently available. Also, with the sets of stations listed above, almost any planform of low to moderate aspect ratio can be handled.

The distribution of lift obtained by the present method is dependent on the subsonic Mach number (see appendix A) at which it is computed. In this report, the Prandtl-Glauert relations (ref. 11) have been used to account for this change but are valid only as long as ΔC_p varies linearly with α.

LOAD DETERMINATION

Because of the nature of the numerical solution, different combinations of N and m for the same planform can result in different answers for the aerodynamic characteristics. Hence, a study was undertaken to try and optimize their combination so that reasonably accurate results are obtained. The results of this study are presented in the next section. Then comparisons of other theoretical methods and experiment with the present method are made to gain confidence in the answers obtained with it. And lastly, illustrative examples are given to show some applications for which the present method can be used.

Optimization of N and m

For any given planform and pair of N and m, a set of chordal loading coefficients $q_j(\eta_n)$ are obtained from the solution of the inverse problem for the flat plate and are used to determine the loading characteristics of the planform. However, since a different set of $q_j(\eta_n)$, and therefore loadings, will be found for each pair of N and m, some criterion is needed by which the most appropriate set of $q_j(\eta_n)$ can be selected. One criterion, suggested by Multhopp (ref. 5), is to examine the chordwise load distribution by paying particular attention to the leading-edge suction force developed. The contention being that when the overall leading-edge suction force, which is assumed equal to the axial force and given in coefficient form for an unswept planform by

$$C_S = \frac{\beta\pi b}{8S_{ref}} \int_{-1}^{1} \frac{1}{c(\eta)} \left[\frac{q_0(\eta)}{q_\infty}\right]^2 d\eta \tag{8}$$

is such as to cause the quantity

$$C_{D,ii} = \alpha C_L - C_A \tag{9}$$

to be equal to the induced drag coefficient given by the equation

$$C_{D,i} = \frac{b^2}{S_{ref}} \int_{-1}^{1} \gamma\alpha_i \, d\eta \tag{10}$$

then the cotangent loading (eq. (2)) can be considered valid. This contention is based on the conclusions of a study made by Munk in reference 12 where he found that the term $C_{D,i}$ was independent of the chordwise loading distribution. In the discussion that follows, the result of equation (9) is called the suction value and the result of equation (10) is called the circulation value.

Upon comparing graphically the two coefficients just discussed for many combinations of N and m for two rectangular planforms of different aspect ratio, as is done in figures 4(a) and 5(a), it is noted that whereas the circulation value is essentially invariant with N and m, and is plotted as a straight line without symbols, the suction value shows a marked dependence upon N and m. If values for the aerodynamic characteristics at each pair of N and m where the two solutions are first equal or have a minimum difference are plotted as solid symbols, it is seen that the aerodynamic center and C_{L_α} values for the A = 2 planform (figs. 4(b) and 4(c)) do not vary appreciably from results obtained when N = 8 at the higher values of m. However, in the aerodynamic center and C_{L_α} graphs (figs. 5(b) and 5(c)) for the A = 7 planform, it appears that the values predicted do not necessarily agree with those at the higher N and m. One reason suggested for the disagreement is that not enough values of m were available to be used at the higher N values (storage limitation) so that the resulting answers found by convergence could have been established. Note that the aerodynamic center is the more sensitive of the two; hence, a major part of the discussion that follows is concerned with it.

From a study of figures 5(b) and 5(c), the curves for N = 2 and 4 seem to show that a particular relationship must exist between N and m in order for the answers to reach a level of convergence. Whatever the relationship is, it leads to results which are close to those given by the solid symbols. From the N = 4 curve in figure 5(b), it seems that a good result from the point of view of convergence would occur at m = 37, a solid symbol. Now if this relationship between m and N is valid, then its multiplication with lower N values to determine new m numbers should lead to results which are as good as those found from the original N and m values.

An application of this procedure would be that of multiplying the ratio of (37/4) by an N value of 2, thereby yielding an m number of approximately 19. When the curves of aerodynamic center and C_{L_α} at N = 2 and m = 19 are examined in figures 5(b) and 5(c), this combination of N and m is seen to give results which approximate well those obtained for N = 4 and m = 37. This occurs even though N = 2 and m = 19 is not a solid symbol which indicates that even though the ratio was obtained from a combination of N and m that was a solid symbol, applications of it at lower values of N do not necessarily result in combinations of N and m which are other solid symbols. It should be noted that had the N = 2 and m = 13 solid symbol been selected as the numbers to be used in determining the ratio of m to N, the m value which would have resulted from the multiplication of the ratio with N = 4 would be 26. This combination of N and m does not give answers which approximate as well the results found from convergence.

Hence, sets of N and m can be calculated that will result in answers for aerodynamic center and C_{L_α} which approximate well those found at a solid symbol provided they have been obtained from a solid symbol which has a larger N value than for the combination sought. In addition, from the results of both figures 4 and 5, the relationship between N and m is seen to indicate that an aspect ratio dependency also exists, requiring the use of more m for a given N at the higher aspect ratios. This is discussed in more detail later.

Examining again the variation of the aerodynamic center with N and m for the A = 2 planform in figure 4(b), it is noted that a part of the aerodynamic-center movement can be correlated with the suction force coefficient which is seen implicitly in figure 4(a). In general, as the suction increases $\left(\text{a decrease in } C_{D,ii}/C_L{}^2\right)$ a corresponding forward movement in the aerodynamic center is observed. This simple relationship implies that if any two sets of N and m give rise to the same suction coefficient, then their aerodynamic centers will also be the same. However, this is not generally true. Look, for example, at a value of $C_{D,ii}/C_L{}^2$ of 0.20 and note all of the different combinations of N and m that will give it and then the corresponding aerodynamic centers. Some differences are seen to exist between the aerodynamic centers predicted by the different combinations of N and m.

There are several possible reasons for this difference. The first one is that the relationship assumed between the leading-edge suction and the aerodynamic center is not a completely valid one since it depends not only on the $q_0(\eta_n)\cot\frac{\vartheta}{2}$ terms (which give rise to the leading-edge suction) but also the $q_2(\eta_n)\sin 2\vartheta$ terms.

The second reason is that since in the solution for the $q_j(\eta_n)$ set the number of control points is required to be equal to the number of unknown coefficients, the flat plate representation of the planform may not be made at enough control points. This could be remedied by an overdetermined solution (i.e., one where there are more control points and number of equations than unknown coefficients).

The third reason follows from the second in that, with the boundary condition only specified at a maximum of 10 points chordwise, the variation of w/U that results by matrix multiplication using the $q_j(\eta_n)$ set determined from the specified boundary conditions does not assume the boundary condition value except at the control points. Elsewhere it is either higher or lower and because of the logarithmic singularity correction term (eq. (A9)) it is singular at the leading and trailing edges. This variation in w/U when acted upon by the chord loading distribution should also give rise to an axial force heretofore unaccounted for. It is called the distributed axial force and is computed by

$$C_{A,d} = \frac{b}{2S_{ref}} \int_{-1}^{1} \int_{0}^{1} c\, \Delta C_p \left(\frac{w}{U} - \alpha\right) d\frac{x}{c}\, d\eta \tag{11}$$

Numerical results have not been obtained for $C_{A,d}$ since every point along the chord at each spanwise position must contain the influence of every loading function at every other spanwise location in order that the quantity w/U can be determined. This implies evaluating integrals similar to those used in finding $q_j(\eta_n)$ but at an extremely large number of locations. In addition, the singularities at the edges of the chord would be difficult to evaluate without a coordinate transformation. (Note that if the mathematical profile were truly flat, then all the axial force generated would be concentrated at the leading edge in the form of a suction force, since w/U would be everywhere equal to α.) Thus, only one solution for the axial-force coefficient has been obtained and is derived solely from the leading-edge suction.

From figures 4 and 5, it appears (as one would probably expect) that for the most part at the higher N and m values the answers for C_{L_α} and aerodynamic center are in what appear to be converging situations. However, it has also been found that one need not always choose the maximum N and m to achieve these answers but may by proper insight and judicious selection obtain equally as valid answers at lower values of N and m. Thus for planforms which have zero sweep on the leading edge, it is suggested that pairs of N and m be selected for the particular planform at the desired Mach number in a manner so as to emphasize its largest dimension; that is, planforms having large values of βA would require a pair of N and m where m was optimized after a suitable value for N was established, and planforms having low values of βA would require that a large value for N be used with a corresponding reduction in m. Selecting pairs of N and m by this procedure should give answers that will be in or be very close to those in the region of converging results. This can be accomplished approximately by using the following expression:

$$m = (4 \text{ to } 5)\beta A\left(\frac{N}{4}\right) \tag{12}$$

A similar type of analysis which leads to equation (12) should be made for wings with sweepback using the leading-edge-suction equation recently developed by Garner in reference 13.

In an attempt to see if the suggestions given would be applicable to arbitrary planforms, aerodynamic-center and C_{L_α} graphs were prepared for two double delta planforms which are shown in figures 6 and 7. It appears that even with taking $N = 8$ the formula does not give quite enough m (only 20) to predict the aerodynamic center at the higher m values (figs. 6(a) and 7(a)). Consequently, for low-aspect-ratio wings with sweepback, an N value of from 6 to 10 should be used with as many m values as the machine storage limitation will allow.

In addition to the overall aerodynamic characteristics which have already been discussed, the influence of different combinations of N and m has been examined with

regard to their influence on the span load distribution. (See figs. 8 to 11.) From this examination, the reason becomes apparent why the induced drag parameter, $C_{D,i}/C_L^2$, was stated to be essentially invariant with different combinations of N and m. The reason is that the span loadings themselves appear for the most part to be independent of N and m.

Comparisons and Illustrative Calculations

The following section contains a number of comparisons with other theoretical methods and experimental data which have been used to verify the results obtained with the present method. After the verifications have been made, illustrative calculations are made to show the present methods' usefulness in computing sweep, Mach number, twist, and camber effects. Additional illustrative calculations of the present method have been made and are given in reference 14.

Comparisons with other theoretical methods.- In order to insure that the computational procedures presently employed give equivalent results to those obtained by Multhopp (ref. 5) and Van Spiegel and Wouters (ref. 6), table I has been prepared to give a tabular comparison of C_{L_α}, aerodynamic center, and $C_{D,i}/C_L^2$. The indications from table I are that all three methods give results for C_{L_α} and $C_{D,i}/C_L^2$ within 2 percent of each other and the aerodynamic centers are within 0.3 percent of the reference chord of each other when at a constant value of N. When the $C_{D,i}/C_L^2$ values are compared with $1/\pi A$ (0.07457 for this case) they are found not to differ from it by more than 2.2 percent, indicating that the computed span loading distributions are nearly elliptical.

With the present method established as giving reliable results when compared with the basic and modified Multhopp procedures (refs. 5 and 6) and with the studies previously conducted, which indicated that an extension in the number of chordwise pressure modes was needed for certain planforms, comparisons of predicted results obtained with the present and other methods are made. The following planforms are offered as examples of this:

(1) The aerodynamic centers and C_{L_α} values for the four simple planforms shown in figure 12 are compared in tables II and III, respectively, with results obtained by DeYoung and Harper in reference 15 by using a Weissinger seven-point solution. (Values of m of 9 or 11 were chosen since $N = 4$, $A = 2$, and $\beta = 1$.)

From table II the aerodynamic centers predicted by the present method are seen to lie from 1.7 to 4.2 percent of the reference chord ahead of those given by reference 15 and from table III the values of C_{L_α} are seen to vary from 1.62 to 5.35 percent below those computed by using the present method. These differences are attributed to the more accurate accounting of the induced camber effects by the present method.

TABLE I.- COMPARISONS OF RESULTS OBTAINED FOR THIS PLANFORM WITH THE PRESENT AND THE MULTHOPP METHODS OF REFERENCES 5 AND 6

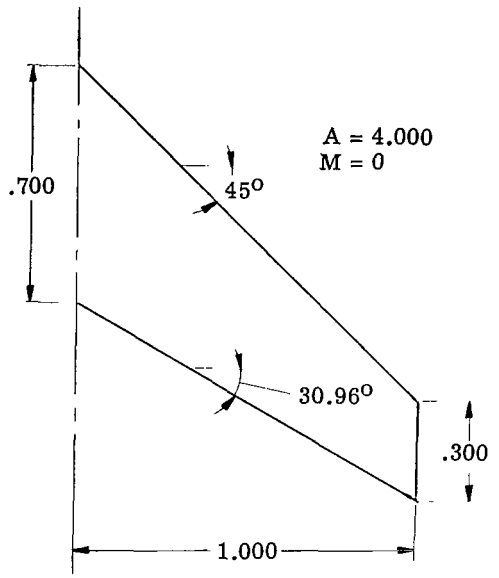

Method	N	m	C_{L_α}	a.c.	$C_{D,i}/C_L^2$
Ref. 5	1	15	0.0564	0.270	0.08125
Present	1	15	.0569	.271	.08129
Ref. 5	2	15	0.0571	0.279	0.08069
Ref. 6	2	15	.0580	.278	.08093
Present	2	15	.0580	.277	.08087
Ref. 6	3	15	0.05836	0.262	0.08090
Present	3	15	.05834	.263	.08086

TABLE II.- AERODYNAMIC CENTERS FOR A = 2 PLANFORMS OF FIGURE 12(a) WHEN N = 4

Method	Aerodynamic center for –			
	$\Lambda = 0^o$, $\lambda = 1.0$, m = 11	$\Lambda = 0^o$, $\lambda = 0.25$, m = 11	$\Lambda = 45^o$, $\lambda = 1.0$, m = 9	$\Lambda = 45^o$, $\lambda = 0.25$, m = 9
Present	0.208	0.191	0.156	0.248
Ref. 15	.250	.245	.192	.265

TABLE III.- LIFT-CURVE SLOPE FOR A = 2 PLANFORMS OF FIGURE 12(b) WHEN N = 4

Method	Lift-curve slope for –			
	$\Lambda = 0^o$, $\lambda = 1.0$, m = 11	$\Lambda = 0^o$, $\lambda = 0.25$, m = 11	$\Lambda = 45^o$, $\lambda = 1.0$, m = 9	$\Lambda = 45^o$, $\lambda = 0.25$, m = 9
Present	0.0432	0.0427	0.0398	0.0432
Ref. 15	.0422	.0415	.0376	.0425

TABLE IV.- DOUBLE-DELTA NONDIMENSIONAL LIFT COMPARISON

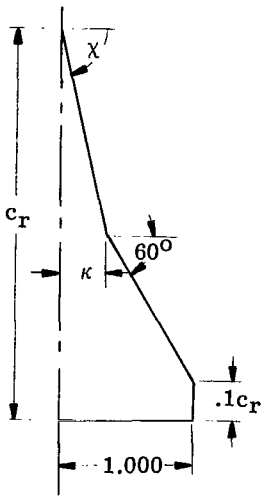

κ	Aspect ratio	χ	$\cos(\Lambda_{c/2})_{eff}$	$\frac{A}{\cos(\Lambda_{c/2})_{eff}}$	$\frac{C_{L_\alpha}}{A}$ (Present) (a)	$\frac{C_{L_\alpha}}{A}$ (Ref. 16)
0	1.88810	0	0.7559	2.4979	0.02086	0.02108
.25	1.41500	82.63	.5212	2.7148	.02234	.02040
.50	1.24920	78.07	.4800	2.6025	.02253	.02075
.75	1.11830	75.00	.5939	1.8830	.02309	.02309
1.00	3.90020	40.00	.9221	4.2297	.01545	.01641

[a] $N = 8$; $m = 23$.

Comparisons of the span loadings are also made between the present method and reference 15 for two of the planforms in figure 12 and are presented in figures 8 and 9 for various combinations of N and m. The span loading distributions computed by the two methods are in good agreement for most sets of N and m.

(2) A series of double-delta planforms, whose general planform parameters are given in table IV, have been used to obtain values of C_{L_α}/A which are also presented in table IV. They are compared with the values of C_{L_α}/A predicted by Spencer in reference 16. From table IV, the C_{L_α}/A predicted values show that a maximum difference of 6 percent or -9 percent exists between the results of the two methods for the planforms examined. The difference is attributed to the method used in reference 16 because it does not consider the distribution in lifting pressure over the surface as the present method does but is a refinement of a mathematical expression relating A and sweep to the value of C_{L_α} for wings which have broken leading edges.

(3) The three predicted span loading curves, given in figure 13 for a sweptback and tapered planform, come from references 15 and 17 and the present method. The span

loadings are seen to differ, in terms of y_{cp}, within 0.9 percent of the semispan from each other. The C_{L_α} results of the present method and Campbell's method (ref. 17) agree quite well and are about 5 percent greater than the result of DeYoung and Harper (ref. 15). For the aerodynamic center, the results of the present method and Campbell's method (ref. 17) are 3.2 and 2.1 percent, respectively, of the reference chord ahead of that presented by DeYoung and Harper (ref. 15).

(4) The two span loading curves (obtained from ref. 8 and the present method) shown in figure 14 for the $A = 3.436$ double-delta planform have both been computed using modifications of the Multhopp approach. The curve of reference 8 is based on the two chordal loading function combinations used by Multhopp with a process of submatrix inversion of the matrix of influence coefficients to arrive at the local nondimensional lift and pitching moment. The results of C_{L_α} and $C_{D,i}/C_L^2$ are within 2 and 1 percent, respectively, of each other, whereas the aerodynamic centers differ by about 3.7 percent of the reference chord. The reason for this larger discrepancy in aerodynamic center than found for C_{L_α} or $C_{D,i}/C_L^2$ can be traced primarily to the different local pitching-moment terms computed by each procedure. The reason for the differences in local pitching moments is not clear.

(5) Three span loadings are presented for the double-delta planform of figure 15 and are computed from the following methods: Campbell's (ref. 17), subsonic kernel function (ref. 18), and present. Since the subsonic kernel function and the present method are basically identical (in the reduced frequency case) except for the handling of the integration across the spanwise singularity, it is not surprising that the span loadings should be quite similar. Consequently, the spanwise centers of pressure y_{cp} differ only by about 2 percent semispan. Further, although the values of C_{L_α} are within 1 percent, reference 18 gives a more stable pitching moment resulting in a more rearward aerodynamic center.

Reference 17 presents a span loading which has more of its loading outboard, therefore, a larger value of y_{cp}. Also, its C_{L_α} is lower and its aerodynamic center is ahead of the others.

In figure 15(b) the same trends in the spanwise variation of the centers of pressure are seen to occur in each of the two lifting surface theories over the first 75 percent of the semispan. However, for $\eta > 89$ percent of the semispan, the subsonic kernel function indicates that the chordwise center of pressure (x_{cp}) lies ahead of the wing. The local center of pressure for Campbell's method is the centroid of the two-dimensional loading and occurs at the local $c/4$.

The difficulty experienced by the subsonic kernel function approach can be attributed to an improper location of collocation points used in that solution. The control points were at $\frac{x}{c} = 0.2, 0.4, 0.6, 0.8$; $\frac{y}{b/2} = 0.15, 0.35, 0.55, 0.75$, and the semispan of the region which contains the control point was set equal to 0.10. However, since there is not an

optimum location procedure specified with this method, it is unclear what number and location of collocation points would yield the best results. Perhaps more realistic results could have been achieved by locating points farther outboard than 0.75. A cosine distribution would have made an interesting comparison, but the collocation points cannot be located very near the tip.

A simple case was attempted using only the outboard panel extended to the root, with the collocation points located the same as previously mentioned $\left(\text{in terms of } x/c \text{ and } \frac{y}{b/2}\right)$ and with a region around the control point of semispan equal to 0.10. In this case reasonable results were found which indicate that the planform shape should be of primary importance in selecting these points.

Concerning the distribution of loading along the chords (fig. 15(b)), it is seen that, in general, both lifting surface theories have the same overall shape and differ mostly in magnitude until the subsonic kernel function becomes influenced by the locations of the collocation points, that is, when x_{cp} is ahead of the planform. Comparing the present method with that of the two-dimensional distribution, the effects of induced camber can be seen concentrated mostly inboard of the leading-edge break. The strength of the two-dimensional loading of any spanwise station was chosen to be that predicted by Campbell's lifting-line solution. This was accomplished by requiring that the total circulation strength be equal to the integral of the two-dimensional distributed loading times a suitable multiplier.

Comparisons with experimental data.- Since experimental data are generally lacking for the planforms previously examined, the ability of the present method to predict the aerodynamic characteristics of these wings cannot be appraised. Therefore, the following discussion will relate to three wings for which experimental data are available and comparisons with theoretical results will be made.

(1) The two predicted span loadings presented in figure 16(a) for the $A = 2$ delta planform agree closely and estimate reasonably the experimental values found in reference 19. Also, the C_L values predicted by the two theoretical methods, present and vortex lattice (ref. 20), are in good agreement with the experimental result computed from the C_{L_α} of the force data, since they differ by only about 5 percent. (From the variation of C_L with α determined from the integrated pressure measurements, the C_L value at $\alpha = 4.30$ is lower than that found by the force tests. The difference is attributed to the lack of enough pressure orifices near the leading edge resulting in a poor integration.)

A comparison of the three aerodynamic centers shows that the value given by the present method is ahead of both the experimental location and the one found by reference 20. (In general, for the lower aspect ratio wings, solutions obtained using higher values of N and m result in a more aft location of the aerodynamic center. (See

figs. 6(a) and 7(a).) From an examination of the local loadings (figs. 16(b) and 16(c)), it is seen that although the experimental local centers of pressure are better predicted by reference 20, over most of the chord (x/c of 0.1 to 0.7), the present method gives better agreement with the experimental pressure distribution. The disagreement between the large pressures predicted near the leading-edge singularity and those measured may have resulted from the thickness effects present in the experimental data. The singularity in pressure at the leading edge also causes the local centers of pressure, predicted by the present method, to be ahead of the experimental value.

(2) The present method predicts quite closely the experimental span loading of the $A = 8.02$ sweptback and tapered wing of figure 17 as found in reference 21. This is seen not only by the distribution but in the y_{cp} location. Also, the agreement between the values of C_L and aerodynamic center is good. From figures 17(b) and 17(c), it can be seen that whereas the local chordal centers of pressure are accurately predicted, the pressures are, in general, underpredicted over the chord from x/c of 0.1 to 0.6 and overpredicted from 0.6 to 1.0. Because of the singularity at the leading edge, the theoretical pressure coefficients in this vicinity are in excess of experimental values.

(3) In figure 18, the theoretical and unpublished[1] experimental loading and moment distribution are given for a variable-sweep wing in one sweep position. The predicted overall C_L at $\alpha = 3.14^\circ$ is over 10 percent higher than that found experimentally from force data and this difference is mentioned later. The predicted aerodynamic center is 7 percent of the reference chord ahead of the experimental value; however, this is not a large discrepancy when one considers that the reference chord in this case is based on the outer panel extended to the root. (See fig. 18.)

The experimental values of span loading which are shown in figure 18(a) agree well with those predicted by theory; however, there is a slight overprediction by the theory over the outermost part of the outer panel which can also be seen in the c_{n_α} graph presented in figure 18(b). This theoretical overprediction of local c_{n_α} leads to the overall C_L being higher than the experimental value. The effect of the leading-edge shed vortex and different amounts of induced angle of attack generated by the theoretical and experimental loading distribution undoubtedly account for some of the disagreement seen in figures 18(a) and (b). Good agreement is found for the c_{m_α} data obtained from theory and experiment. The x_{cp} graph is just the result of the c_{n_α} and c_{m_α} curves and hence shows the local center of pressure slightly off of that predicted by theory.

At the four different spanwise stations shown in figure 18(c), the chordal loadings are compared and the agreement is found to be reasonable at most locations.

Illustrative calculations.- Effect of variable sweep: Changes in the aerodynamic characteristics due to increasing or decreasing the outer panel wing sweep (from the

[1]Tests performed in the Langley high-speed 7- by 10-foot tunnel.

streamwise tip position) can also be predicted with the present method. For example, the planform in figure 18 has its sweep varied from 15^{o} to 40^{o} at a Mach number of 0.23 and the results, shown in figure 19, are based on the area and mean geometric chord of the outer panel extended to the root when $\Lambda = 30^{o}$. Those results presented are from the present method and unpublished experimental data measured on a semispan pressure wing at the Langley Research Center.

The agreement obtained between theoretical and experimental results is only fair in that the theory shows the proper trends and similar increments, but not absolute levels. Experimental values for $C_{D,i}/C_L{}^2$ were not available from force data. As reported in references 22 and 23, the variations presented in figure 19 are typical of variable-sweep wings.

Effect of Mach number: The effect of increasing the subsonic Mach number on the wing-alone aerodynamic characteristics is accounted for by use of the Prandtl-Glauert compressibility rule as mentioned earlier. (See ref. 11.) In general, the results obtained appear to be questionable above a Mach number 0.8 because of the inapplicability of the Prandtl-Glauert transformation as $M \rightarrow 1$ (ref. 11).

Some results obtained by applying this rule to a highly sweptback and tapered wing are presented in figure 20 along with those determined from Mach numbers 1.2 to 2.8 by use of the supersonic lifting-surface theory of reference 4. Experimental values for the wing-body combination are presented for comparison.

In general, the theoretical methods are able to predict reasonably well the experimental flat wing overall aerodynamic characteristics (which for subsonic speeds have not been published but are found in ref. 24 for supersonic speeds) even though the experimental data contained the influence of a body. The one exception is the induced drag parameter which does differ considerably. However, this is not unexpected since the real leading edge is sharp and the leading-edge suction is considerably less than the 100 percent assumed by the theory. Further, no induced drag, called vortex drag at supersonic speeds, is given supersonically since it was not available separate from the wave drag.

In the transonic region (dashed lines) the results are obtained by fairing from subsonic to supersonic speeds.

Warped wing: The determination of the aerodynamic characteristics for a warped wing can also be found by using the present method when the local surface slope distribution is specified. In addition to the flat plate loading characteristics, which are always found, the basic loading features are also computed by the use of the appropriate equations given in appendix B. Also determined are the zero-lift angle of attack α_o, pitching-moment coefficient $C_{m,o}$, and root bending-moment coefficient $C_{B,o}$. Illustrative results of this procedure are presented in figure 21 for a double-delta planform with 5^{o}

of linear twist and 2-percent circular arc camber. (Other details of this planform and loading distribution are to be found in the "Supplement to NASA TN D-4427" since it is one of the sample cases given.)

MEAN CAMBER SURFACE DETERMINATION

The problem of determining the mean camber surface required to support a prescribed loading on a given planform is easier to solve from the basic formulation than finding the loading associated with a prescribed surface shape for the same planform. This can be seen from the fundamental equation in compressible subsonic flow which is equation (1) and is given as follows:

$$\left(\frac{w}{U}\right)_{z=0} = \frac{1}{8\pi q_\infty} \int_{-1}^{1} \int_{\xi_{le}}^{\xi_{te}} \frac{\Delta p(\xi,\eta)}{(y-\eta)^2} \left[1 + \frac{(x-\xi)/\beta}{\sqrt{\frac{(x-\xi)^2}{\beta^2} + (y-\eta)^2}}\right] d\xi \, d\eta$$

from which the mean camber surface is found by use of the following equation:

$$\frac{z}{c} = \int_{(x/c)_{te}}^{x'/c} \frac{w}{U} \, d\frac{x}{c} \tag{13}$$

The determination of the local $\Delta p(\xi,\eta)$ from equation (1) has been shown to involve solving the equations inversely for a part of its integrand; whereas, to find w/U at any point, the individual specified loading must be simply multiplied with the appropriate kernel function value and summed over the surface. Thus, if the more difficult problem is solved or programed first (as in the present study), then the other only requires, in addition to those changes mentioned, the deletion of the matrix inversion and the addition of the w/U integration to find z/c.

Since values of w/U are only computed at the control points, some representation at other chordwise locations is needed in order that the integration of equation (13) can be carried out. A least-square polynomial curve fit of the w/U values at the control points was chosen to represent the variation of w/U along the chord between the first and last control points. The polynomial curve fit is specified to have a degree of one less than the number of chordal control points to insure that a good fit can be obtained. Outside the range of the control points, a linear extrapolation of the polynomial curve fit is used to the nearest chordwise edge.

Optimization of N and m

As in the load determination section, a study was undertaken here to find the relationship that N and m should have in order that the best mean camber lines could be obtained. It was intuitively felt that these mean camber lines would occur when the most control points were employed. For the A = 2 delta planform shown in figure 22, four combinations of N and m were selected and in each case the same surface loading distribution was used. It was composed of only a $\sin \vartheta$ chordwise loading which varied elliptically from tip to tip and was adjusted to give an overall lift coefficient of unity. All other pressure mode coefficients were set equal to zero.

Figure 22(a) shows that the computed downwash w/U values at a constant m with varying N do not lead to a much changed polynomial curve fit, whereas at a constant value of N varying m does. The curves appearing in this figure are integrated and appear in figure 22(b). As would be expected, sets of N and m which have essentially the same curve fit lead to the same mean camber line. Thus, the mean camber lines for the sets N = 4 and N = 8 at m = 11 are the same. This is also true for the sets of N = 4 and N = 8 at m = 23.

Thus it appears that for the given surface loading, increasing the number of spanwise stations at which the desired chord loadings are defined is more important in obtaining the best mean camber lines than increasing the number of chordal pressure modes involved (much above those needed to define the shape) at each spanwise station. This is a similar conclusion to that reached in reference 25. (Note that the prescribed loading does not contain any leading-edge suction and hence it is not known what the effects of including the suction term would have on the camber for optimum combinations of N and m.)

With the relationship that N and m should have for certain loadings established, some comparisons with other theoretical methods are made and follow in the next section.

Comparisons

The accuracy of the present method may be appraised by comparing in figure 23 the downwash distribution at the plane of symmetry of an A = 10 rectangular wing with that of a two-dimensional wing with the same $\sin \vartheta$ chord loading at each span station.

Over most of the chord the three-dimensional downwash is slightly lower than that of the two dimensional by a constant amount. If a much higher aspect ratio wing had been used in the computation, this difference would become smaller.

At the edges, where $x/c \to 0$ and 1, the three-dimensional downwash is seen to tend toward plus and minus infinity, respectively. This is caused by the logarithmic

singularity correction term, which results from the second-order singularity $\left(\frac{1}{y - \eta}\right)^2$ in the integrand, containing a term which increases without bound at all edges. (See eq. (A9).)

From figure 23, it can also be noted that by using only a $\sin \vartheta$ loading increasing the number of chordal control points does not change the downwash distribution at or in the vicinity of the chordal control points already computed but does give a more detailed representation of the distribution.

As another check, the mean camber lines obtained with the present method for the sweptback wing shown in figure 24 are presented there[2] for comparison with those predicted by the mean camber surface solution of Katzoff, Faison, and DuBose (ref. 26). Three differences are apparent in the procedures used and are

1. The present method rounds any kinks that occur in the wing planform (i.e., at the root) which results in a closer representation of the isobars on the planform (ref. 5) and hence gives a better downwash distribution than the method used in reference 25 (ref. 27).

2. The uniform chord loadings ΔC_p used in reference 26 are approximated herein by a Fourier series of four odd sine terms $-\sin \vartheta$, $\sin 3\vartheta$, $\sin 5\vartheta$, and $\sin 7\vartheta$. This series or others like it composed of $\cot \frac{\vartheta}{2}$ and even sine functions give greater flexibility in approximating arbitrary pressure loadings. The amplitudes of the chord loading were uniform over the entire area and produced a lift coefficient of 1.0.

3. The present method uses the least-square polynomial curve fit and constant slope scheme to determine the downwash values all along the chord as discussed earlier. This procedure differs from that used in reference 26 where the downwash distribution computed at selected internal constant chord lines is completed by fairing except near the edges of the chord. There the downwash is assumed to be equal to that required to produce a constant pressure all along the resulting mean camber lines.

The curves which are discussed in the previous paragraph are then integrated to find the mean camber height z/c above the x-y plane. Despite the differences discussed between these two methods, figure 24 shows that the agreement between them is good except near the plane of symmetry. This is explained in part by the first difference listed. (See also ref. 27.)

Application.- An application of the present method to the highly sweptback and tapered planform shown in figure 25[3] is made where the lift coefficient for this planform

[2]The results of reference 26 were found by integrating from the leading edge rearward and hence were adjusted in figure 24 to the same zero level for comparison.

[3]Tabular results for this planform and loading distribution are to be found in the "Supplement to NASA TN D-4427" since it is used as the sample case.

was taken as unity at a Mach number of 0.30. The chordal loading function coefficients were specified so that there was (1) a zero $\cot \frac{\vartheta}{2}$ distribution, (2) an elliptical distribution of $\sin \vartheta$ across the span, (3) a $\sin 2\vartheta$ distribution such that the local x_{cp} varied parabolically from 50 percent of the local chord at the plane of symmetry to 20 percent at the break and from the break linearly back to 50 percent at the tip, and (4) a $\sin 3\vartheta$ distribution which caused the slope of the chordal loadings to be zero at the trailing edge.

Figure 25 shows that the mean camber lines have a rearward movement of the x/c location of maximum camber and a twist which increases toward the tip. The mean camber line at $\eta = 0.997$ is typical of stations near the tip and should be examined carefully before a direct application is made since the downwash distribution which produced it may be overly influenced by the singular nature of the downwash at the tip.

CONCLUSIONS

The results obtained with a modified version of Multhopp's lifting-surface theory programed for the IBM 7094 electronic data processing system and Control Data 6400 computer system to find the surface loadings and mean camber surfaces have been studied and the following conclusions are drawn:

For the surface loading program:

1. It has been found that the loading program may be applied with reasonable accuracy to conventional and composite planforms to find their flat plate characteristics and to wings with twist and/or camber to determine the basic loading distribution as well as the force and moment coefficients at zero lift.

2. In predicting the surface loading, the number and spacing of control points is more important when seeking an accurate overall aerodynamic center than when a solution for the lift-curve slope, span loading, or spanwise location of center of pressure is being sought. It has been found that at least four, and preferably more, chordal control points should be used in obtaining aerodynamic centers. This number should depend upon the βA of the planform being considered, since the more control points used (100 available) at each spanwise station necessitates a decrease in the number of spanwise stations. This may lead to a problem when values of βA are large. However, in general, the number of chordal control points should be kept between 6 and 10 to insure that the resulting values of aerodynamic center lie within the region of converging results.

3. Reasonable agreement is generally obtained with both experiment and other theories concerning local and overall loading characteristics.

4. The effect of Mach number can be determined and the resulting agreement with experiment is found to be reasonable.

For the mean camber surface program:

1. Good agreement is achieved between the downwash required by two-dimensional theory for a $\sin \vartheta$ loading and that predicted by a three-dimensional uniform $\sin \vartheta$ loading at the plane of symmetry of an aspect-ratio-10 rectangular wing.

2. The agreement with results from other mean camber predictions is found to be fairly good and the present method has the capability of approximating most chord loading shapes by the use of a Fourier sine series.

3. For an acceptable prediction of mean camber surfaces which includes no leading-edge suction, the number of chordwise stations should be nearly equal and never less than the number of pressure loading terms required to properly define the desired shape and the number of spanwise stations should be as many as can be accommodated by the machine for that number of chord stations.

4. The resultant mean camber surface predicted for a composite planform whose loading includes no leading-edge suction was found to have a reasonable twist and camber distribution inboard of the tip. In the vicinity of the tip, the mean camber surface does not appear to be as reasonable due to the singular nature of the downwash at the tip.

Langley Research Center,
National Aeronautics and Space Administration,
Langley Station, Hampton, Va., January 19, 1968,
126-13-01-50-23.

APPENDIX A

FORMULATING THE INFLUENCE COEFFICIENT MATRIX

The formulation of the influence coefficients $\bar{L}^{j}_{\nu n}(\phi_s)$ is accomplished by integrating (or approximating) the chordal influence that the pressure loading functions exert on each control point from every other spanwise station. (See ref. 6.) Then, for symmetrical spanwise loadings, the chordal influence at η_{-n}, $L^{j}_{\nu -n}(\phi_s)$, is added to that of η_n, $L^{j}_{\nu n}(\phi_s)$, to give the total $\bar{L}^{j}_{\nu n}(\phi_s)$, and for antisymmetrical loadings the influence at η_{-n}, $L^{j}_{\nu -n}(\phi_s)$, is subtracted from that at η_n, $L^{j}_{\nu n}(\phi_s)$. The value at the plane of symmetry, $\bar{L}^{j}_{\nu 0}(\phi_s)$, is just equal to $L^{j}_{\nu 0}(\phi_s)$ when the loading is symmetrical and zero when antisymmetrical.

Now, for $\nu \neq n$,

$$L^{j}_{\nu n}(\phi_s) = -b_{\nu n} K_j(\phi_s, y_\nu; \eta_n) \qquad (j \geq 0) \qquad \text{(A1)}$$

with

$$\nu = -\frac{m-1}{2}, -\frac{m-3}{2}, \ldots, 0, \ldots, \frac{m-3}{2}, \frac{m-1}{2}$$

where

$$b_{\nu n} = \begin{cases} \dfrac{\sin \theta_n}{(m+1)(\cos \theta_n - \cos \theta_\nu)^2} & (|n-\nu| \text{ odd}) \\ 0 & (|n-\nu| \text{ even}) \end{cases} \qquad \text{(A2)}$$

$$K_j(\phi_s, y_\nu; \eta_n) = \begin{cases} \displaystyle\int_0^\pi \cot \frac{\vartheta}{2} \sin \vartheta \, K(\phi_s, y_\nu; \vartheta, \eta_n) d\vartheta & (j = 0) \\ \displaystyle\int_0^\pi \sin j\vartheta \sin \vartheta \, K(\phi_s, y_\nu; \vartheta, \eta_n) d\vartheta & (j \geq 1) \end{cases} \qquad \text{(A3)}$$

and the subsonic kernel function is given by

$$K(\phi, y; \vartheta, \eta) = 1 + \frac{\left[-c(y)\cos \phi + d(y) + c(\eta)\cos \vartheta - d(\eta)\right]/\beta}{\sqrt{\left[-c(y)\cos \phi + d(y) + c(\eta)\cos \vartheta - d(\eta)\right]^2/\beta^2 + (y-\eta)^2}} \qquad \text{(A4)}$$

where

$$\left.\begin{aligned} x &= -c(y)\cos\phi + d(y) \\ \xi &= -c(\eta)\cos\vartheta + d(\eta) \end{aligned}\right\} \tag{A5}$$

Now, for $n = \nu$,

$$L^{j}_{\nu\nu}(\phi_s) = b_{\nu\nu}K_j(\phi_s,y_\nu;\eta_\nu) + \text{Logarithmic singularity correction} \tag{A6}$$

where

$$b_{\nu\nu} = \frac{m + 1}{4 \sin\theta_\nu} \tag{A7}$$

$$K_j(\phi_s,y_\nu;\eta_\nu) = \left\{\begin{aligned} &2\phi_s + 2\sin\phi_s && (j = 0) \\ &\phi_s - \tfrac{1}{2}\sin 2\phi_s && (j = 1) \\ &\frac{\sin(j - 1)\phi_s}{j - 1} - \frac{\sin(j + 1)\phi_s}{j + 1} && (j > 1) \end{aligned}\right\} \tag{A8}$$

The logarithmic singularity correction term (LSC) arises because of the spanwise integration across the second-order singularity $\frac{1}{(y - \eta)^2}$. Its derivation is discussed by Multhopp in reference 5, Mangler and Spencer in reference 28, and Van Spiegel and Wouters in reference 6. Its best form is

$$\text{LSC} = \frac{\left(df_j(\phi)/d\phi\right)_{\phi=\phi_s}}{c(y_\nu)^2(m + 1)\sin\theta_\nu \sin\phi_s}\left[\frac{m + 1}{8}(\cos 2\theta_\nu - \ln 4)\right.$$

$$\left. - \sum_{n=-\frac{m-1}{2}}^{\frac{m-1}{2}}{}' \sin^2\theta_n \ln|y_\nu - \eta_n|\right] \qquad (|n - \nu| \text{ odd}) \tag{A9}$$

where the prime on the summation sign means that the term when $n = \nu$ is eliminated in the summation process and

APPENDIX A

$$f_j(\phi) = \begin{cases} \cot \dfrac{\phi}{2} & (j = 0) \\ \sin j\phi & (j \geq 1) \end{cases} \qquad \text{(A10)}$$

APPENDIX B

EQUATIONS USED IN THE COMPUTATIONS

The following equations are used to determine the total local characteristics at the design lift coefficient as well as the overall characteristics for wings with twist and/or camber. Note that the $qt_j(\eta_n)$ terms represent the pressure mode coefficients associated with the twist and/or camber boundary conditions, and the $q_j(\eta_n)$ terms represent the pressure mode coefficients associated with the flat plate boundary conditions. The $qt_j(\eta_n)$ terms are arrived at in a manner similar to that of the $q_j(\eta_n)$ terms, as given by the matrix inversion of equation (4), except that the $\frac{-4w(\phi_s,y_\nu)}{U}$ values are now the local angle of attack for the warped wing at the flat plate control points when the root chord is at zero angle of attack.

Local Aerodynamic Characteristics

(a) Pressure coefficient

$$\Delta C_p(\vartheta,\eta_n) = \frac{1}{c(\eta_n)q_\infty}\left\{\left[qt_0(\eta_n) - q_0(\eta_n)\left(\frac{C_{L,1} - C_{L,desired}}{C_{L,\alpha=1\ rad}}\right)\right]\cot\frac{\vartheta}{2} + \sum_{j=1}^{N}\left[qt_j(\eta_n) - q_j(\eta_n)\left(\frac{C_{L,1} - C_{L,desired}}{C_{L,\alpha=1\ rad}}\right)\right]\sin j\vartheta\right\}$$

(b) Chord loading

$$\left(c_\ell cq_\infty\right)_n = \pi\left\{\left[qt_0(\eta_n) + \frac{1}{2}qt_1(\eta_n)\right] - \left[q_0(\eta_n) + \frac{1}{2}q_1(\eta_n)\right]\left(\frac{C_{L,1} - C_{L,desired}}{C_{L,\alpha=1\ rad}}\right)\right\}$$

(c) Nondimensional lift coefficient (called circulation in the "Supplement to NASA TN D-4427")

$$\gamma_n = \left(\frac{c_\ell c}{2b}\right)_n = \frac{\pi}{2bq_\infty}\left\{\left[qt_0(\eta_n) + \frac{1}{2}qt_1(\eta_n)\right] - \left[q_0(\eta_n) + \frac{1}{2}q_1(\eta_n)\right]\left(\frac{C_{L,1} - C_{L,desired}}{C_{L,\alpha=1\ rad}}\right)\right\}$$

(d) Pitching moment about local leading edge

$$\left(c_m c^2 q_\infty\right)_n = c(\eta_n)\pi\left\{\left[qt_0(\eta_n) + \frac{1}{2}qt_1(\eta_n) - \frac{1}{2}qt_0(\eta_n) - \frac{1}{4}qt_2(\eta_n)\right] - \left[q_0(\eta_n) + \frac{1}{2}q_1(\eta_n) - \frac{1}{2}q_0(\eta_n) - \frac{1}{4}q_2(\eta_n)\right]\left(\frac{C_{L,1} - C_{L,\text{desired}}}{C_{L,\alpha=1\text{ rad}}}\right)\right\}$$

(e) Location of center-of-pressure loading from Y-axis

$$\left(\xi_{cp}\right)_n = -\frac{c(\eta_n)}{2}\left\{\frac{\left[qt_0(\eta_n) + \frac{1}{2}qt_2(\eta_n)\right] - \left[q_0(\eta_n) + \frac{1}{2}q_2(\eta_n)\right]\left(\frac{C_{L,1} - C_{L,\text{desired}}}{C_{L,\alpha=1\text{ rad}}}\right)}{\left[qt_0(\eta_n) + \frac{1}{2}qt_1(\eta_n)\right] - \left[q_0(\eta_n) + \frac{1}{2}q_1(\eta_n)\right]\left(\frac{C_{L,1} - C_{L,\text{desired}}}{C_{L,\alpha=1\text{ rad}}}\right)}\right\} + d(\eta_n)$$

(f) Center-of-pressure loading in fractions of local chord

$$\left(x_{cp}\right)_n = \frac{\left(\xi_{cp}\right)_n - d(\eta_n) + c(\eta_n)}{2c(\eta_n)}$$

(g) Span load coefficient

$$\left(\frac{c_\ell c}{c_{av}}\right)_n = \frac{\pi}{c_{av} q_\infty}\left\{\left[qt_0(\eta_n) + \frac{1}{2}qt_1(\eta_n)\right] - \left[q_0(\eta_n) + \frac{1}{2}q_1(\eta_n)\right]\left(\frac{C_{L,1} - C_{L,\text{desired}}}{C_{L,\alpha=1\text{ rad}}}\right)\right\}$$

Overall Aerodynamic Characteristics

(a) Flat plate lift

$$\frac{b}{2}\int_{-1}^{1} c_\ell c q_\infty \, d\eta \approx \frac{\pi^2(b/2)}{m+1}\sum_{n=-\frac{m-1}{2}}^{\frac{m-1}{2}}\left[q_0(\eta_n) + \frac{1}{2}q_1(\eta_n)\right]\sin\theta_n$$

(b) Flat plate pitching moment about the total wing $\bar{c}/4$

$$\frac{b}{2}\int_{-1}^{1} c_m c^2 q_\infty \, d\eta \approx -\frac{\pi^2(b/2)}{m+1} \sum_{n=-\frac{m-1}{2}}^{\frac{m-1}{2}} \left\{ \left[d(\eta_n) - x_{\bar{c}} - \frac{\bar{c}}{4} \right] \left[q_0(\eta_n) + \frac{1}{2} q_1(\eta_n) \right] \right.$$

$$\left. - c(\eta_n) \left[\frac{1}{2} q_0(\eta_n) + \frac{1}{4} q_2(\eta_n) \right] \right\} \sin \theta_n$$

(c) Flat plate pitching moment about the reference wing $c_{ref}/4$ =

$$(\text{Flat plate pitching moment})_{\text{total wing}} - \text{Lift}\left(x_{\bar{c}} + \frac{\bar{c}}{4} - x_{c_{ref}} - \frac{c_{ref}}{4} \right)$$

(d) Flat plate rolling moment about the X-axis

$$\left(\frac{b}{2}\right)^2 \int_{-1}^{1} \eta c_l c q_\infty \, d\eta \approx \frac{\pi^2(b/2)^2}{m+1} \sum_{n=-\frac{m-1}{2}}^{\frac{m-1}{2}} \eta_n \left[q_0(\eta_n) + \frac{1}{2} q_1(\eta_n) \right] \sin \theta_n$$

(e) Flat plate location of the aerodynamic center

$$(\xi_{cp})_{\text{overall}} = -\frac{(\text{Flat plate pitching moment})_{\text{reference wing}}}{\text{Lift}} + x_{c_{ref}} + \frac{c_{ref}}{4}$$

(f) Flat plate aerodynamic center in fractions of reference chord, measured from the $x_{c_{ref}}$

$$\text{a.c.} = -\frac{(\text{Flat plate pitching moment})_{\text{reference wing}}}{\text{Lift}(c_{ref})} + \frac{1}{4}$$

(g) Angle of attack at zero lift

$$\alpha_o = -\frac{C_{L,1}}{C_{L_\alpha}}$$

where $C_{L,1}$ is determined similarly to flat plate C_L

(h) Pitching-moment coefficient at zero lift

$$C_{m,o} = C_{m,1} + C_{m_\alpha}\alpha_o$$

where $C_{m,1}$ is determined similarly to flat plate C_m

(i) Root bending-moment coefficient at zero lift

$$C_{B,o} = \frac{b}{S_{ref}} \int_0^1 (c_l c)_{basic} \eta \, d\eta$$

$$C_{B,o} \approx \frac{b\pi^2}{(m+1)q_\infty S_{ref}} \sum_{n=-\frac{m-1}{2}}^{\frac{m-1}{2}} \left[qt_0(\eta_n) + \frac{1}{2} qt_1(\eta_n) \right] \eta_n \sin \theta_n$$

REFERENCES

1. Crigler, John L.: A Method for Calculating Aerodynamic Loadings on Thin Wings at a Mach Number of 1. NASA TN D-96, 1959.

2. Smith, J. H. B.: Calculation of the Shape of a Thin Slender Wing for a Given Load Distribution and Planform. C.P. No. 385, Brit. A.R.C., 1958.

3. Carlson, Harry W.; and Middleton, Wilbur D.: A Numerical Method for the Design of Camber Surfaces of Supersonic Wings With Arbitrary Planforms. NASA TN D-2341, 1964.

4. Middleton, Wilbur D.; and Carlson, Harry W.: A Numerical Method for Calculating the Flat-Plate Pressure Distributions on Supersonic Wings of Arbitrary Planform. NASA TN D-2570, 1965.

5. Multhopp, H.: Methods for Calculating the Lift Distribution of Wings (Subsonic Lifting-Surface Theory). R. & M. No. 2884, Brit. A.R.C., Jan. 1950.

6. Van Spiegel, E.; and Wouters, J. G.: Modification of Multhopp's Lifting Surface Theory With a View to Automatic Computation. NLR-TN W.2, Nat. Lucht- Ruimtevaartlab. (Amsterdam), June 1962.

7. Milne-Thomson, L. M.: Theoretical Aerodynamics. Second ed., MacMillan and Co., Ltd., 1952, p. 225.

8. Nagaraj, V. T.: Theoretical Calculation of the Aerodynamic Characteristics of a Double Delta Wing (by Lifting Surface Theory). M.E. Thesis, Indian Inst. Sci., 1961.

9. Van de Vooren, A. I.: An Approach to Lifting Surface Theory. Rep. F. 129, Nat. Luchtvaartlab. (Amsterdam), June 1953.

10. Garner, H. C.; and Lehrian, Doris E.: Non-Linear Theory of Steady Forces on Wings With Leading-Edge Flow Separation. NPL Aero Rep. 1059, Brit. A.R.C., Feb. 15, 1963.

11. Kuethe, A. M.; and Schetzer, J. D.: Foundations of Aerodynamics. Second ed., John Wiley & Sons, Inc., c.1959, pp. 200-203.

12. Munk, Max M.: The Minimum Induced Drag of Aerofoils. NACA Rep. 121, 1921.

13. Garner, H. C.: Some Remarks on Vortex Drag and Its Spanwise Distribution in Incompressible Flow. NPL Aero Note 1048, Brit. A.R.C., Nov. 4, 1966.

14. Lamar, John E.; and Alford, William J., Jr.: Aerodynamic-Center Considerations of Wings and Wing-Body Combinations. NASA TN D-3581, 1966.

15. DeYoung, John; and Harper, Charles W.: Theoretical Symmetric Span Loading at Subsonic Speeds for Wings Having Arbitrary Plan Form. NACA Rep. 921, 1948.

16. Spencer, Bernard, Jr.: A Simplified Method for Estimating Subsonic Lift-Curve Slope at Low Angles of Attack for Irregular Planform Wings. NASA TM X-525, 1961.

17. Campbell, George S.: A Finite-Step Method for the Calculation of Span Loadings of Unusual Plan Forms. NACA RM L50L13, 1951.

18. Watkins, Charles E.; Woolston, Donald S.; and Cunningham, Herbert J.: A Systematic Kernel Function Procedure for Determining Aerodynamic Forces on Oscillating or Steady Finite Wings at Subsonic Speeds. NASA TR R-48, 1959.

19. Wick, Bradford H.: Chordwise and Spanwise Loadings Measured at Low Speed on a Triangular Wing Having an Aspect Ratio of Two and an NACA 0012 Airfoil Section. NACA TN 1650, 1948.

20. Dulmovits, John: A Lifting Surface Method for Calculating Load Distributors and the Aerodynamic Influence Coefficient Matrix for Wings in Subsonic Flow. Rep. No. ADR 01-02-64.1, Grumman Aircraft Eng. Corp., Aug. 1964.

21. Graham, Robert R.: Low-Speed Characteristics of a 45^{o} Sweptback Wing of Aspect Ratio 8 From Pressure Distributions and Force Tests at Reynolds Numbers From 1,500,000 to 4,800,000. NACA RM L51H13, 1951.

22. Baals, Donald D.; and Polhamus, Edward C.: Variable Sweep Aircraft. Astronaut. Aerosp. Eng., vol. 1, no. 5, June 1963, pp. 12-19.

23. Alford, William J., Jr.; Luoma, Arvo A.; and Henderson, William P.: Wind-Tunnel Studies at Subsonic and Transonic Speeds of a Multiple-Mission Variable-Wing-Sweep Airplane Configuration. NASA TM X-206, 1959.

24. Morris, Odell A.; and Fournier, Roger H.: Aerodynamic Characteristics at Mach Numbers 2.30, 2.60, and 2.96 of a Supersonic Transport Model Having a Fixed, Warped Wing. NASA TM X-1115, 1965.

25. Garner, H. C.: Accuracy of Downwash Evaluation by Multhopp's Lifting-Surface Theory. NPL Aero Rep. 1110, Brit. A.R.C., July 1964.

26. Katzoff, S.; Faison, M. Frances; and DuBose, Hugh C.: Determination of Mean Camber Surfaces for Wings Having Uniform Chordwise Loading and Arbitrary Spanwise Loading in Subsonic Flow. NACA Rep. 1176, 1954. (Supersedes NACA TN 2908.)

27. Thwaites, Bryan, ed.: Incompressible Aerodynamics. Clarendon Press (Oxford), 1960, pp. 321 and 363.

28. Mangler, K. W.; and Spencer, B. F. R.: Some Remarks on Multhopp's Subsonic Lifting-Surface Theory. R. & M. No. 2926, Brit. A.R.C., 1956.

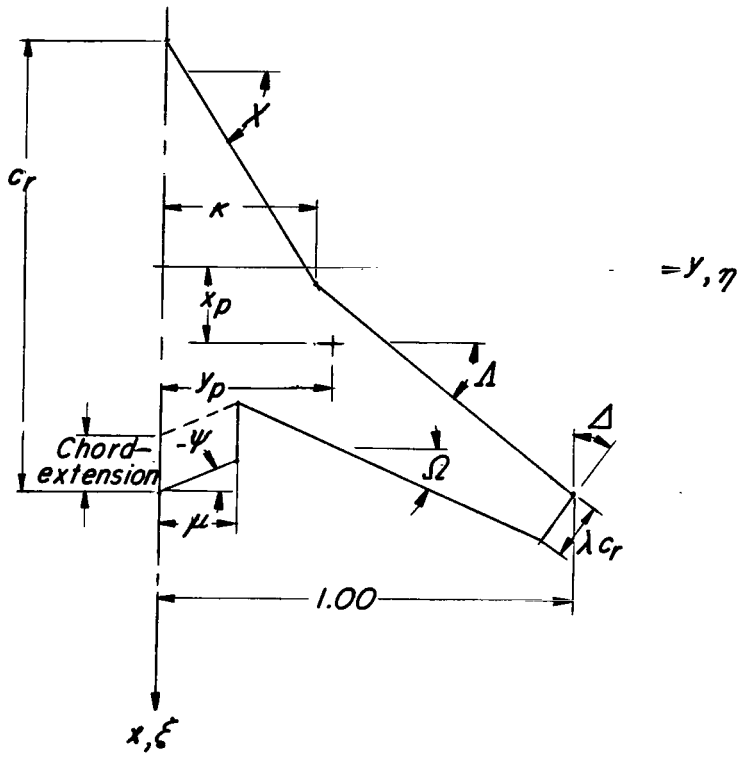

(a) Planform variables.

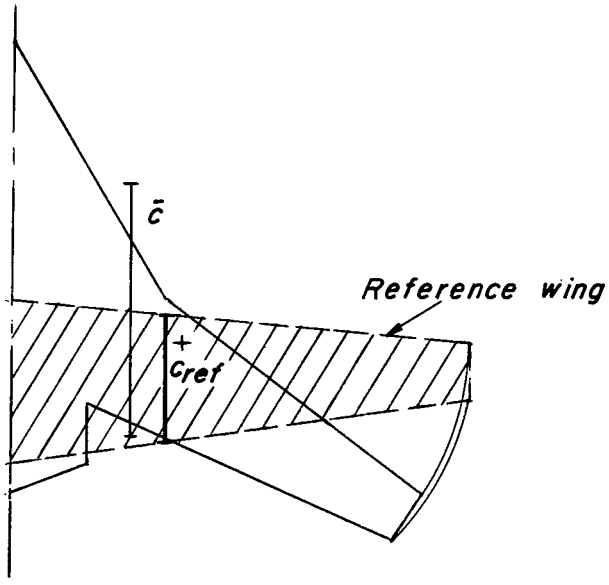

(b) Reference wing geometry.

Figure 1.- General planform which can be used in these programs along with its coordinate system and reference wing geometry.

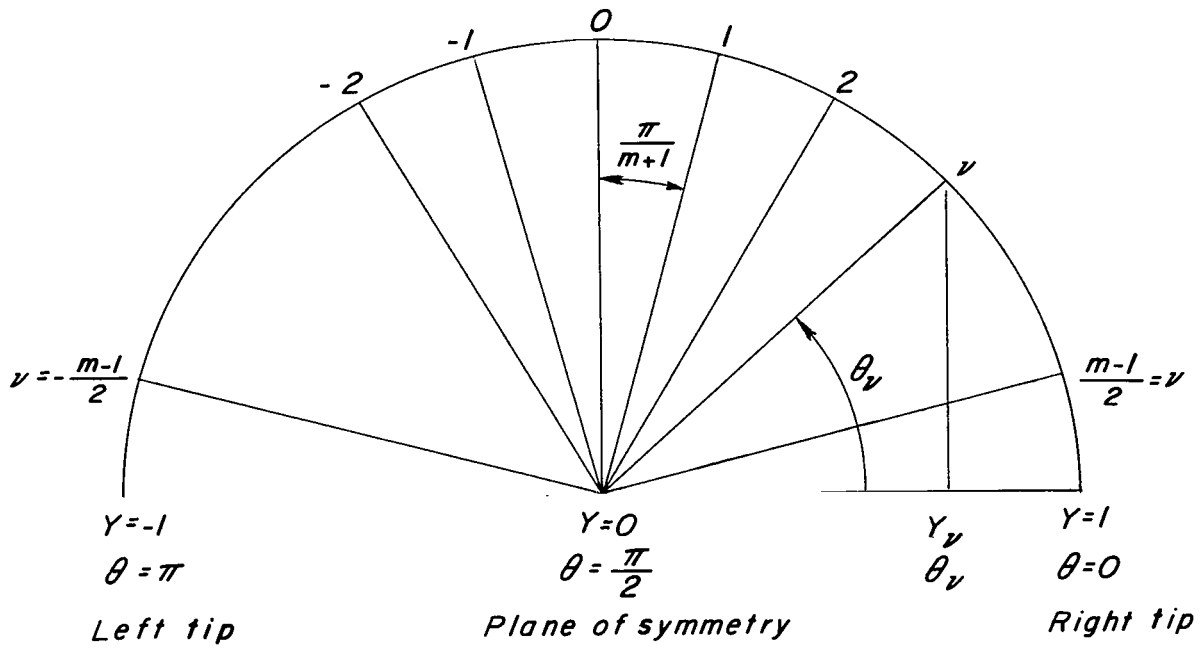

(a) Spanwise. $\theta_\nu = \frac{\pi}{2} - \frac{\nu\pi}{m+1}$, where ν ranges from $-\frac{m-1}{2}$ to $\frac{m-1}{2}$.

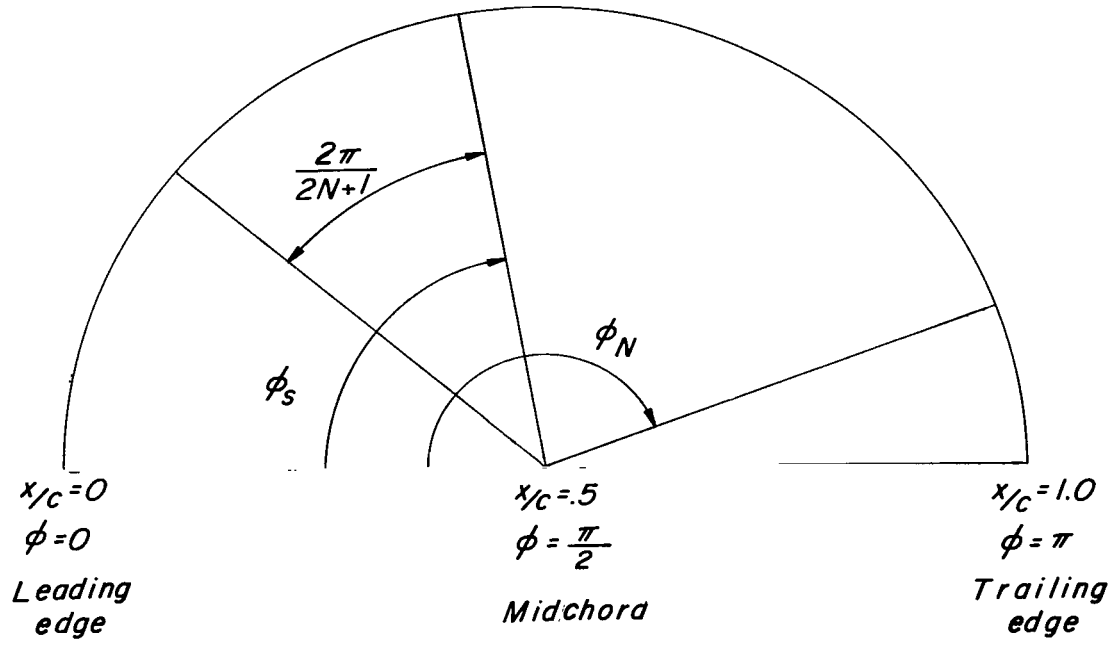

(b) Chordwise. $\Phi_s = \frac{2s\pi}{2N+1}$, where s ranges from 1 to N.

Figure 2.- Control-point locations.

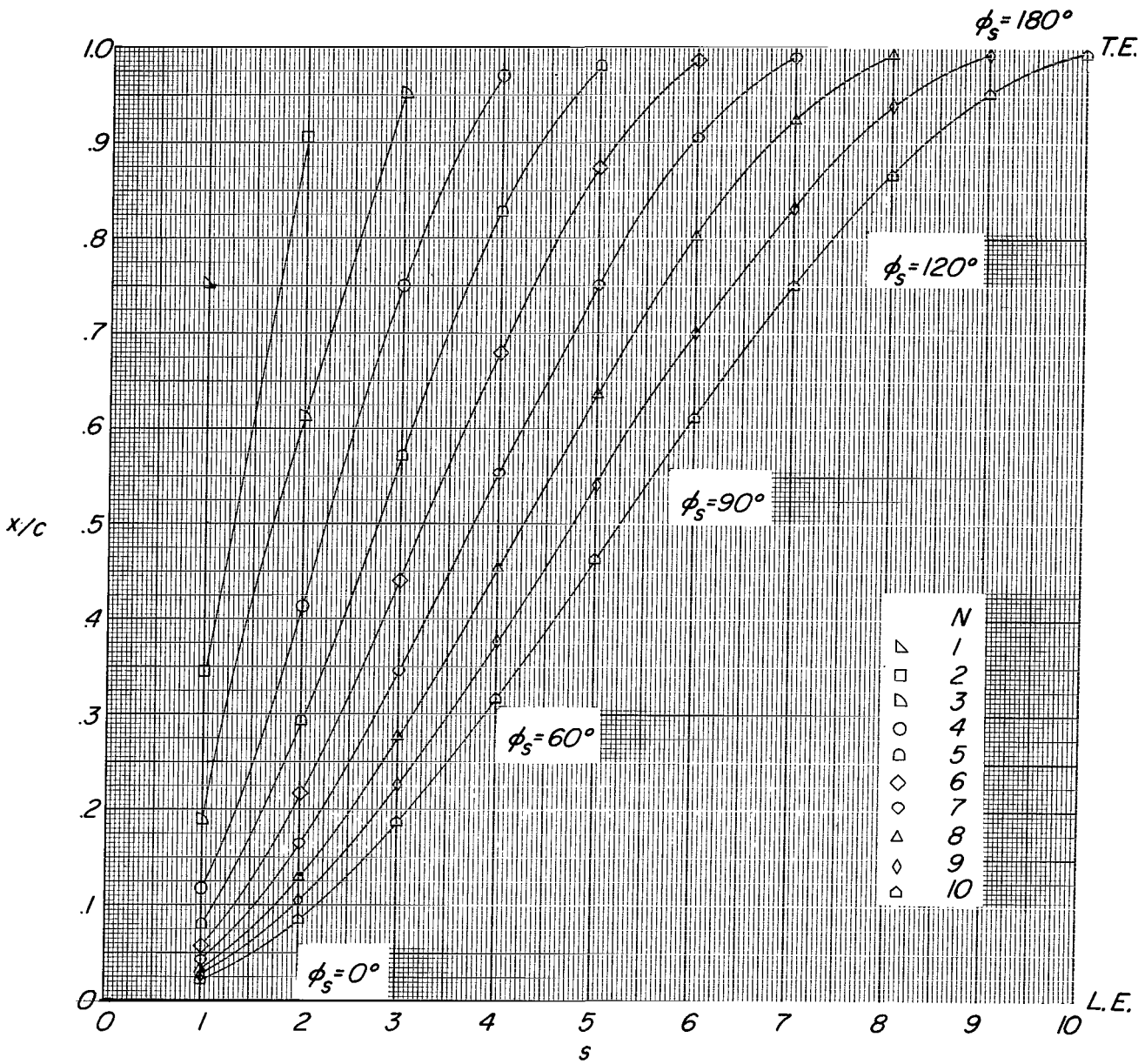

Figure 3.- Detailed chordwise location of control points. $\frac{x}{c} = \frac{1}{2}(1 - \cos \Phi_s)$.

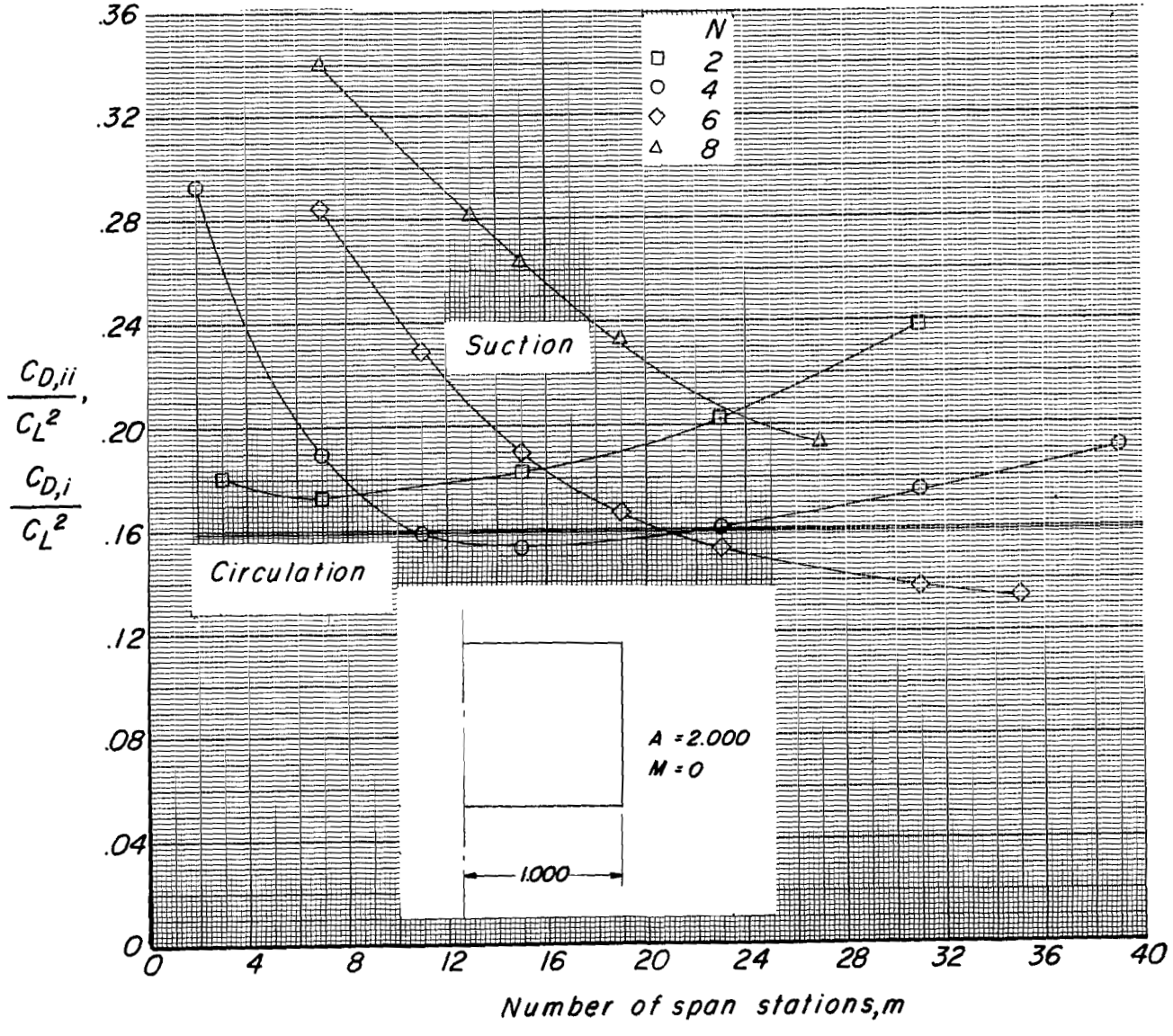

(a) Induced drag parameter.

Figure 4.- Effect of varying number and locations of control points and chordal loading functions on aerodynamic characteristics of A = 2 rectangular planform at M = 0.

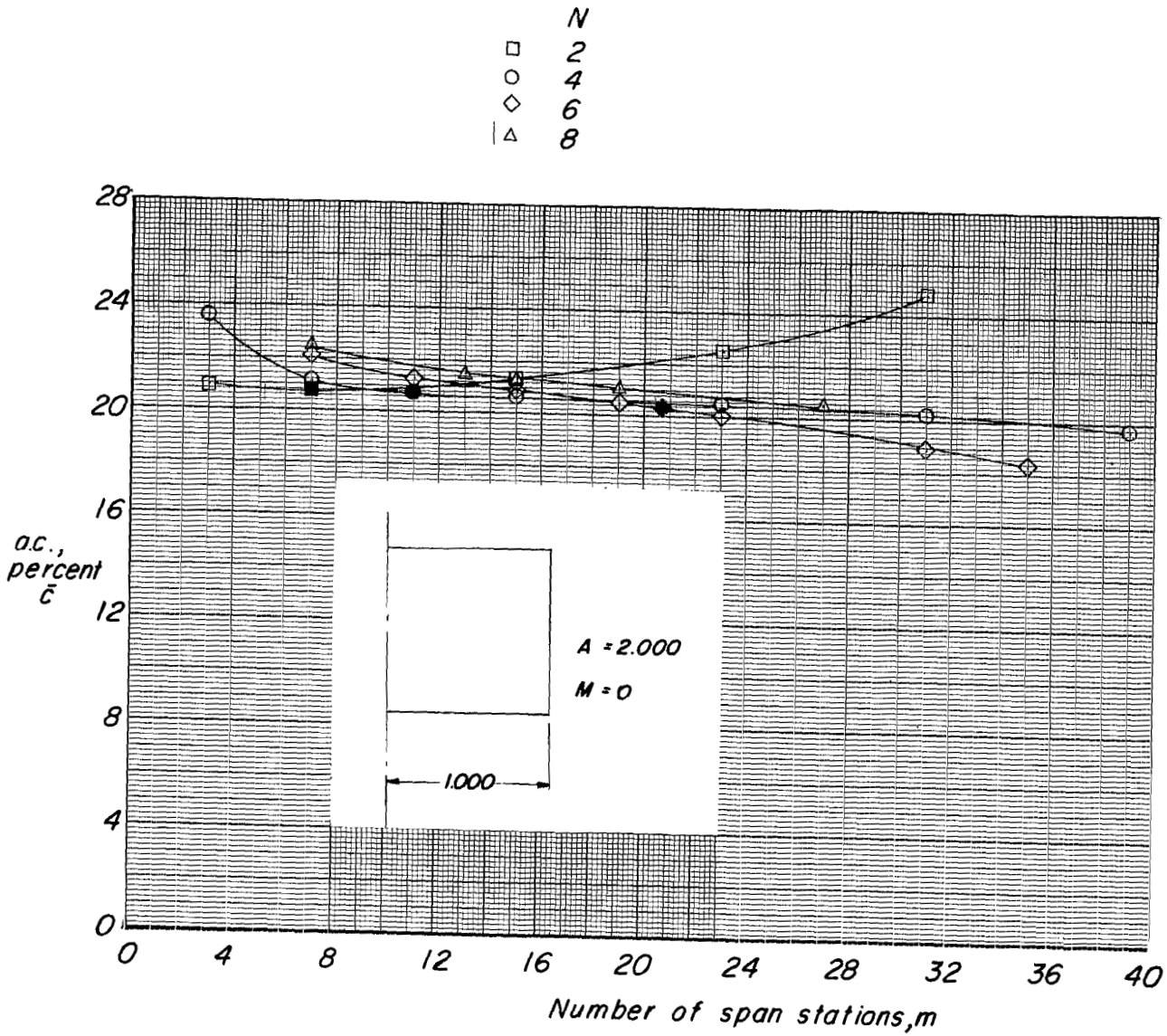

(b) Aerodynamic center.

Figure 4.- Continued.

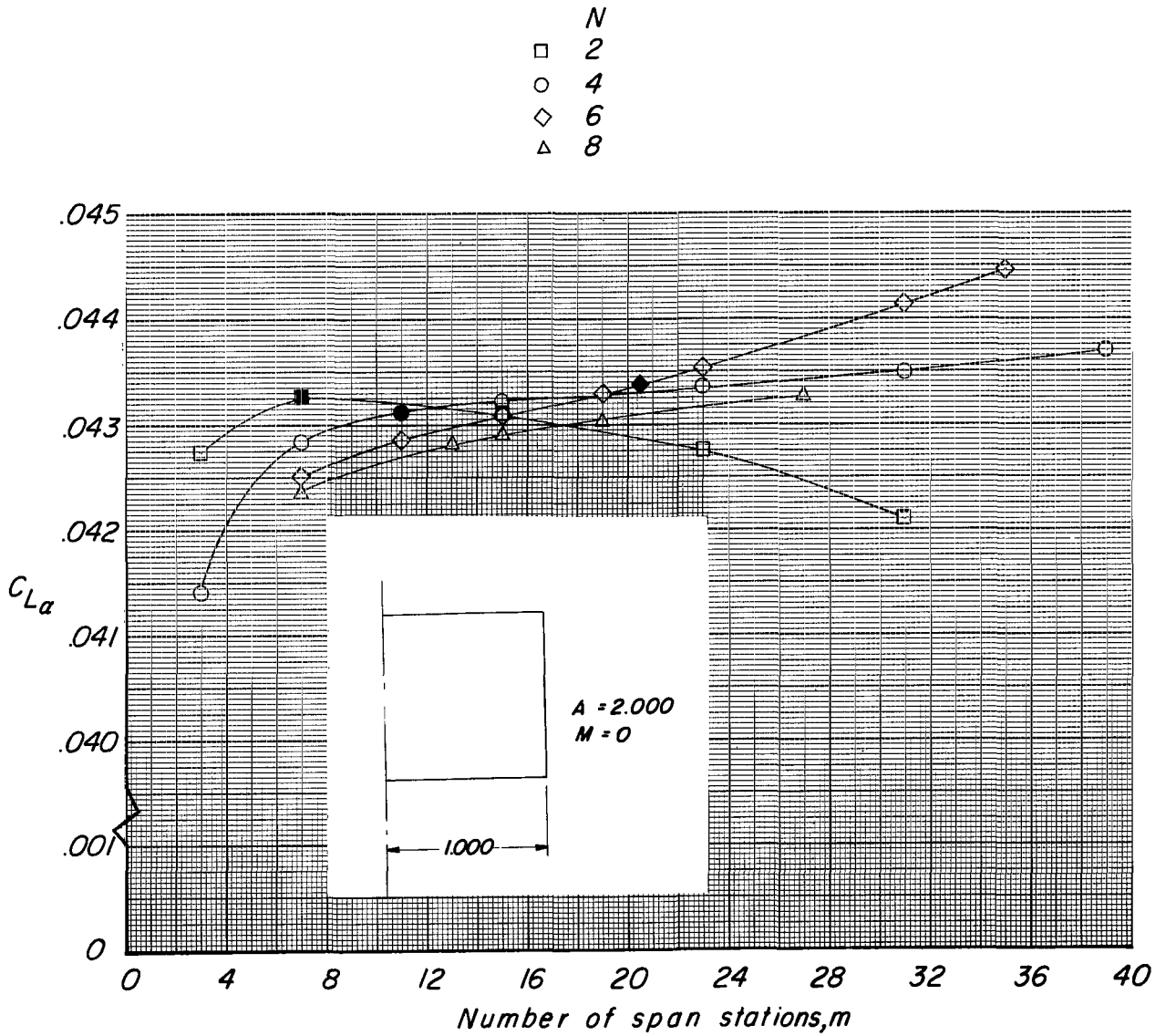

(c) C_{L_α}.

Figure 4.- Concluded.

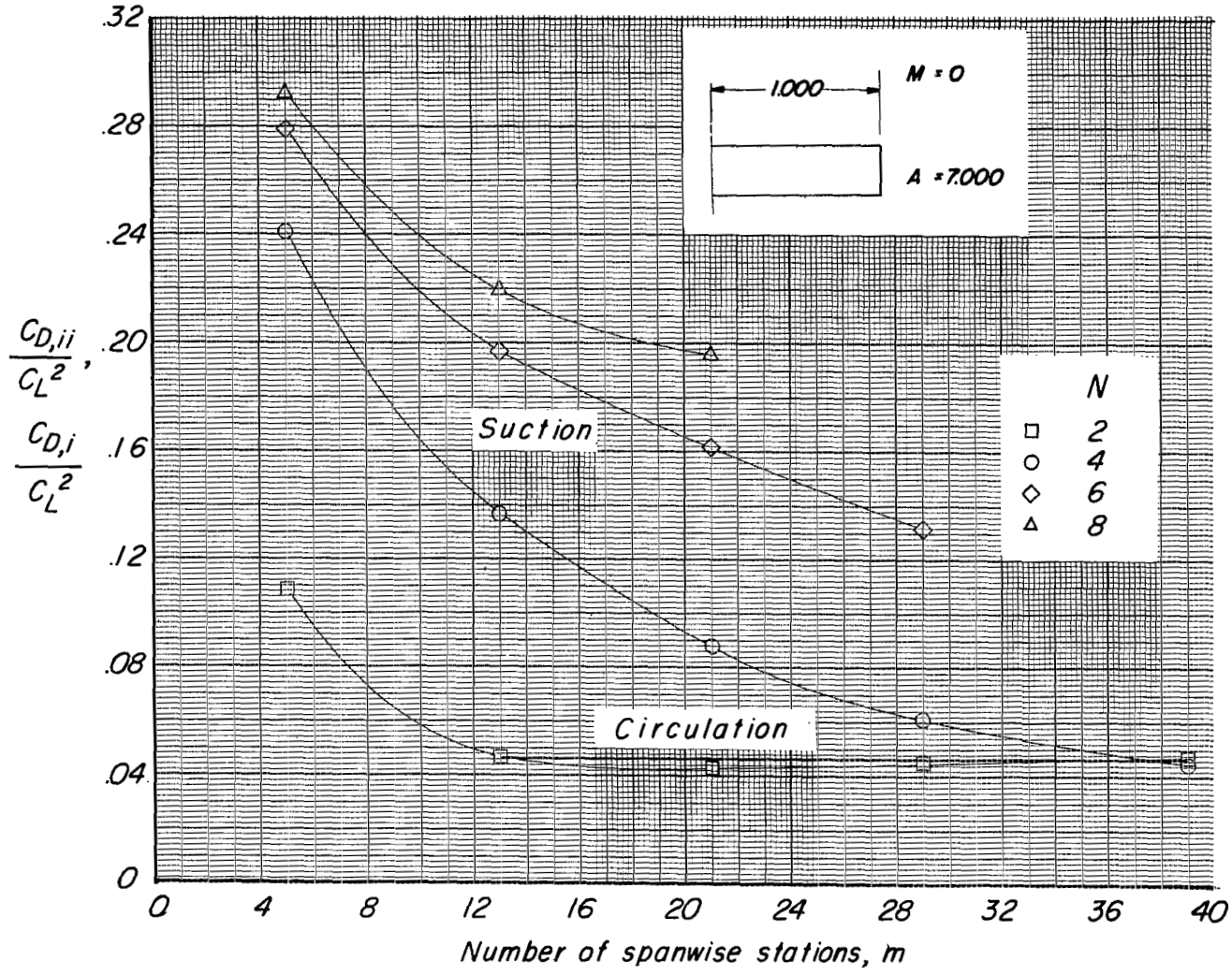

(a) Induced drag parameter.

Figure 5.- Effect of varying number and locations of control points and chordal loading functions on aerodynamic characteristics of A = 7 rectangular planform at M = 0.

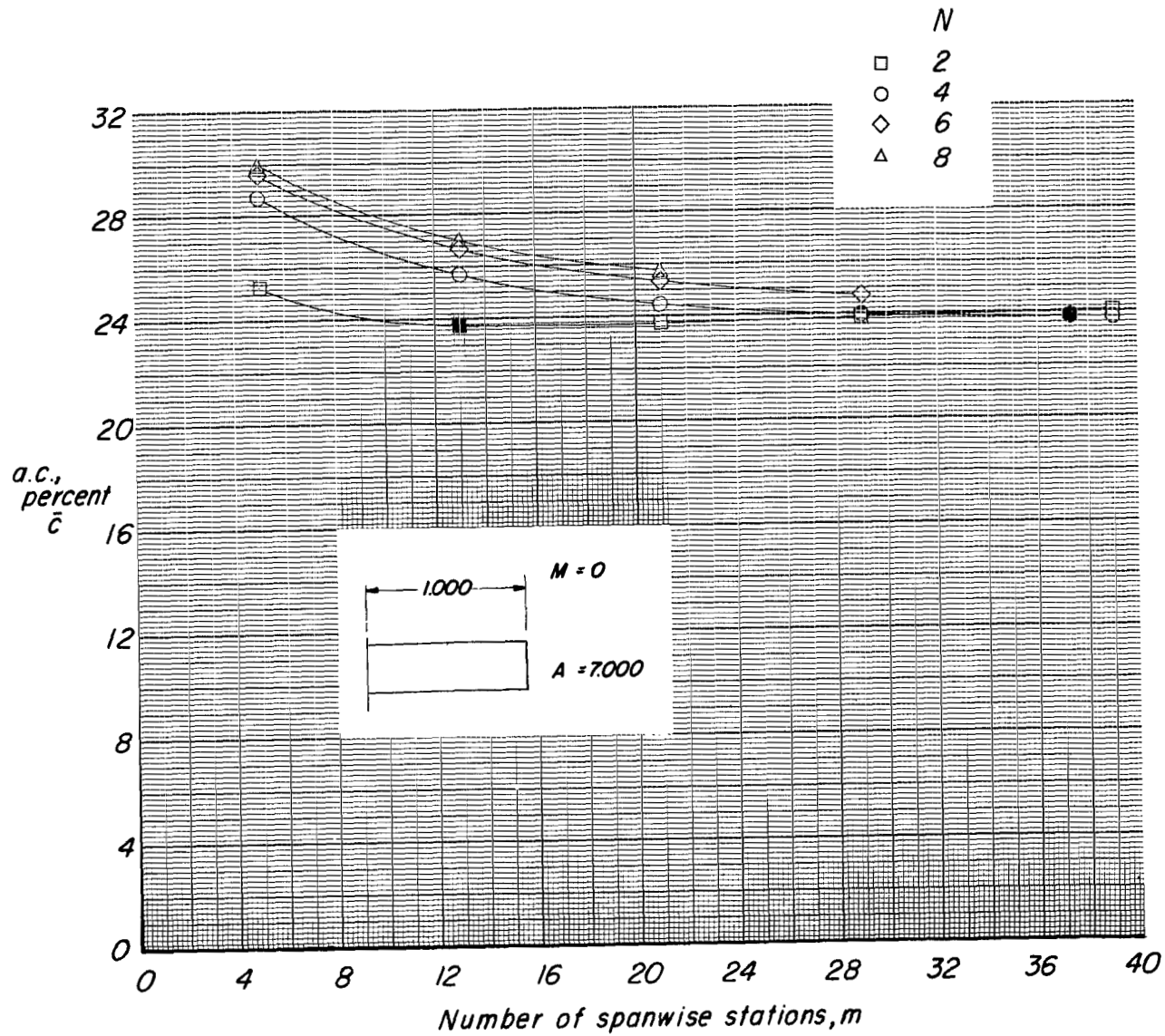

(b) Aerodynamic center.

Figure 5.- Continued.

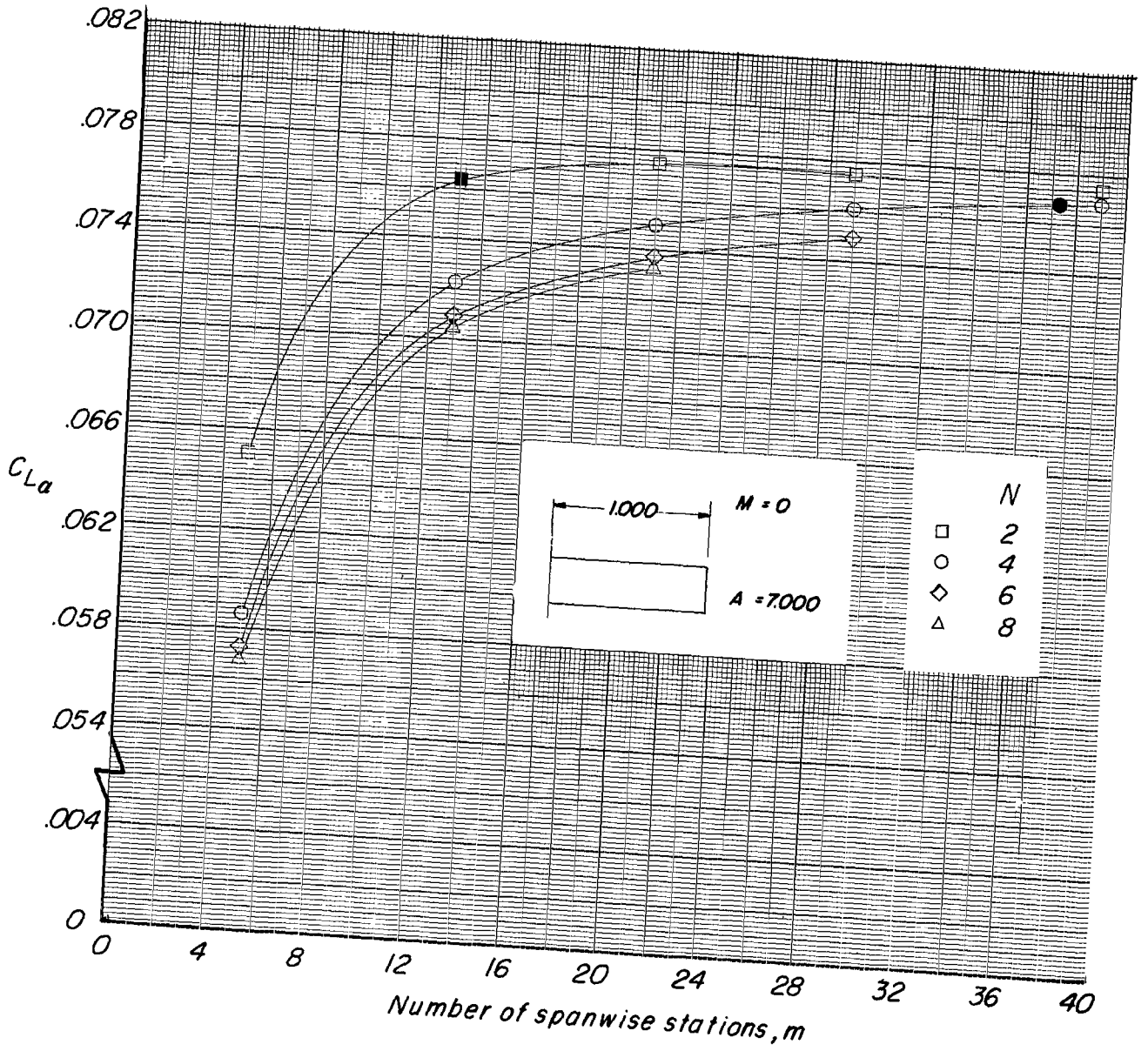

(c) C_{L_α}.

Figure 5.- Concluded.

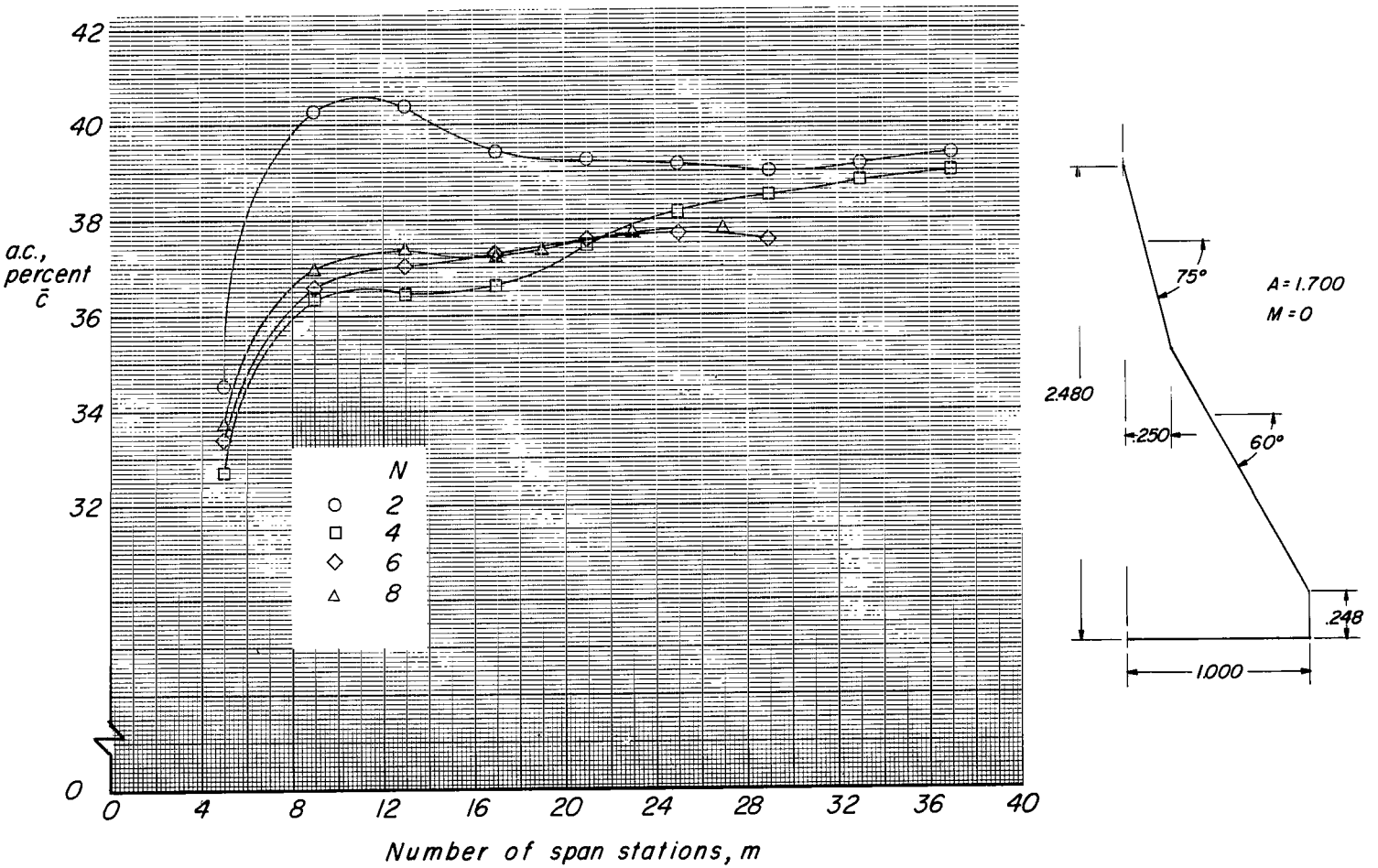

(a) Aerodynamic center.

Figure 6.- Effect of varying number and locations of control points and chordal loading functions on aerodynamic characteristics of A = 1.7 double-delta planform at M = 0.

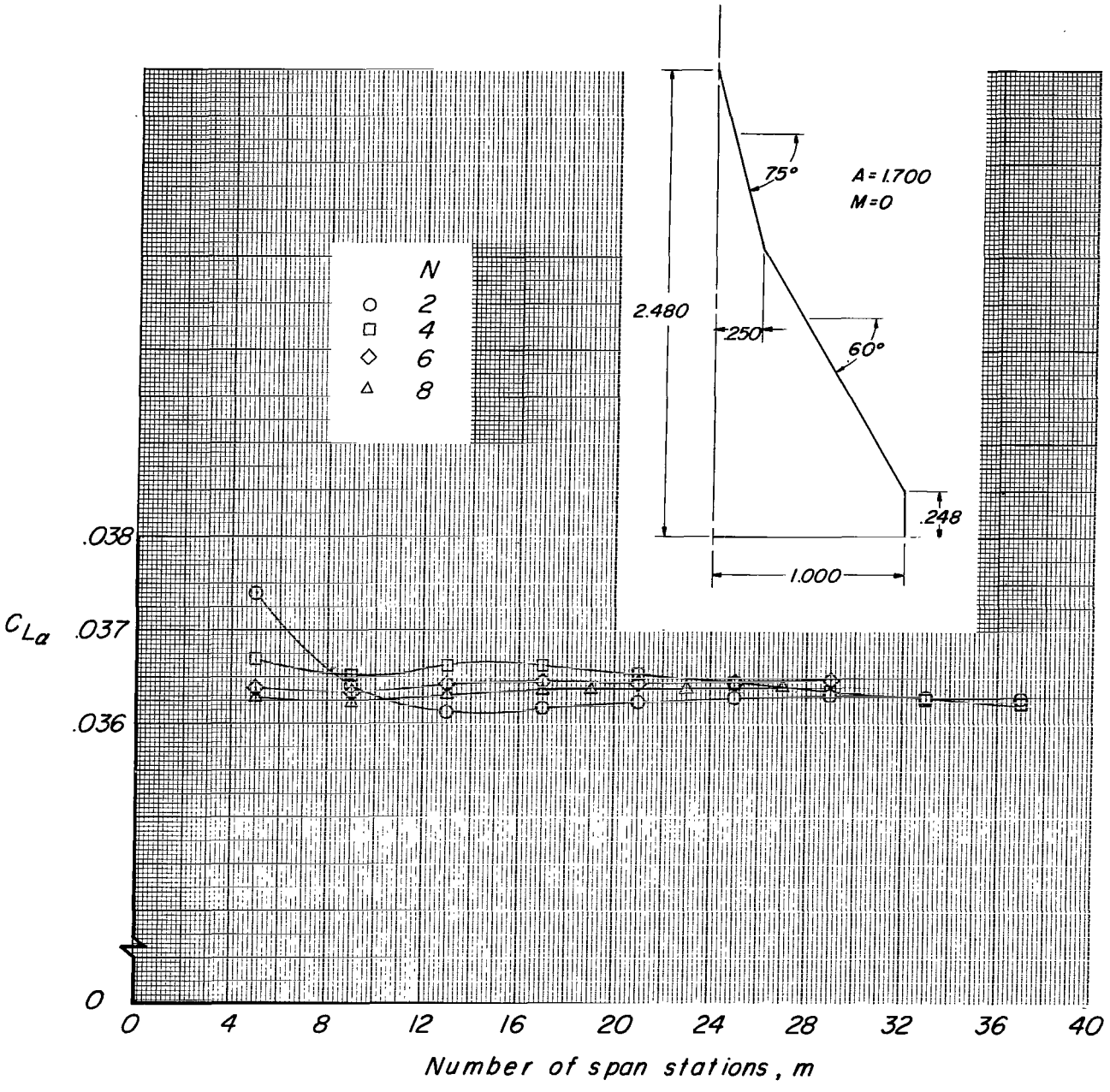

(b) C_{L_α}.

Figure 6.- Concluded.

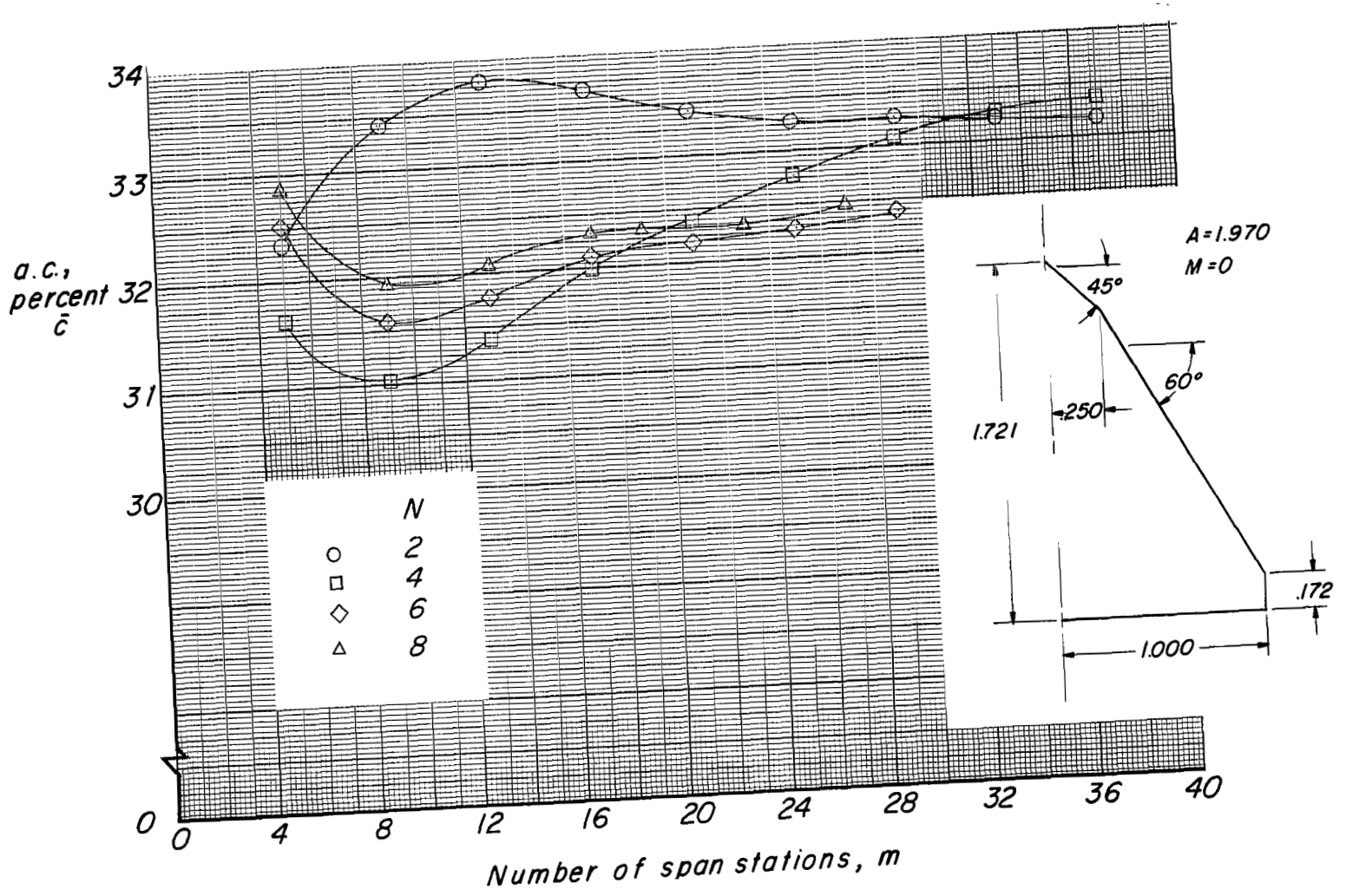

(a) Aerodynamic center.

Figure 7.- Effect of varying number and locations of control points and chordal loading functions on aerodynamic characteristics of A = 1.97 double-delta planform at M = 0.

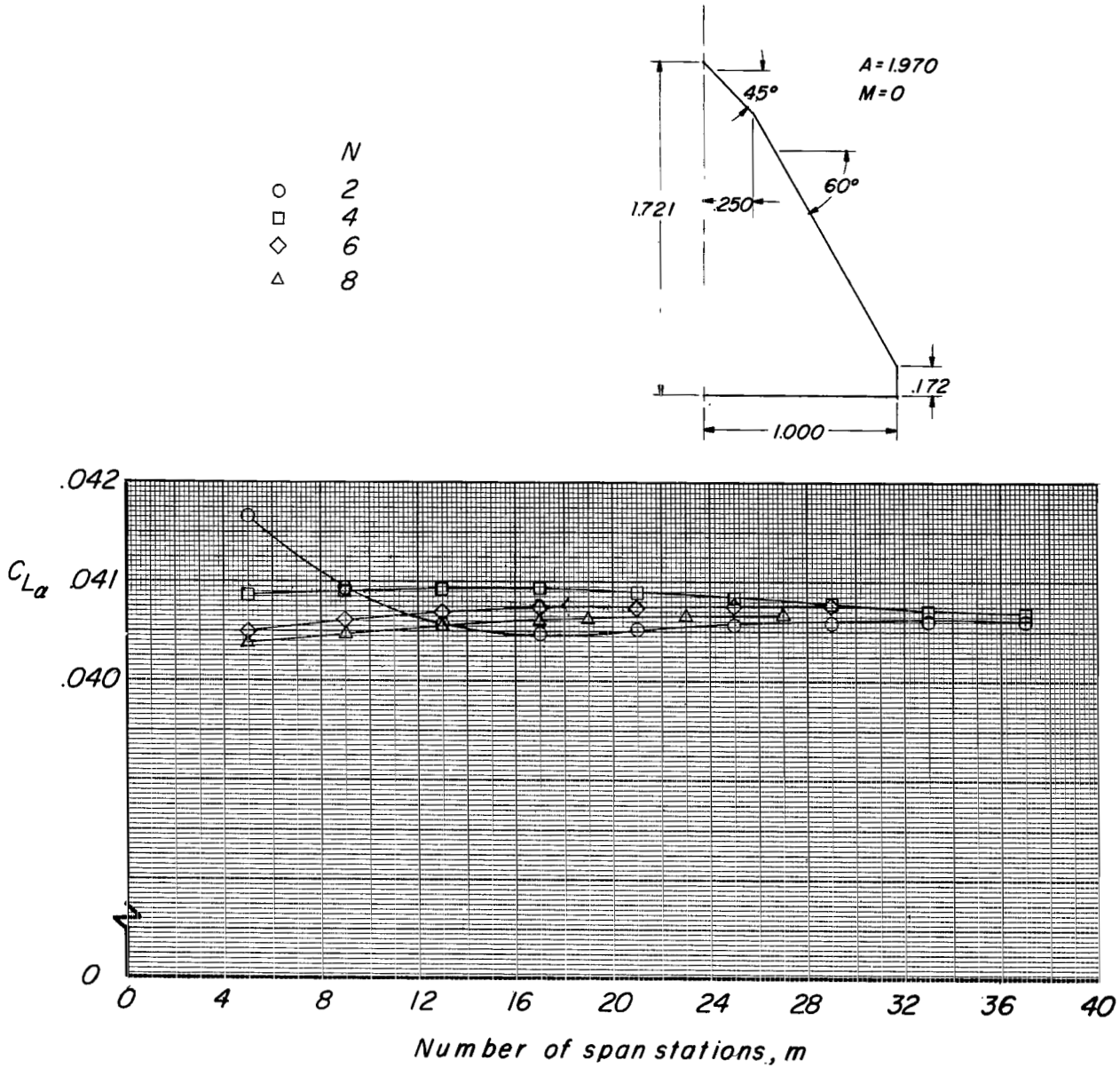

(b) C_{L_α}.

Figure 7.- Concluded.

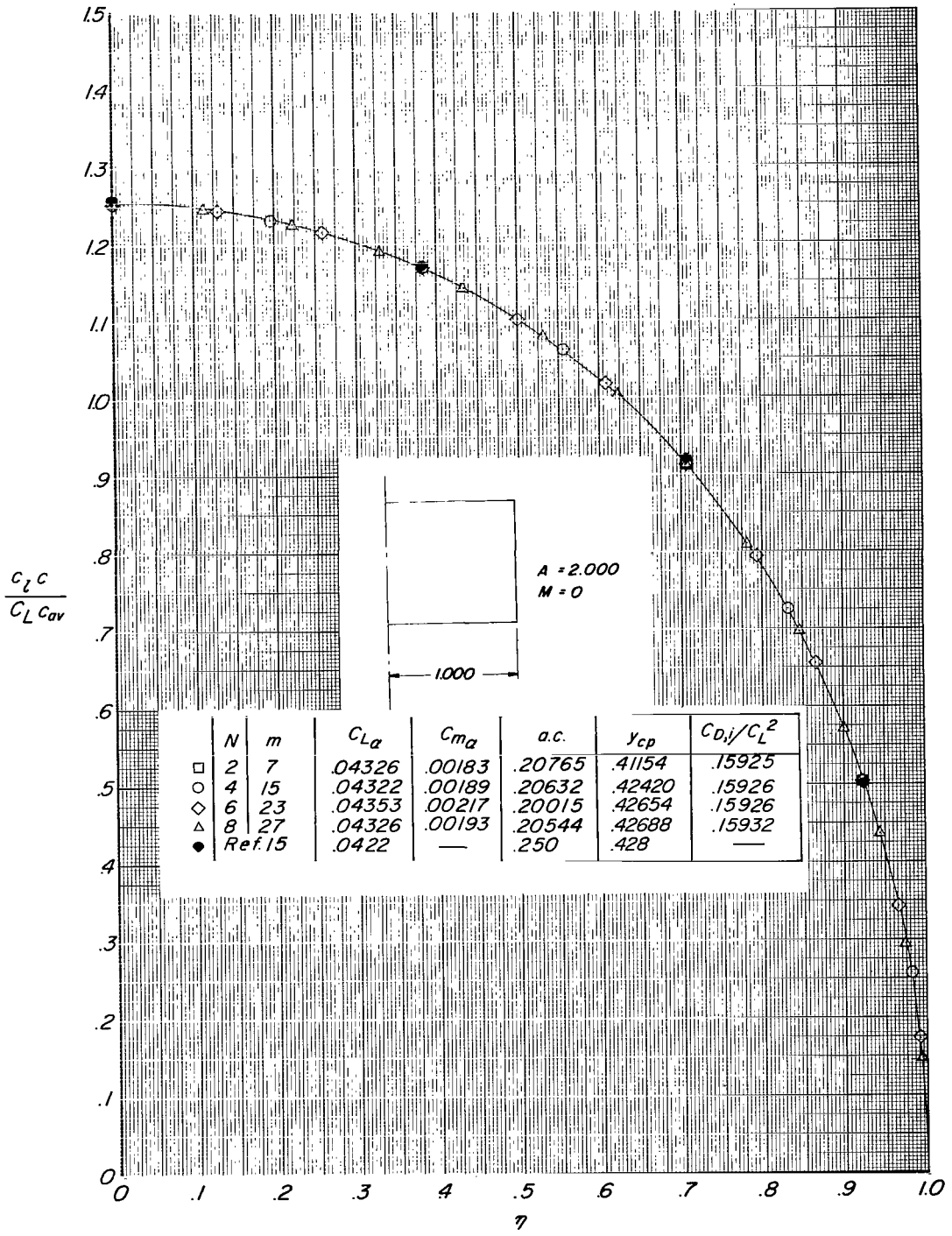

(a) Ratio of m to N is approximately constant.

Figure 8.- Span loading coefficient variation with different combinations of N and m for A = 2 rectangular planform at M = 0.

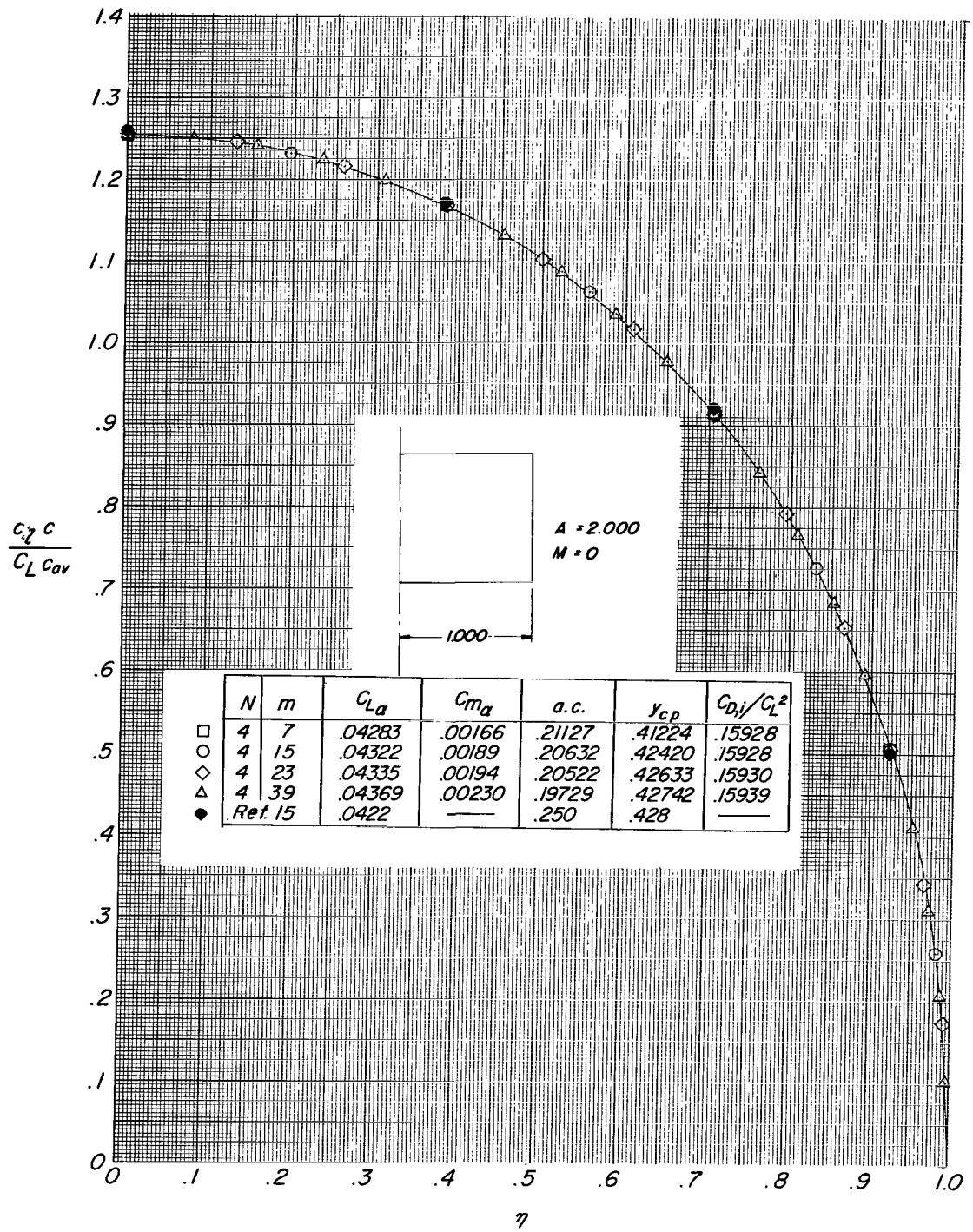

(b) Constant N.

Figure 8.- Continued.

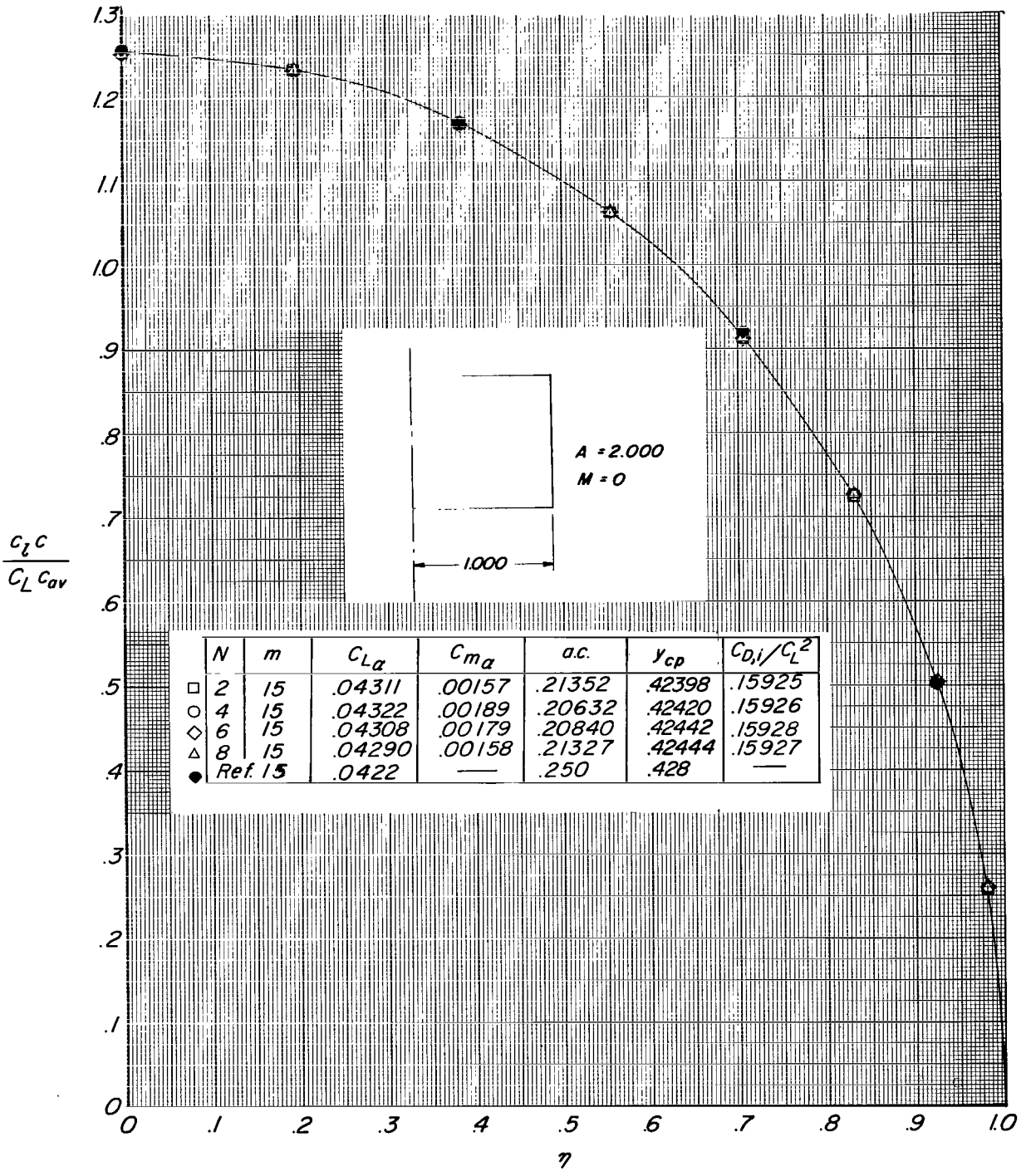

	N	m	C_{L_α}	C_{m_α}	a.c.	y_{cp}	$C_{D,i}/C_L^2$
□	2	15	.04311	.00157	.21352	.42398	.15925
○	4	15	.04322	.00189	.20632	.42420	.15926
◇	6	15	.04308	.00179	.20840	.42442	.15928
△	8	15	.04290	.00158	.21327	.42444	.15927
●	Ref. 15		.0422	—	.250	.428	—

(c) Constant m.

Figure 8.- Concluded.

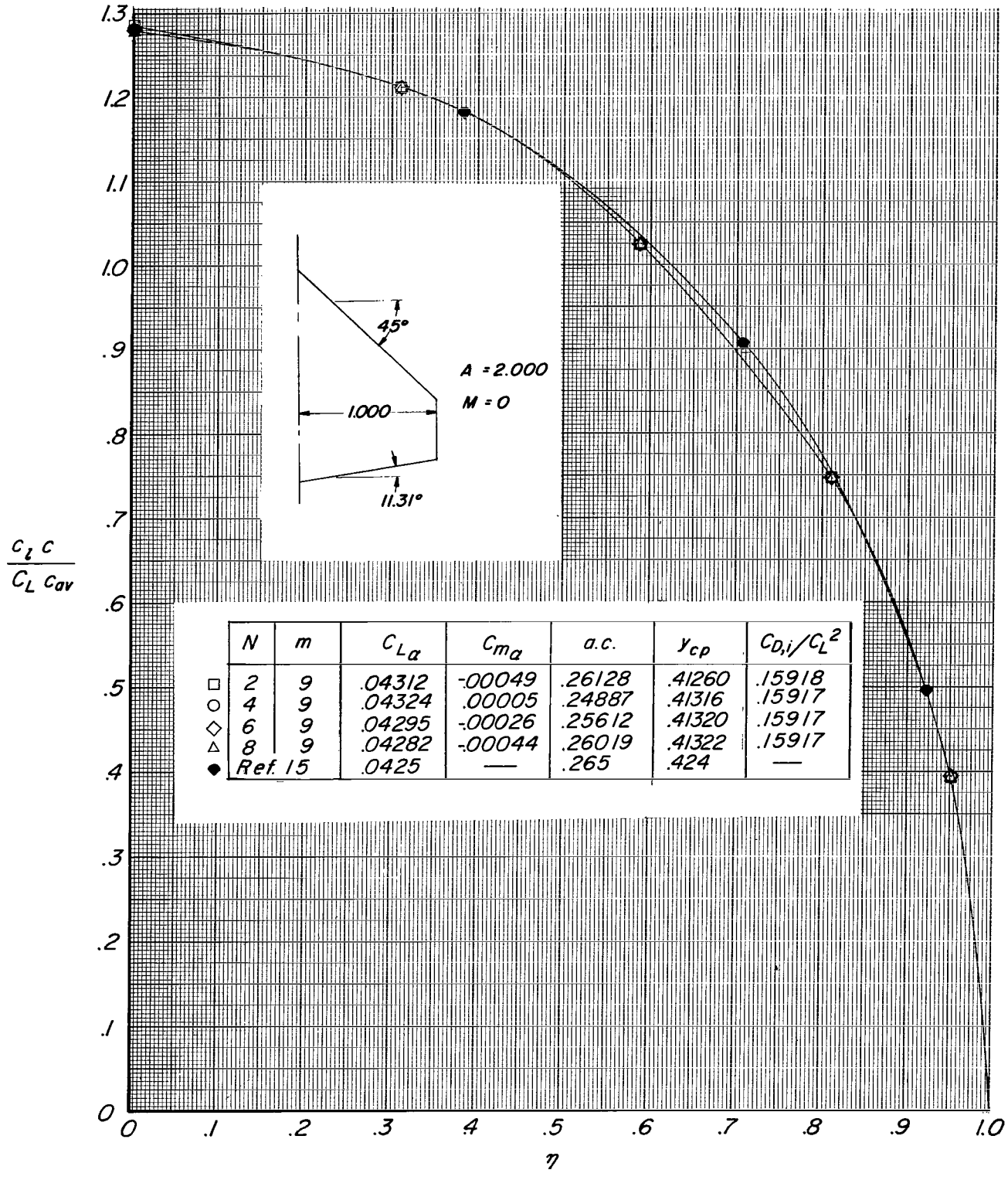

	N	m	C_{L_α}	C_{m_α}	a.c.	y_{cp}	$C_{D,i}/C_L^2$
□	2	9	.04312	-.00049	.26128	.41260	.15918
○	4	9	.04324	.00005	.24887	.41316	.15917
◇	6	9	.04295	-.00026	.25612	.41320	.15917
△	8	9	.04282	-.00044	.26019	.41322	.15917
●	Ref. 15		.0425	—	.265	.424	—

Figure 9.- Span loading coefficient variation with different values of N for A = 2 sweptback and tapered planform at M = 0 when m = 9.

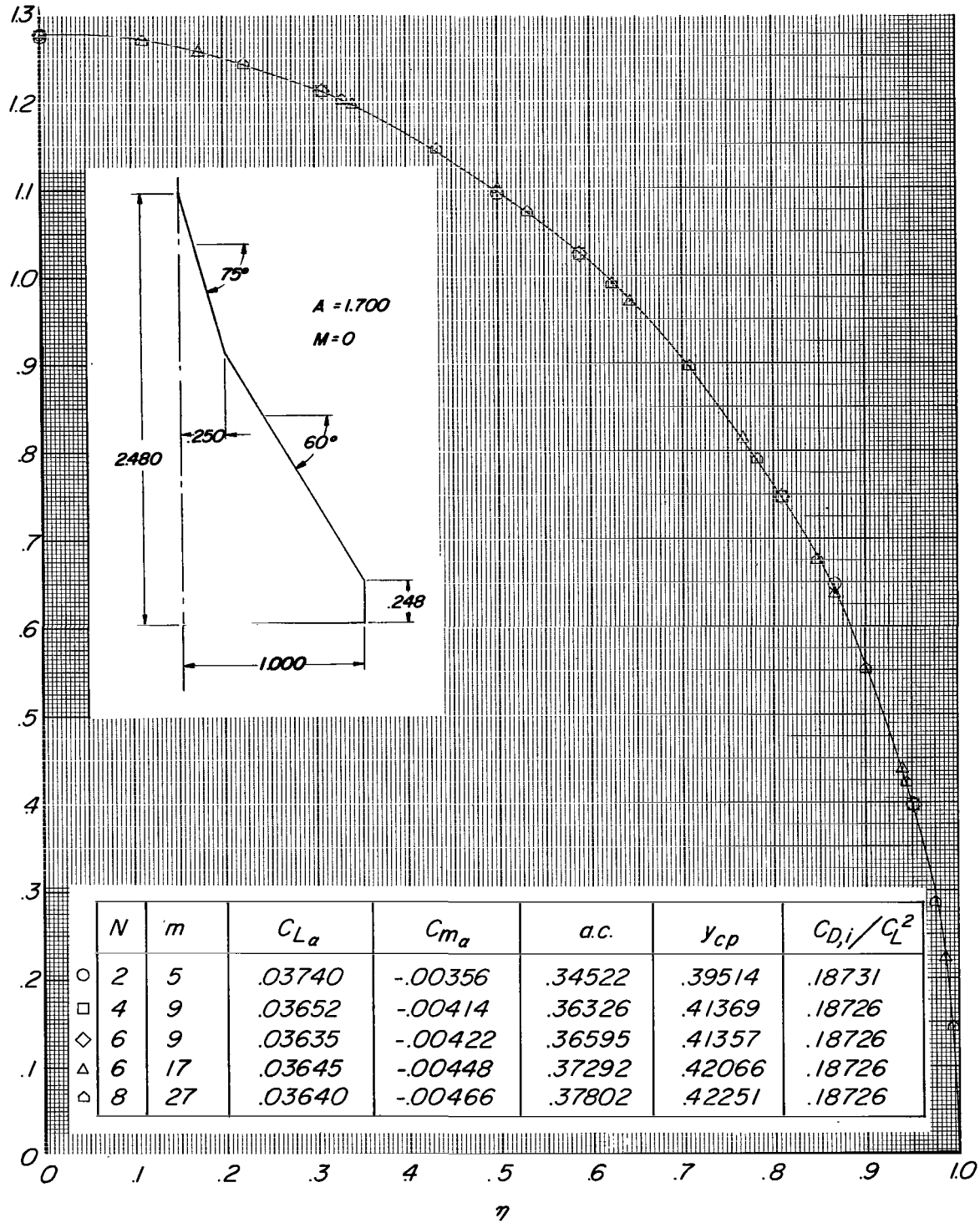

	N	m	C_{L_α}	C_{m_α}	a.c.	y_{cp}	$C_{D,i}/C_L^2$
○	2	5	.03740	-.00356	.34522	.39514	.18731
□	4	9	.03652	-.00414	.36326	.41369	.18726
◇	6	9	.03635	-.00422	.36595	.41357	.18726
△	6	17	.03645	-.00448	.37292	.42066	.18726
⌓	8	27	.03640	-.00466	.37802	.42251	.18726

Figure 10.- Span loading coefficient variation with different combinations of N and m for A = 1.7 double-delta planform at M = 0.

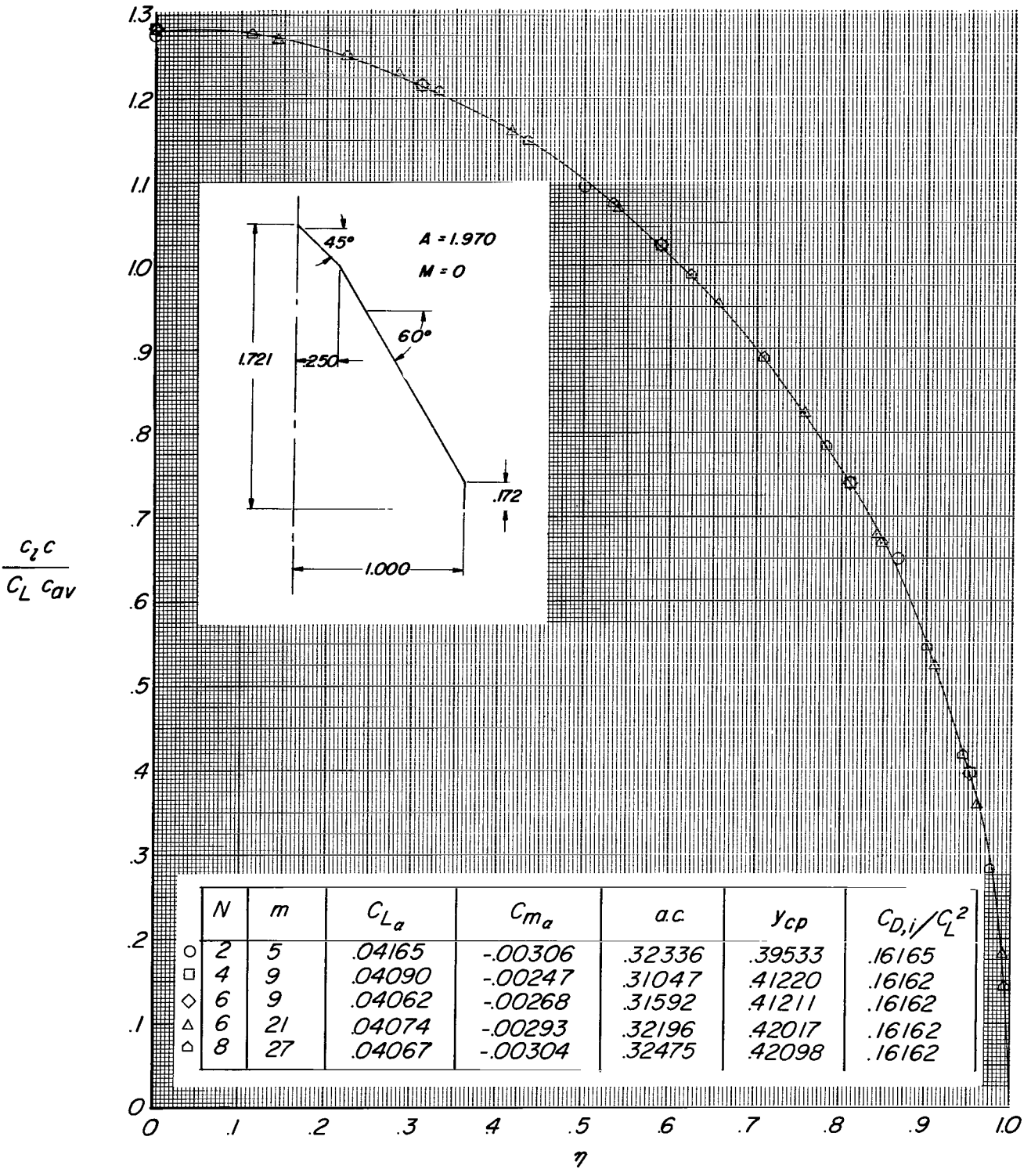

	N	m	C_{L_a}	C_{m_a}	a.c.	y_{cp}	$C_{D,i}/C_L^2$
○	2	5	.04165	-.00306	.32336	.39533	.16165
□	4	9	.04090	-.00247	.31047	.41220	.16162
◇	6	9	.04062	-.00268	.31592	.41211	.16162
△	6	21	.04074	-.00293	.32196	.42017	.16162
⌂	8	27	.04067	-.00304	.32475	.42098	.16162

Figure 11.- Span loading coefficient variation with different combinations of N and m for A = 1.97 double-delta planform at M = 0.

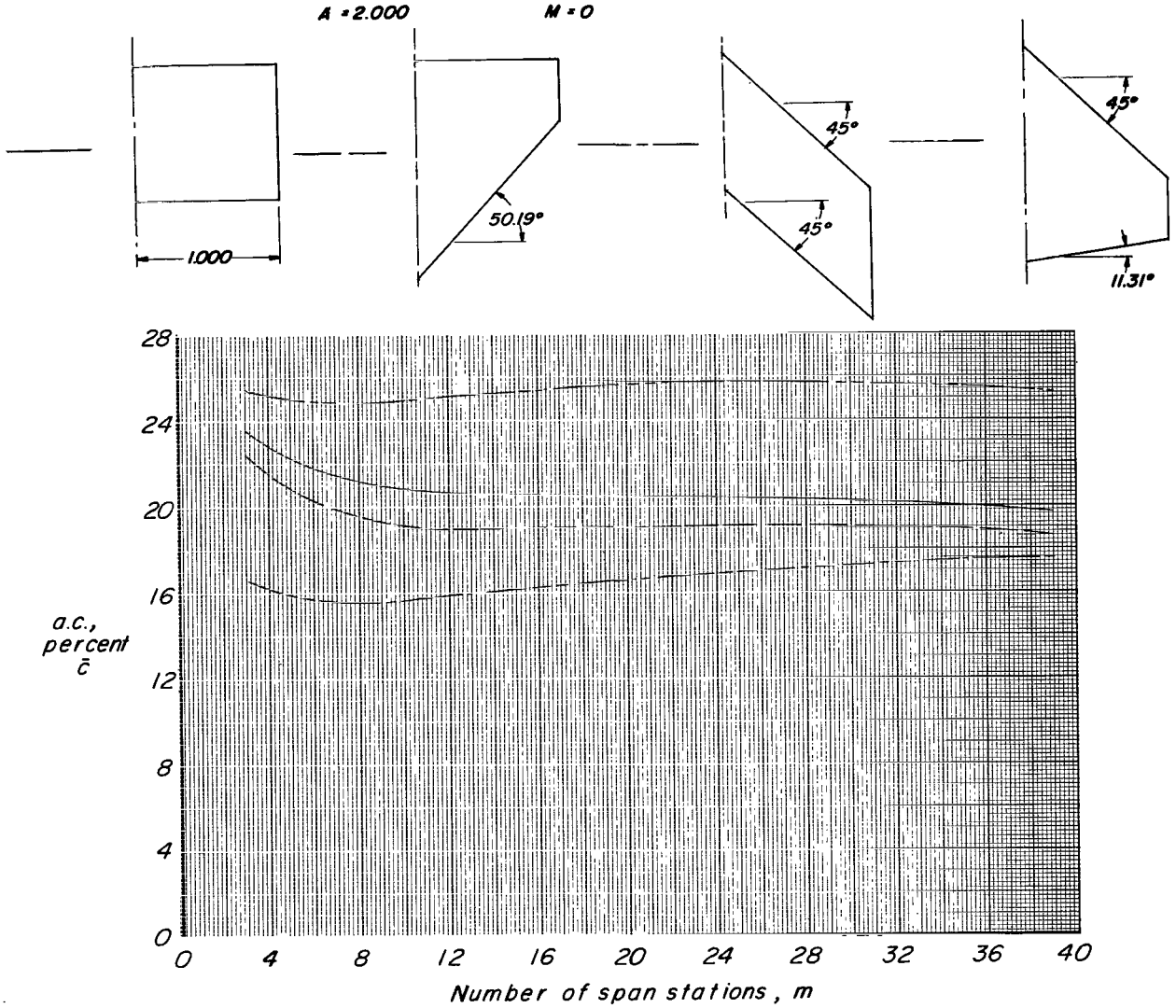

(a) Aerodynamic center.

Figure 12.- Effect of varying number and locations of control points on aerodynamic characteristics for four A = 2 planforms at M = 0 when N = 4.

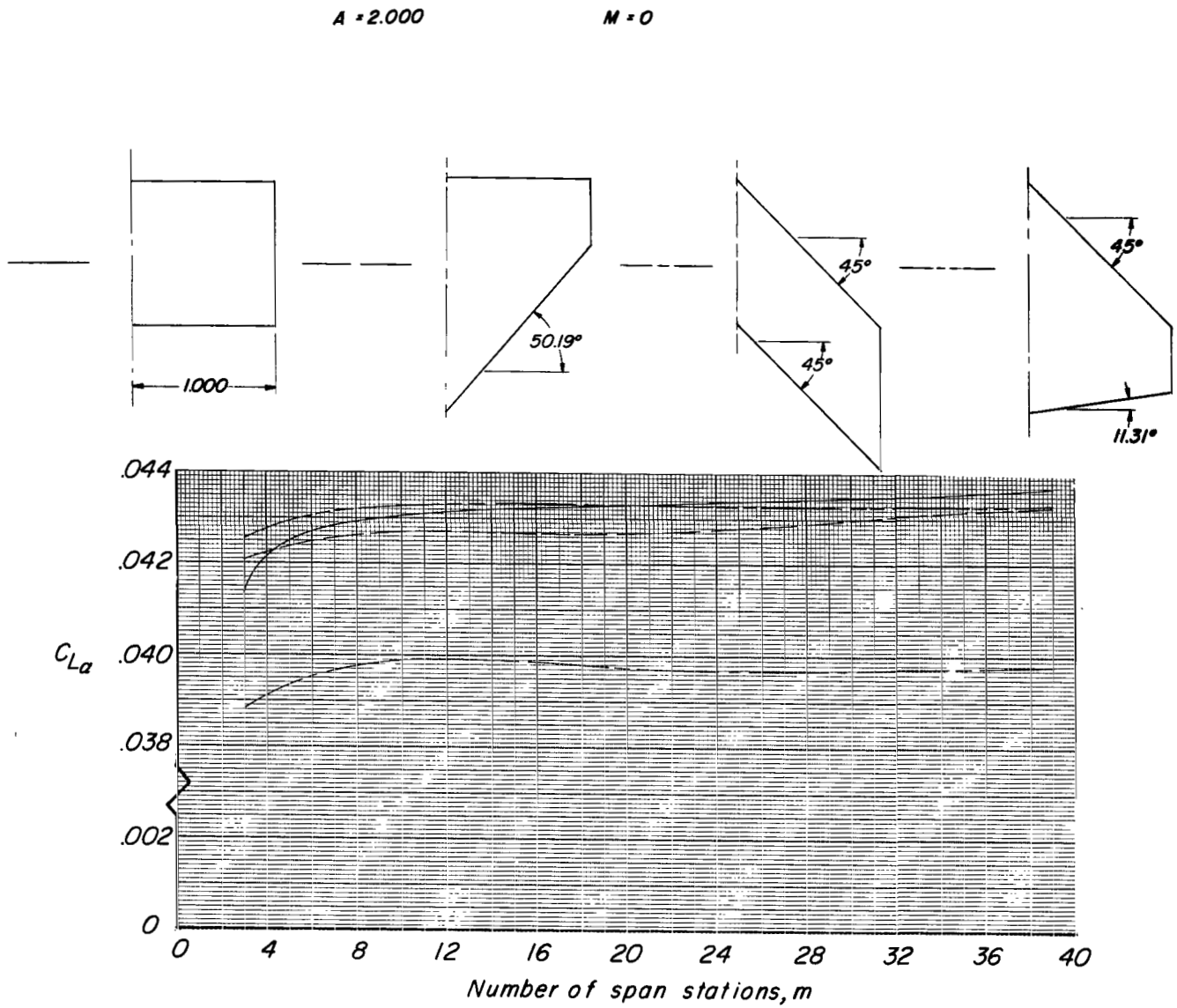

(b) C_{L_α}.

Figure 12.- Concluded.

Method	C_{L_α}	a.c.	y_{cp}
——— N = 4, m = 31	.0615	.252	.460
— — — Ref. 17	.0613	.263	.463
— — — — Ref. 15	.0583	.284	.469

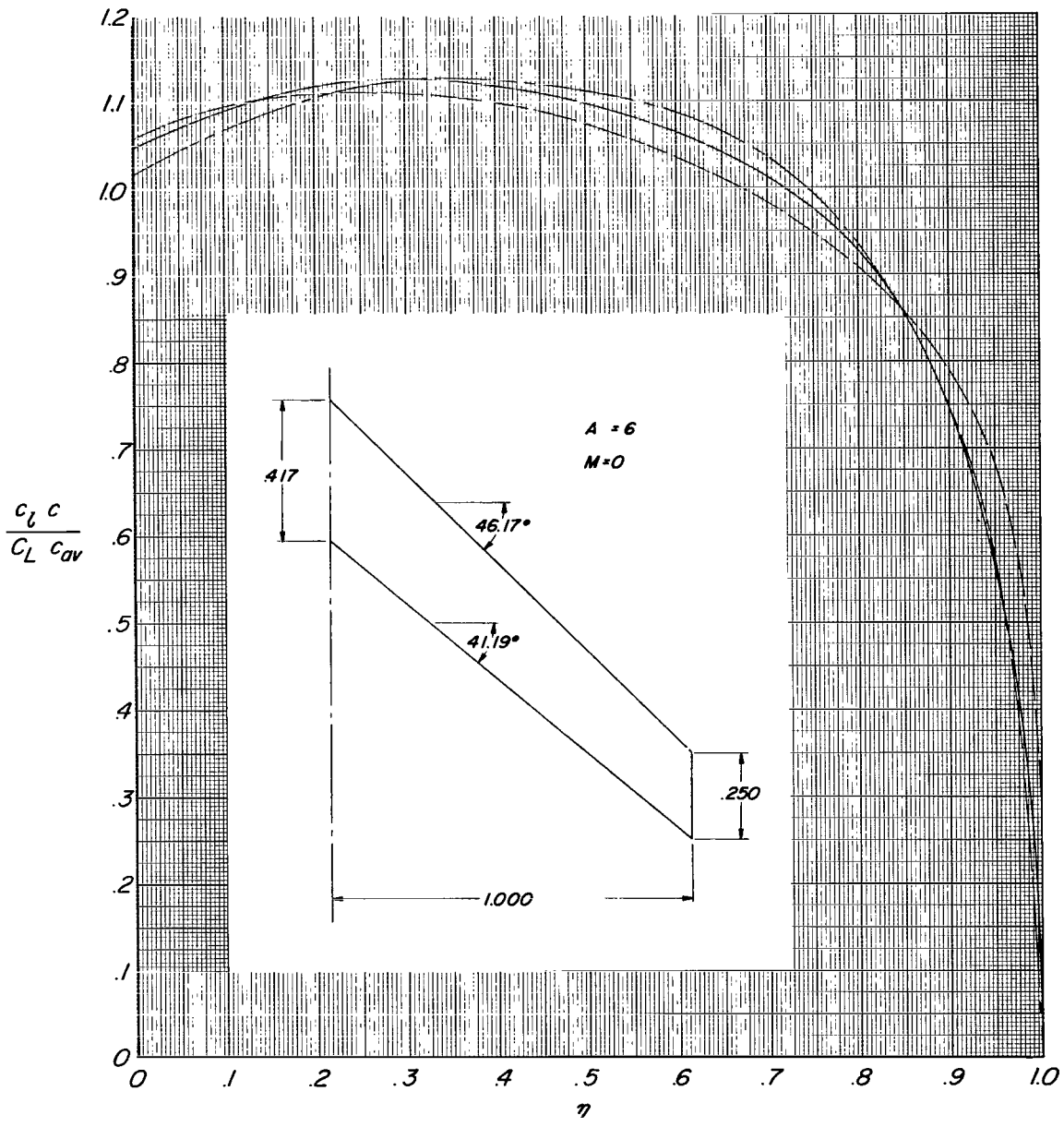

Figure 13.- Span loading distributions predicted by three different theoretical methods for A = 6 sweptback and tapered planform at M = 0.

Method	C_{L_α}	C_{m_α}	a.c.	y_{cp}	$C_{D,i}/C_L^2$
——— N=2, m=15	.05722	-.00525	.34184	.420	.09270
— — N=2, m=15, ref. 8	.05792	-.00318	.30500	.427	.09259

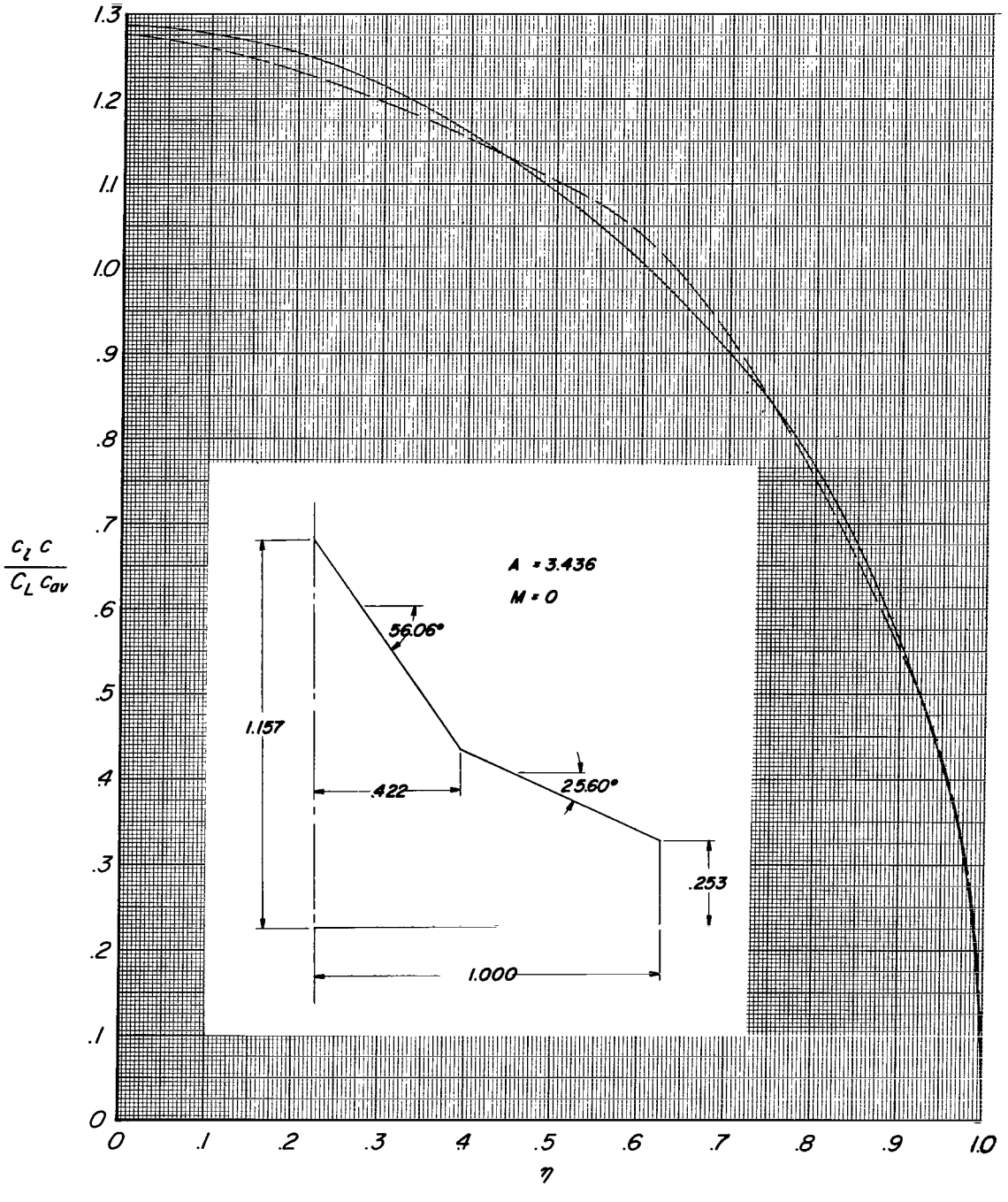

Figure 14.- Span loading distributions predicted by two different theoretical methods for A = 3.436 double-delta planform at M = 0.

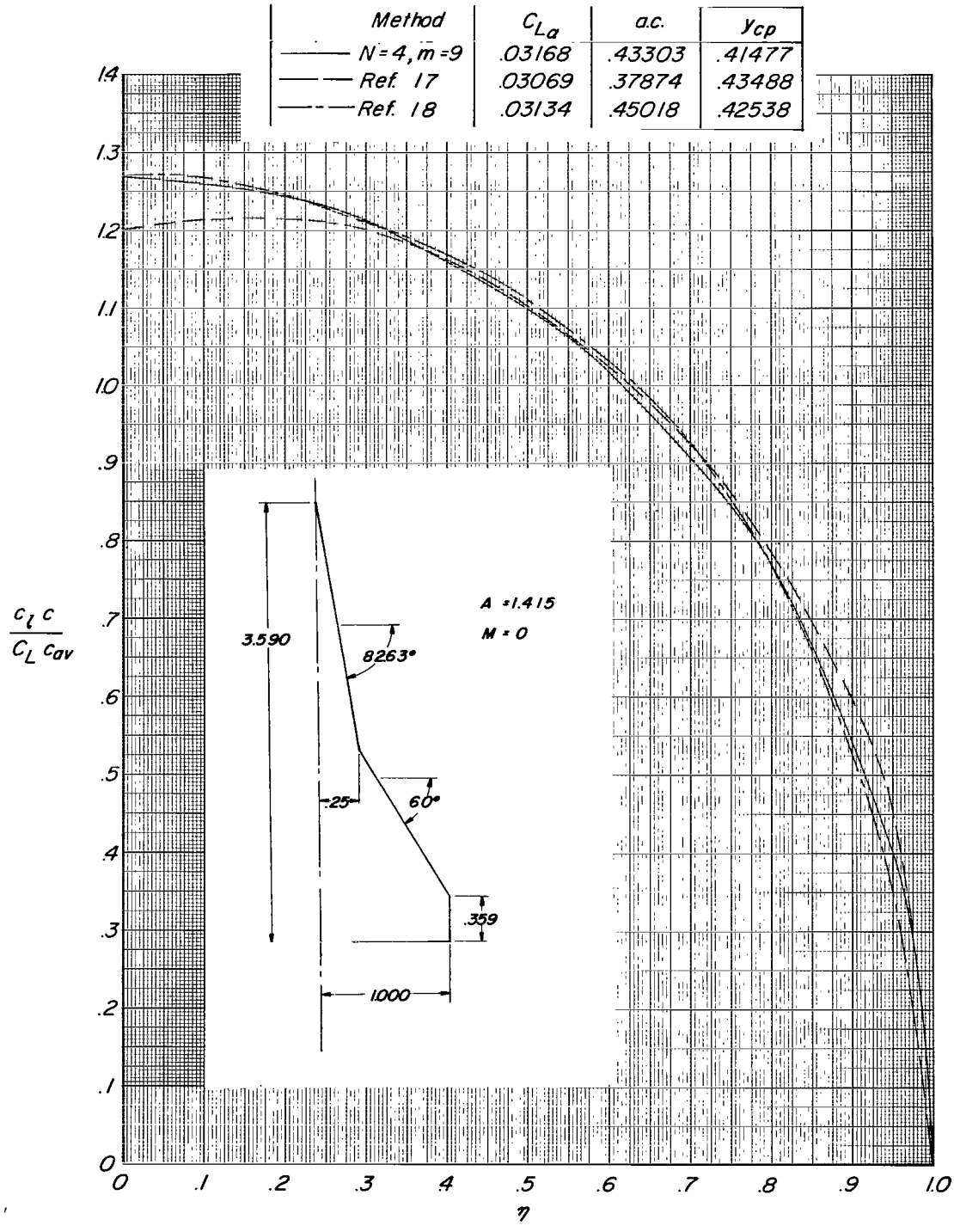

(a) Spanwise.

Figure 15.- Loading distributions predicted by three different theoretical methods for A = 1.415 double-delta planform at M = 0.

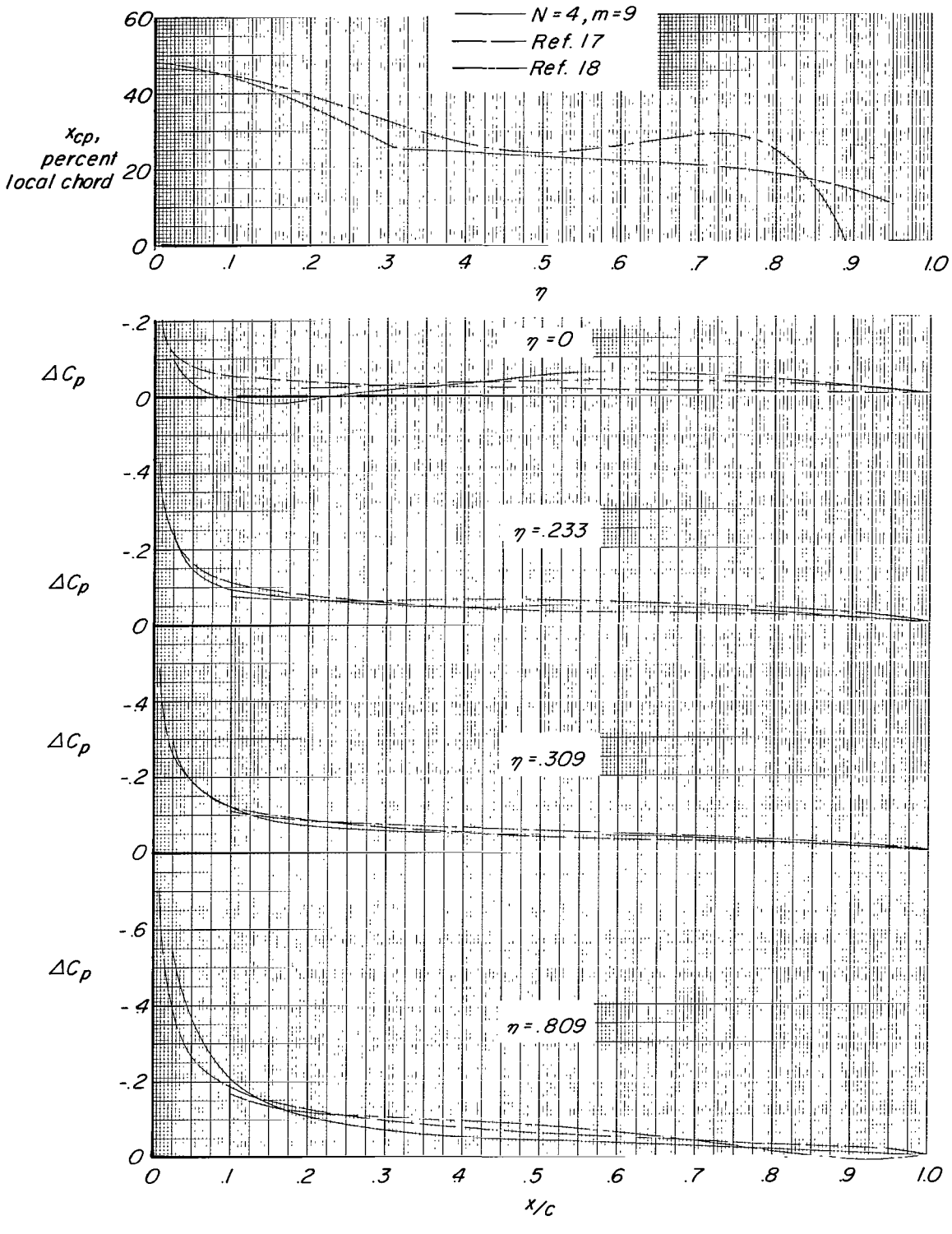

(b) Local spanwise centers of pressure and chordwise load distribution.

Figure 15.- Concluded.

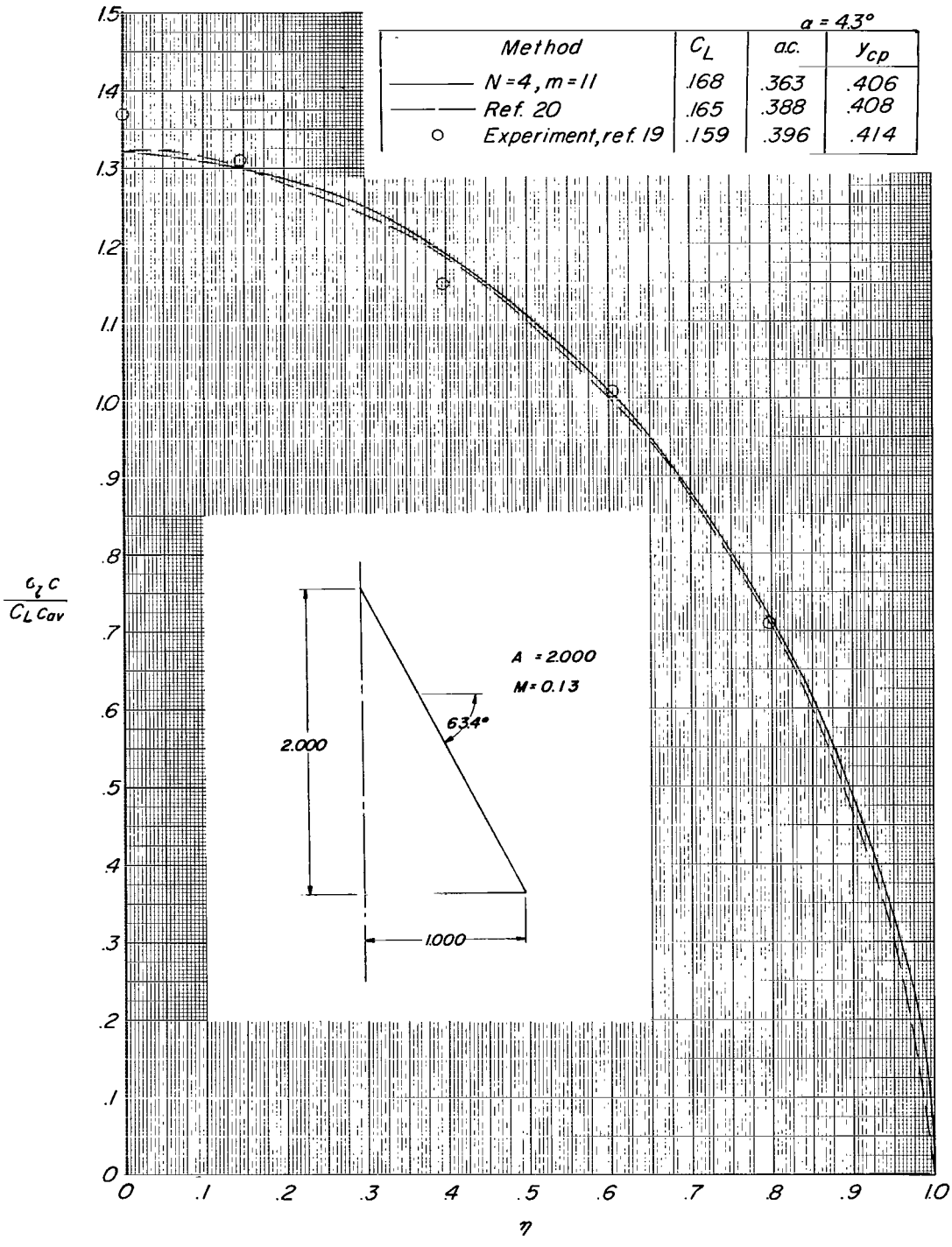

(a) Spanwise.

Figure 16.- Loading distributions predicted by two different theoretical methods and compared with experiment for A = 2 delta planform at M = 0.13.

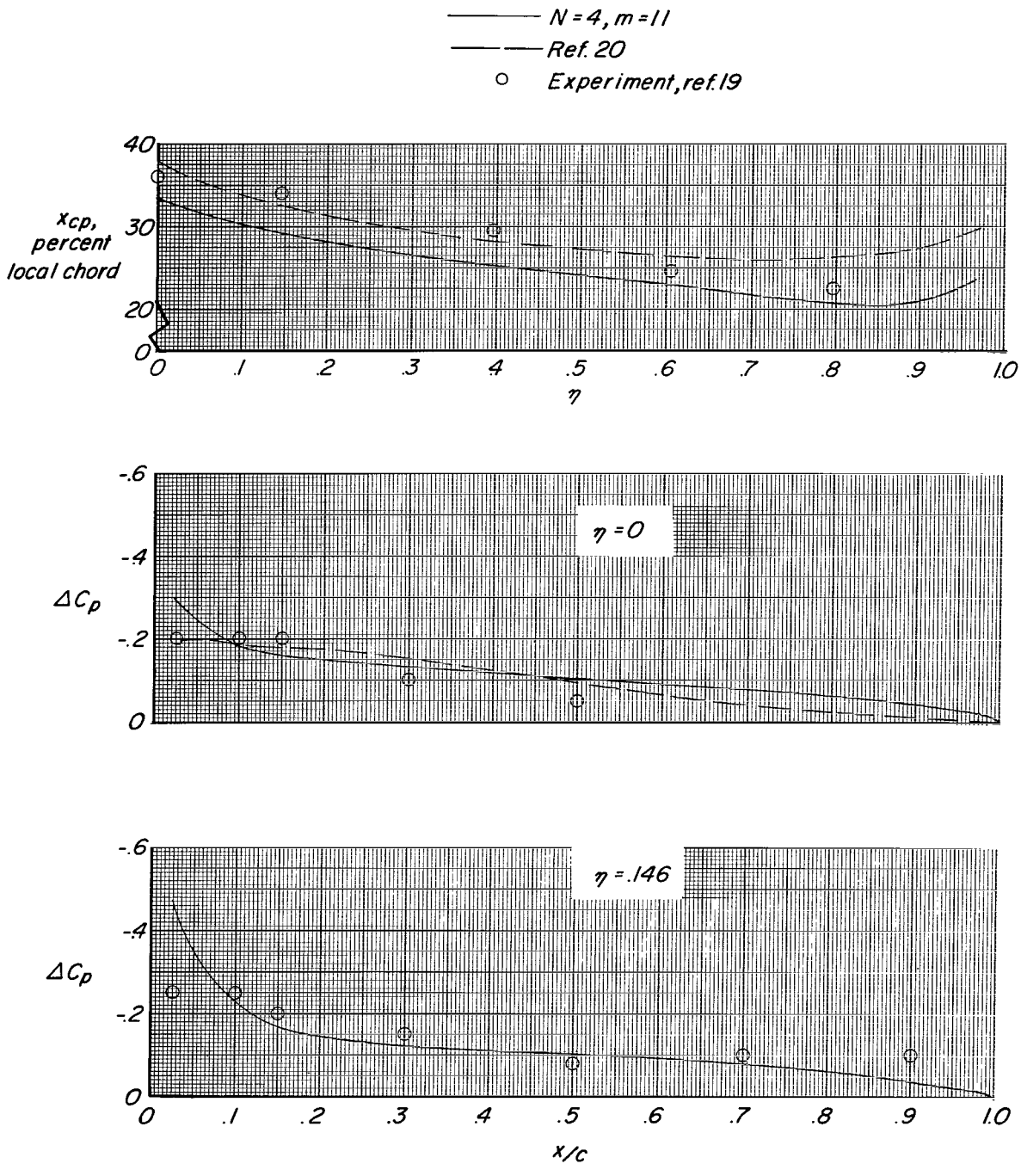

(b) Local spanwise centers of pressure and chordwise load distributions.

Figure 16.- Continued.

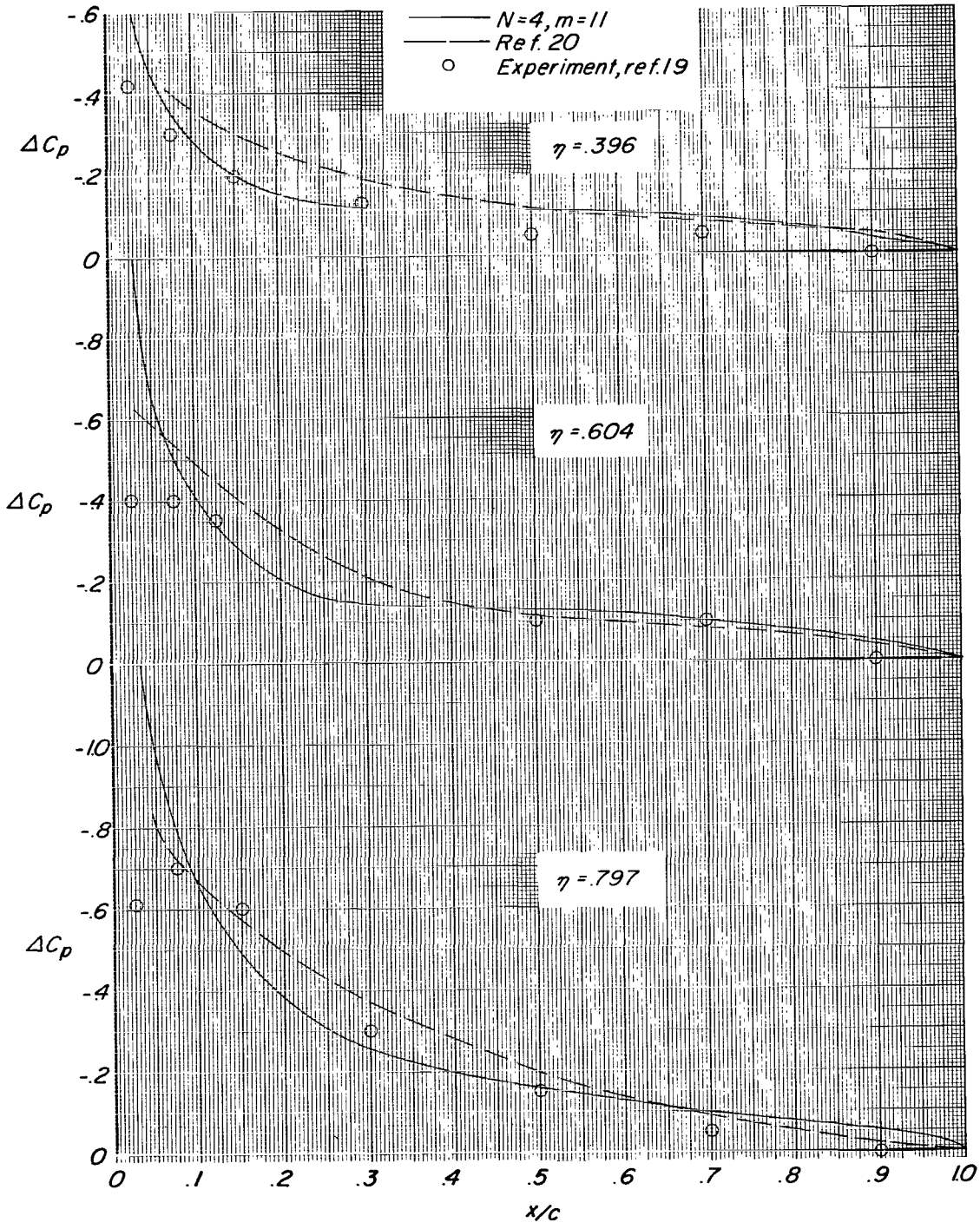

(b) Concluded.

Figure 16.- Concluded.

$\alpha = 4.7°$

Method	C_L	a.c.	y_{cp}
——— N = 4, m = 37	.312	.317	.454
○ Experiment, ref. 21	.315	.328	.455

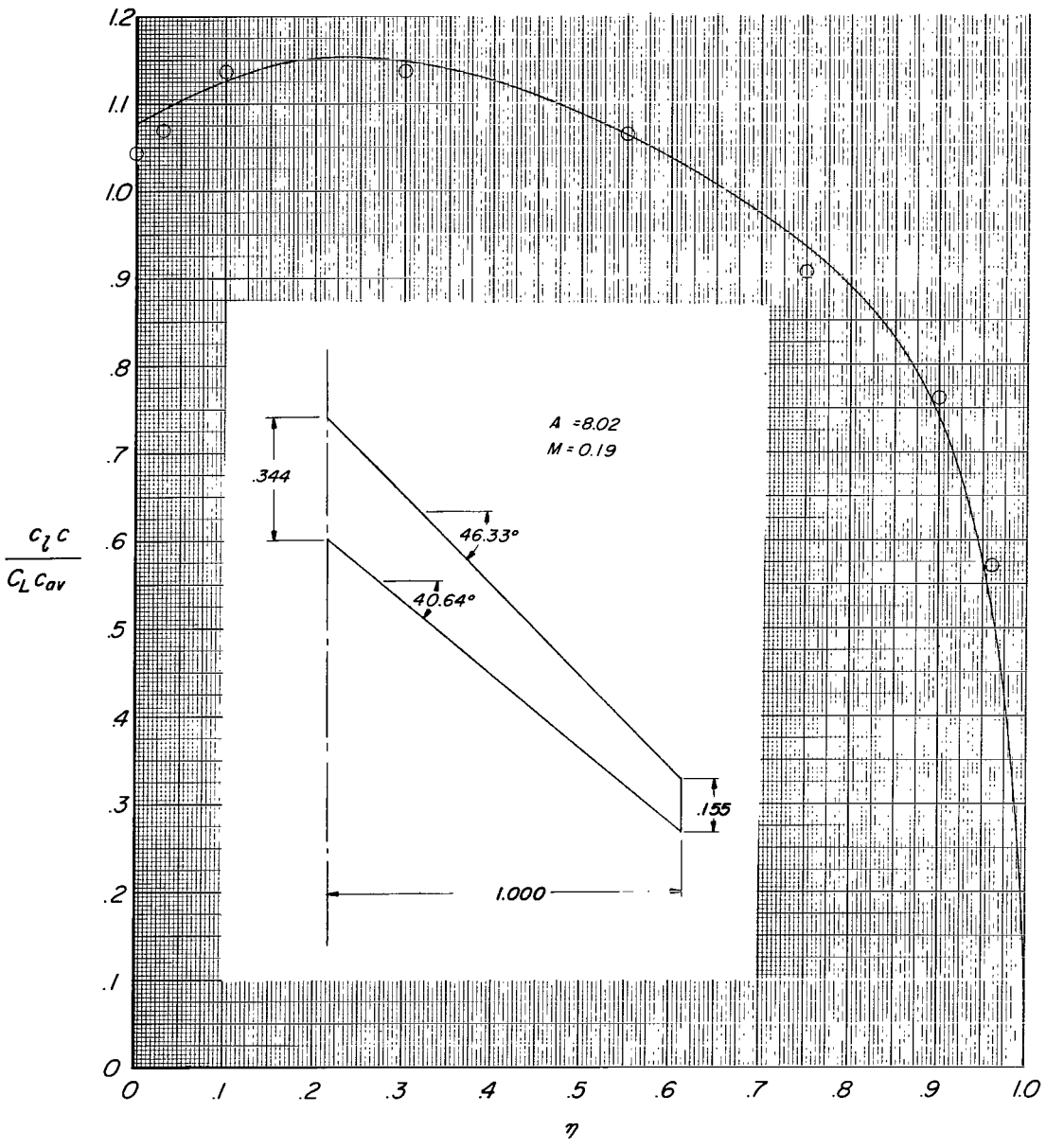

(a) Spanwise.

Figure 17.- Loading distributions predicted by present method and compared with experiment for A = 8.02 sweptback and tapered planform at M = 0.19.

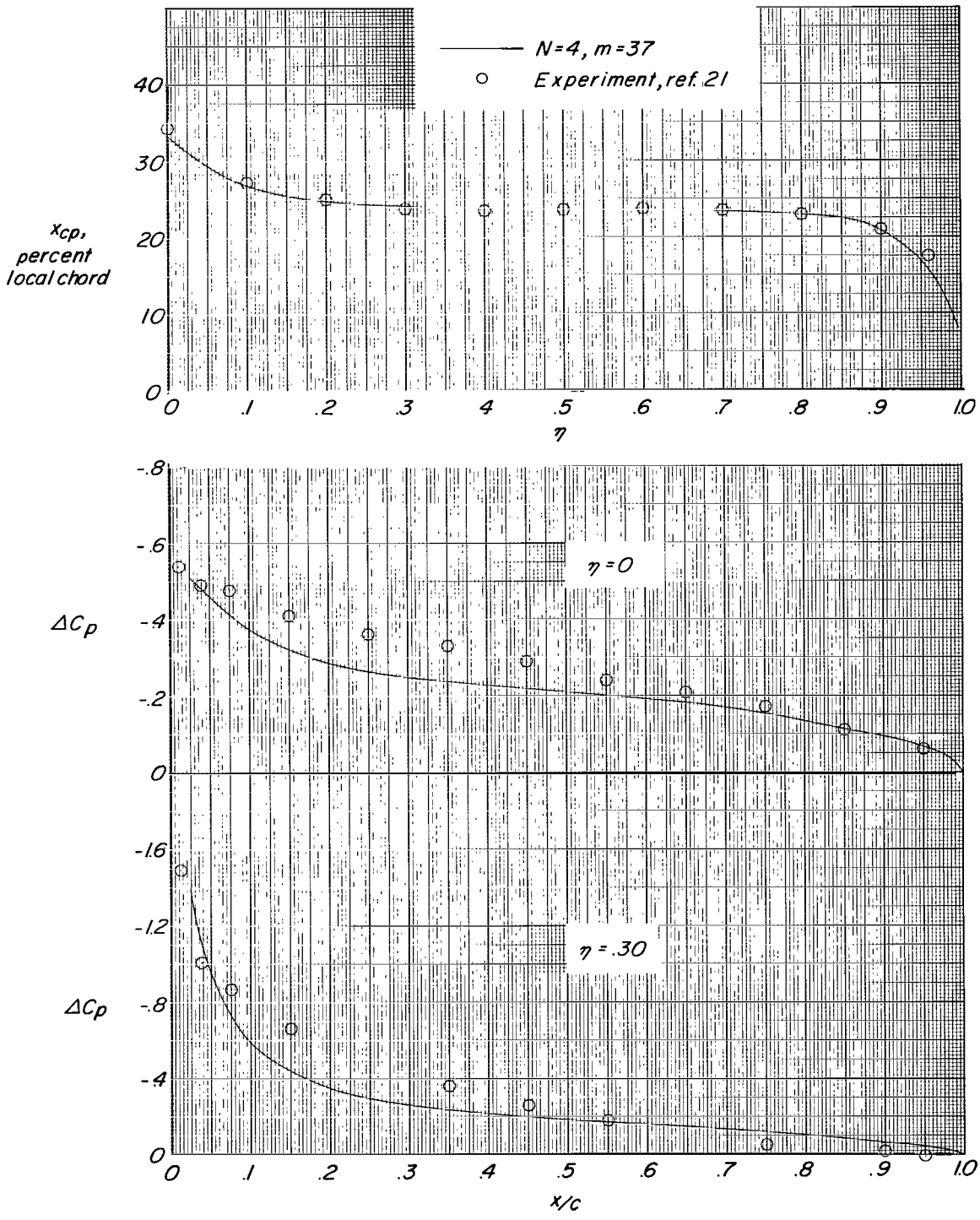

(b) Local spanwise centers of pressure and chordwise load distributions.

Figure 17.- Continued.

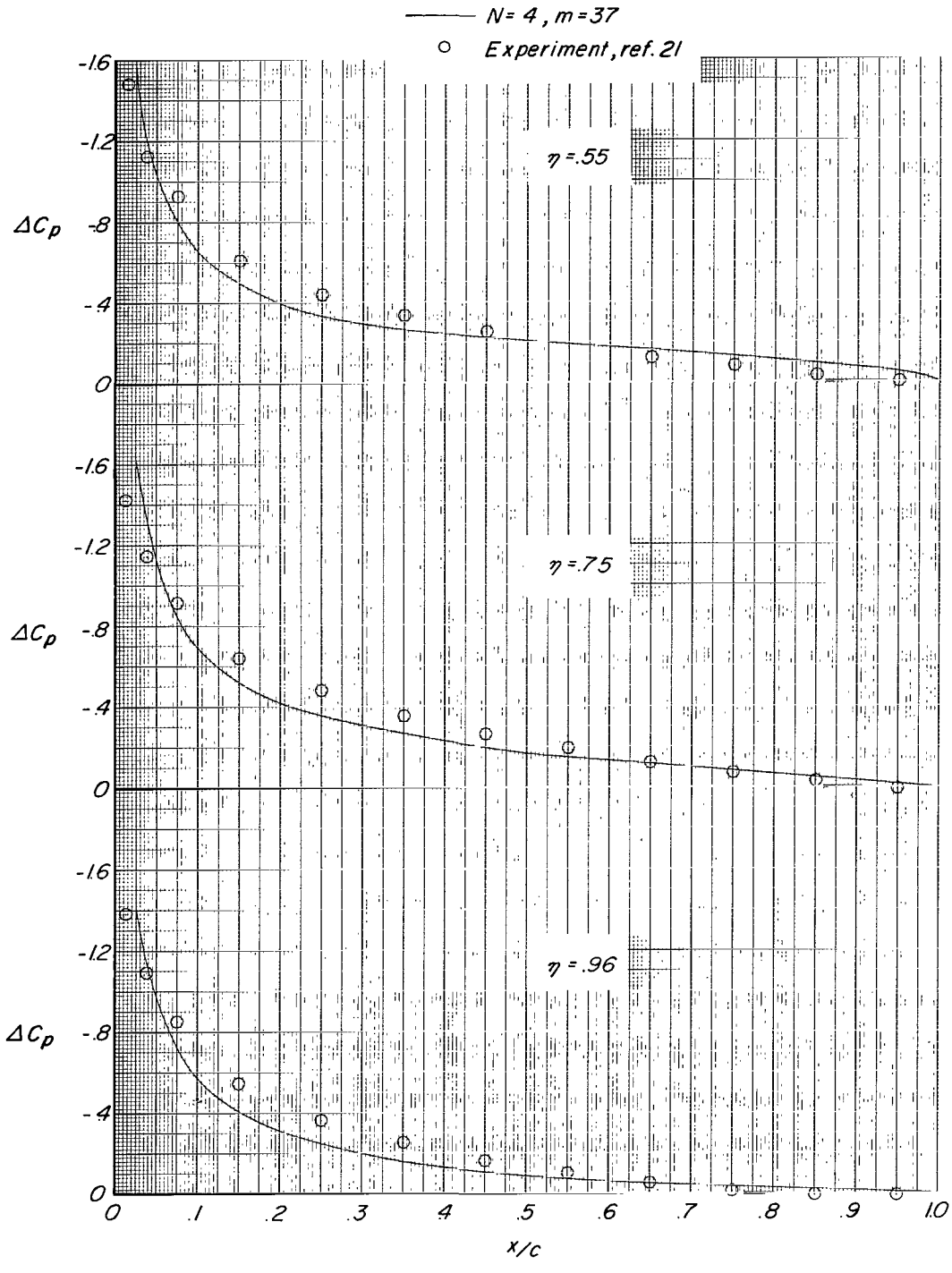

(b) Concluded.

Figure 17.- Concluded.

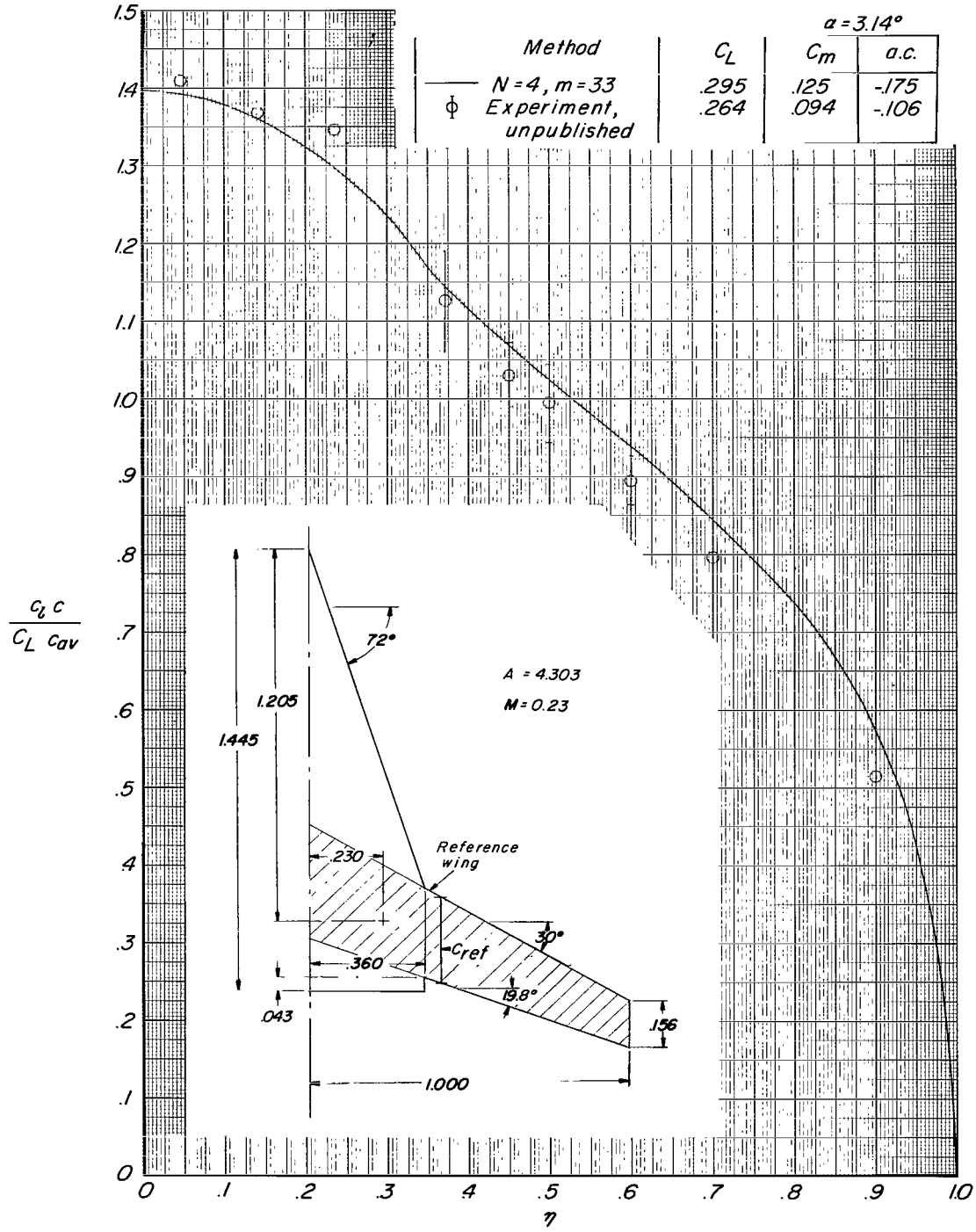

(a) Spanwise.

Figure 18.- Loading and moment distributions predicted by present method and compared with experiment for A = 4.303 variable-sweep planform at M = 0.23.

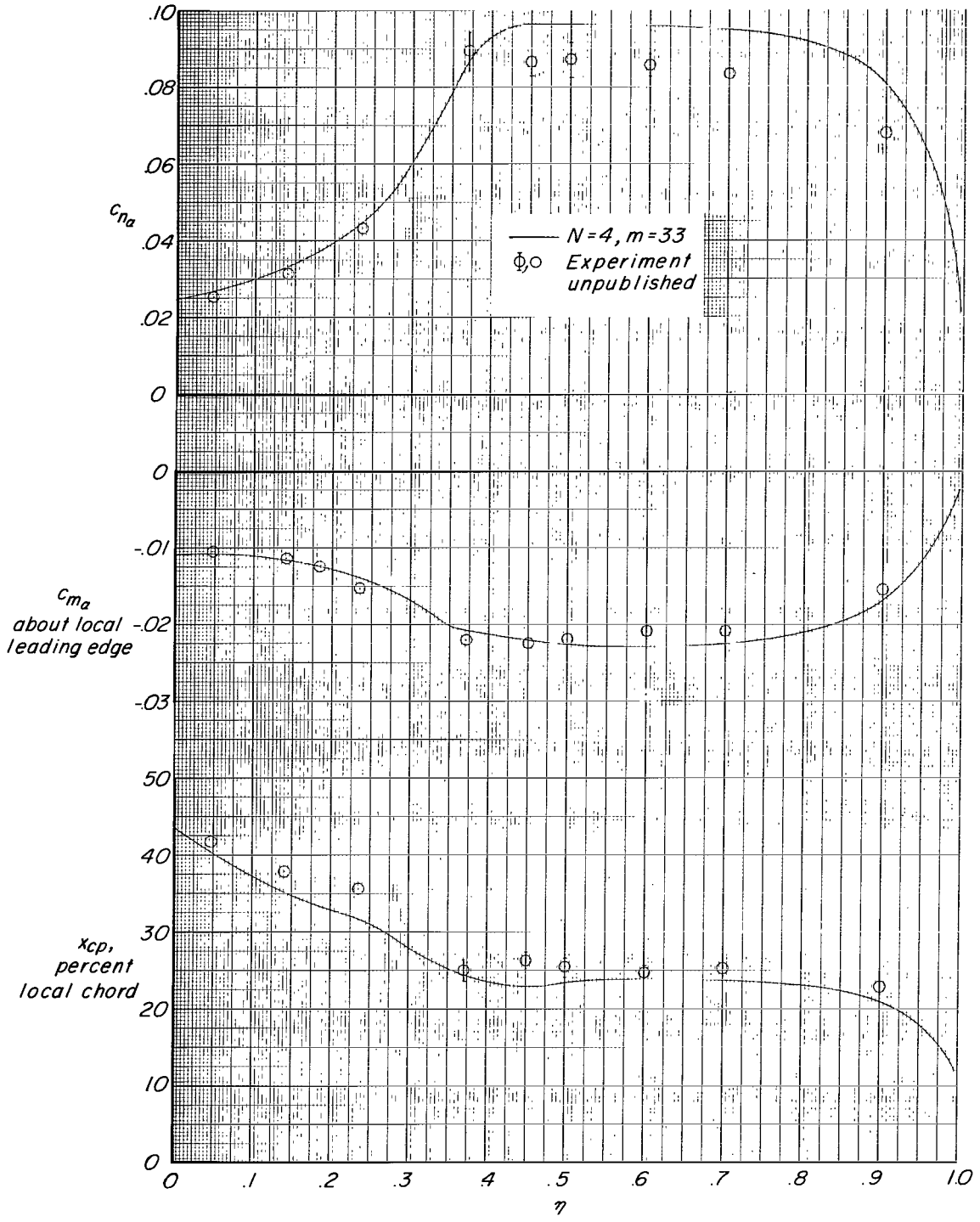

(b) Local slope of normal-force and pitching-moment coefficients and centers of pressure.

Figure 18.- Continued.

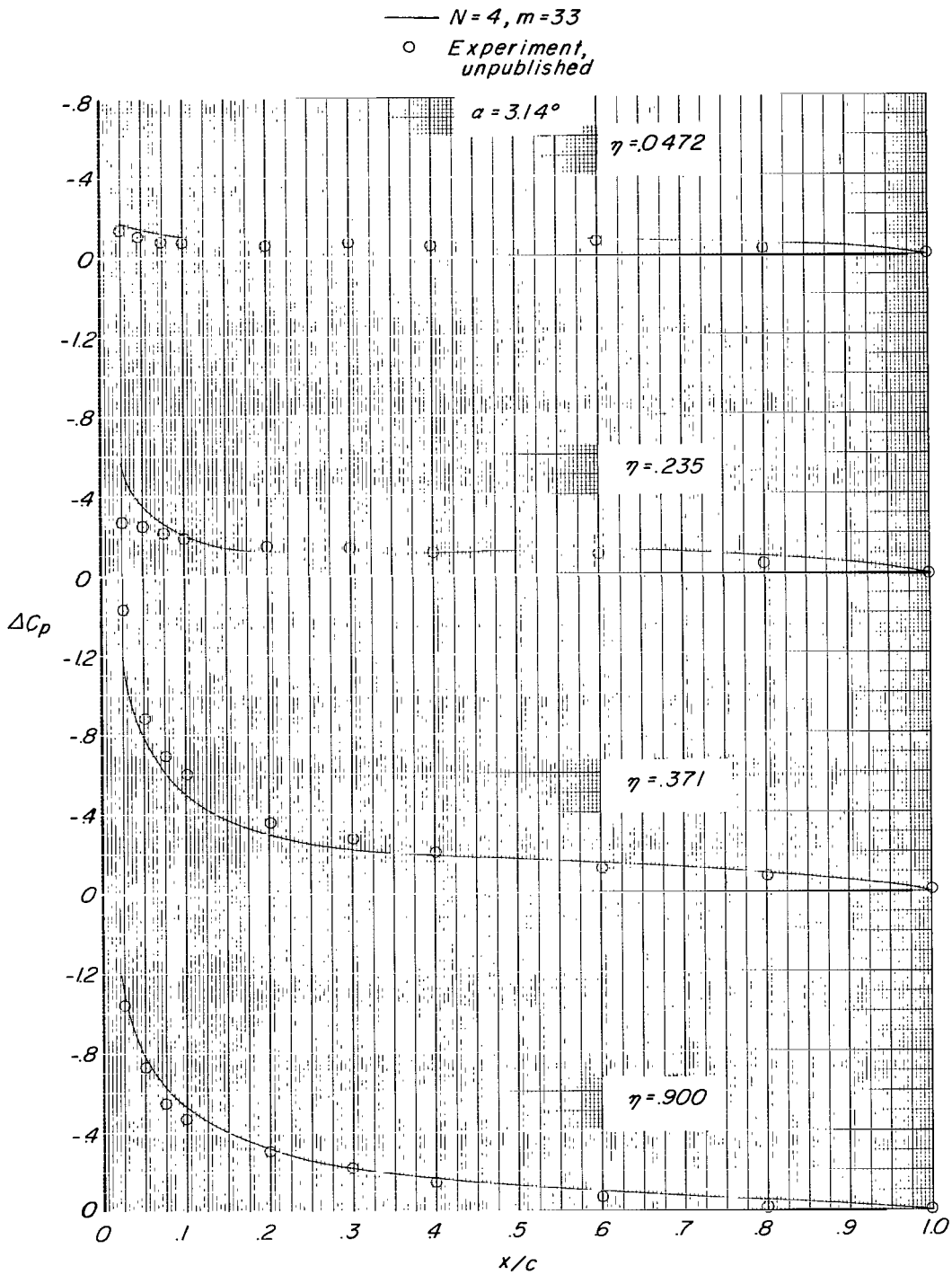

(c) Local chordwise loadings.

Figure 18.- Concluded.

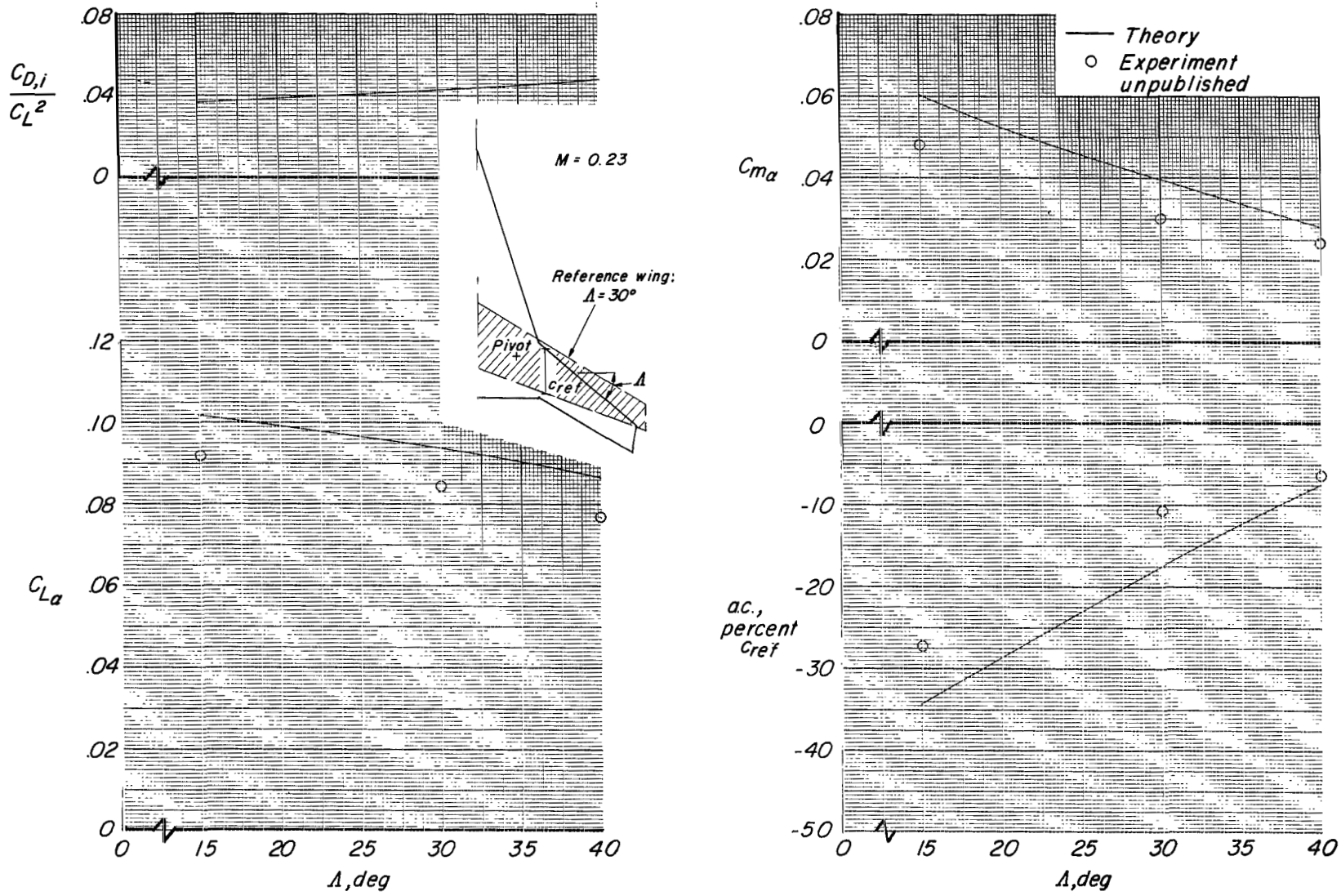

Figure 19.- Effect of leading-edge outboard sweep on some longitudinal aerodynamic characteristics of variable-sweep wing (N = 4, m = 37, 33, and 29 for $\Lambda = 15^0$, 30^0, and 40^0, respectively) at M = 0.23.

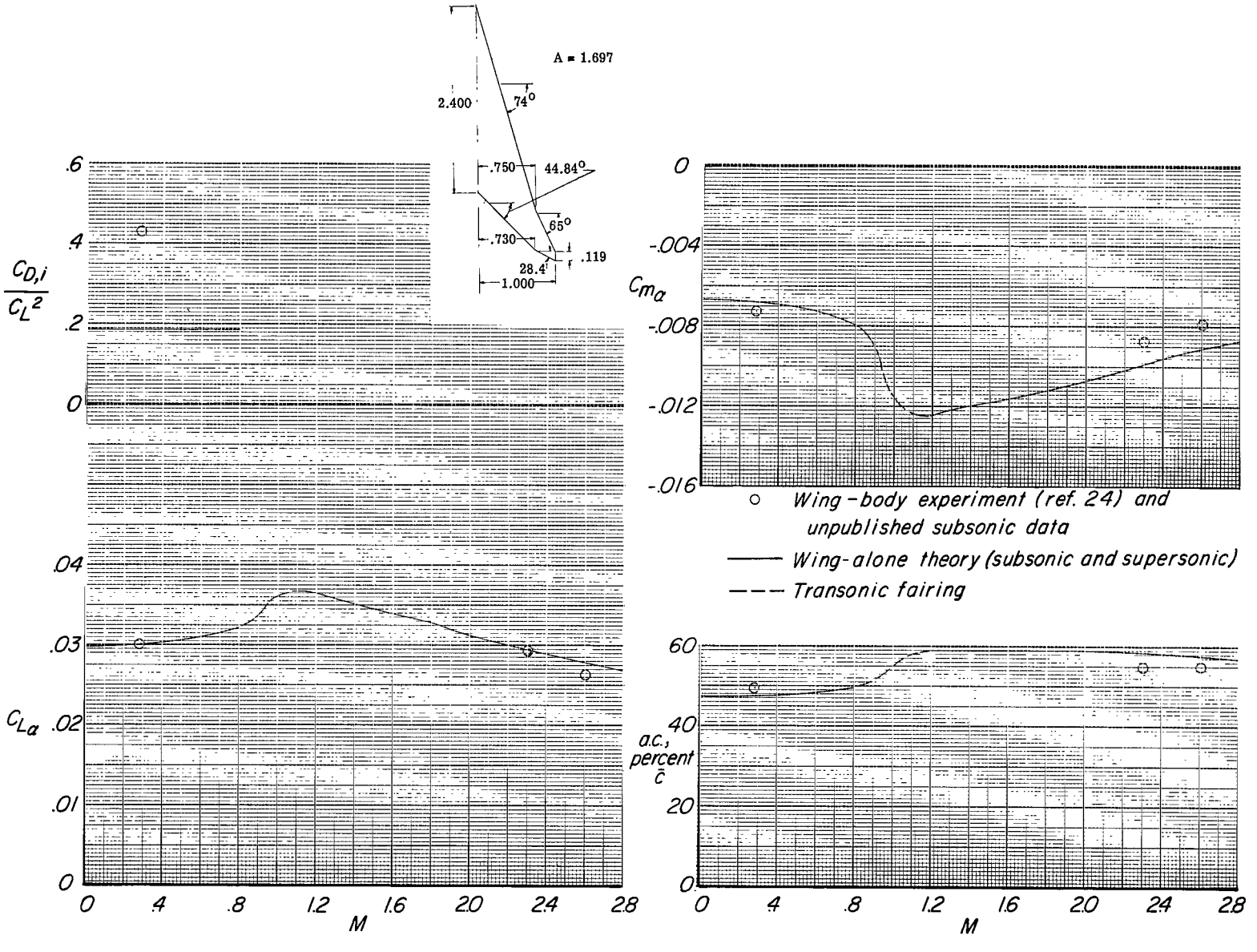

Figure 20.- Effect of Mach number on some longitudinal aerodynamic characteristics of highly sweptback and tapered wing (subsonic theory, N = 8, m = 23).

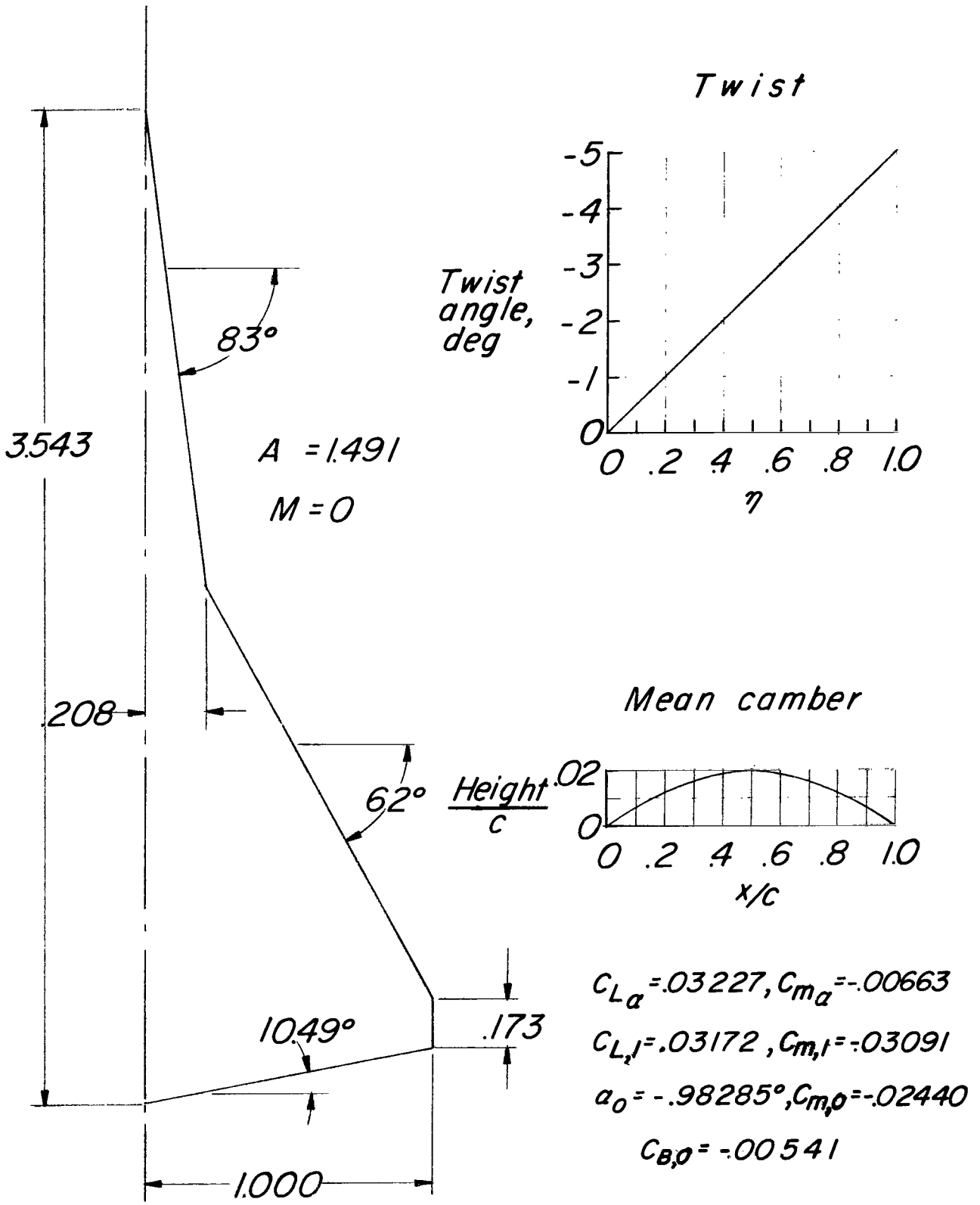

Figure 21.- Warped A = 1.491 double-delta planform at M = 0 and computer results.

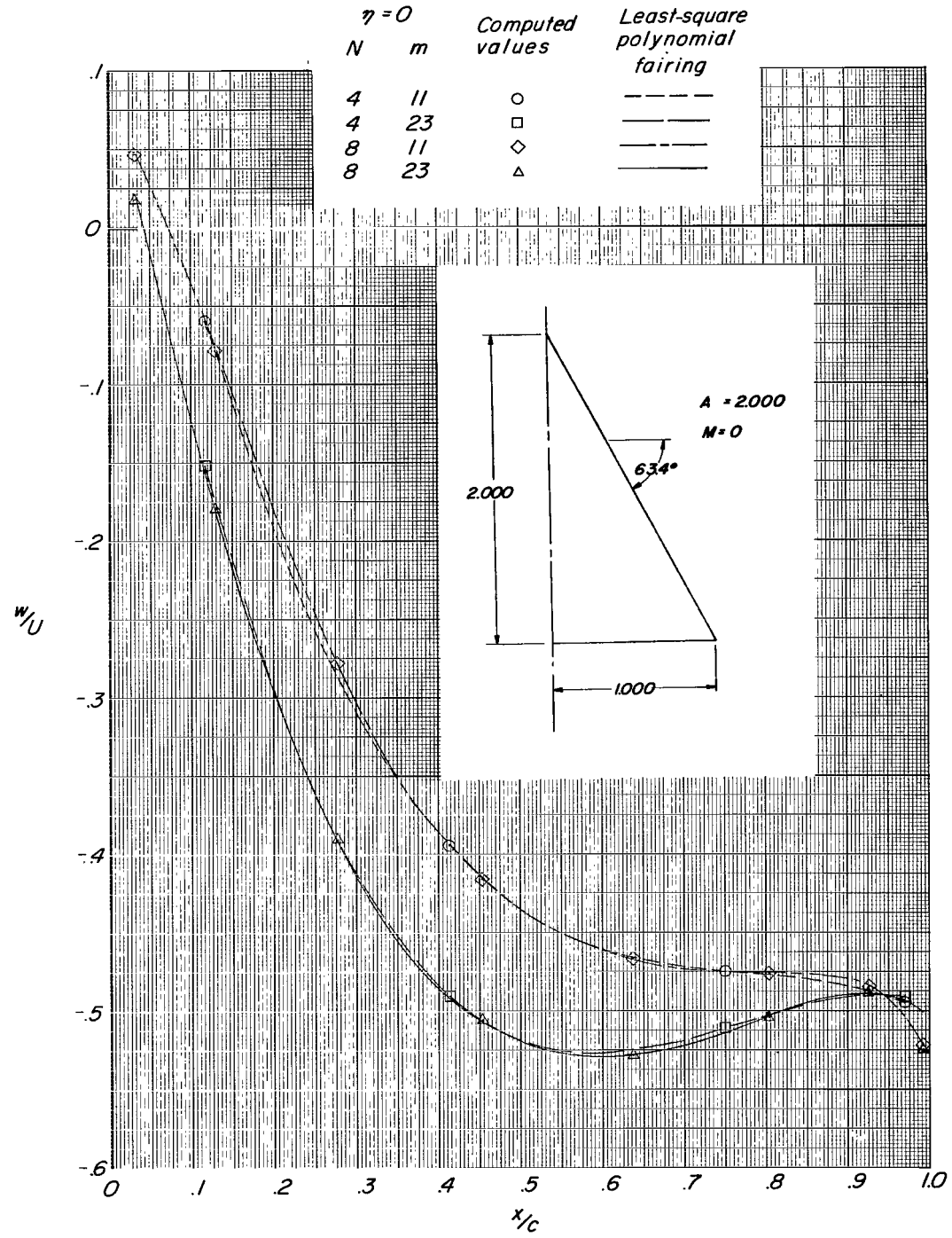

(a) Computed w/U and least-square polynomial curve fit.

Figure 22.- Effect of varying number and locations of control points on downwash distribution and shape of mean camber lines for A = 2 delta planform at M = 0.

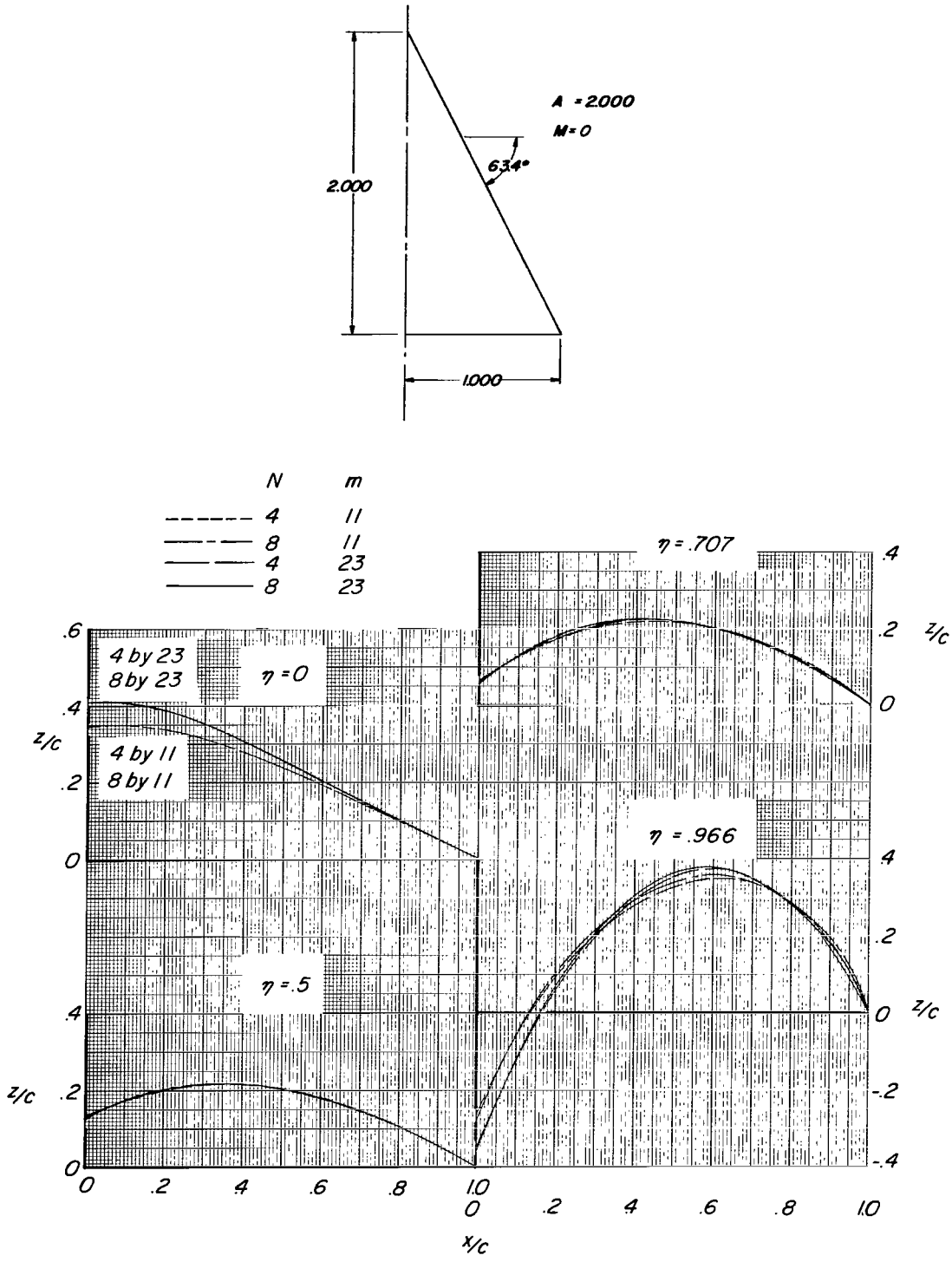

(b) Mean camber lines.

Figure 22.- Concluded.

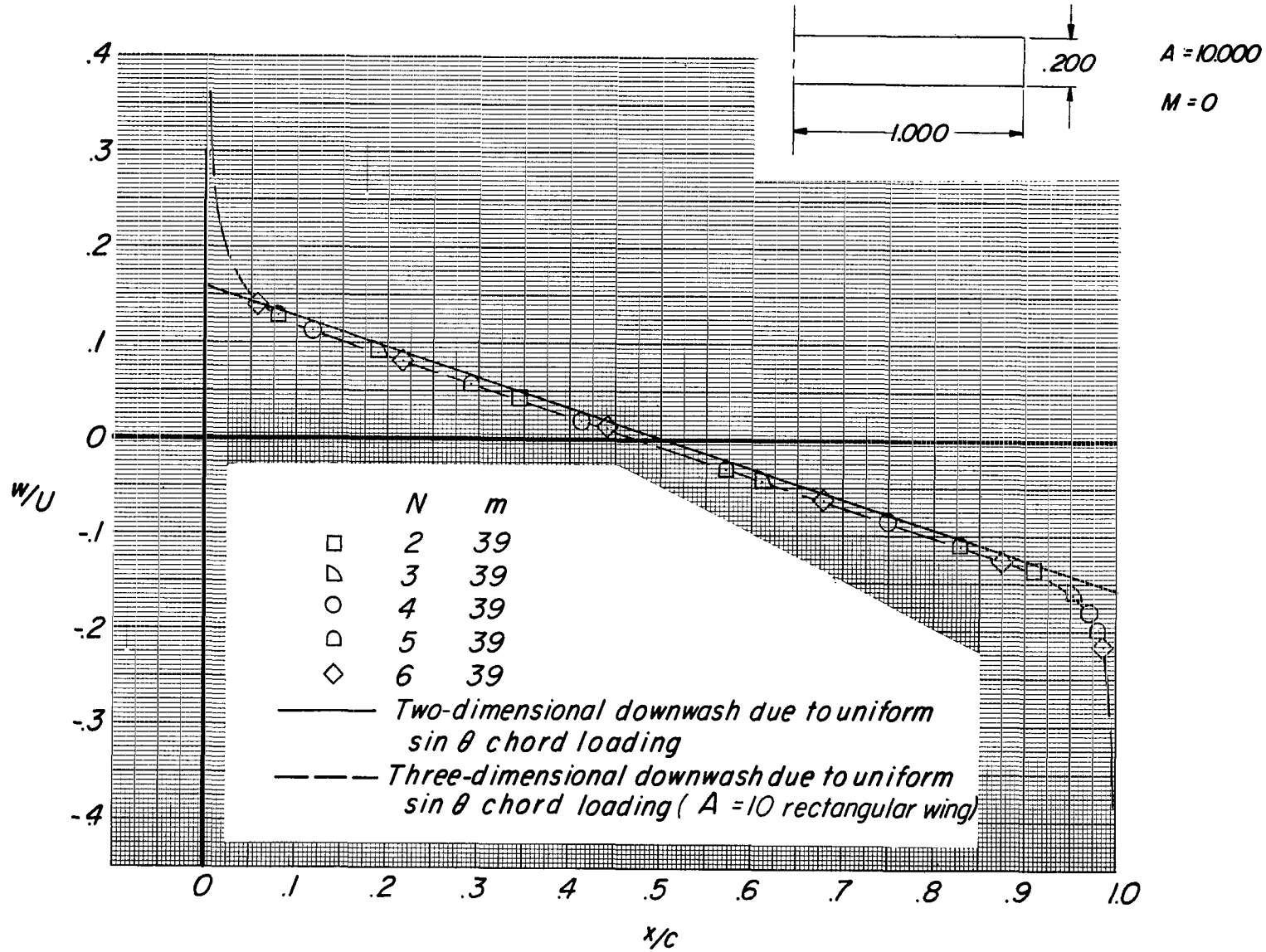

Figure 23.- Comparison of two- and three-dimensional downwash predictions from uniform sin θ chord loading at η = 0.000.

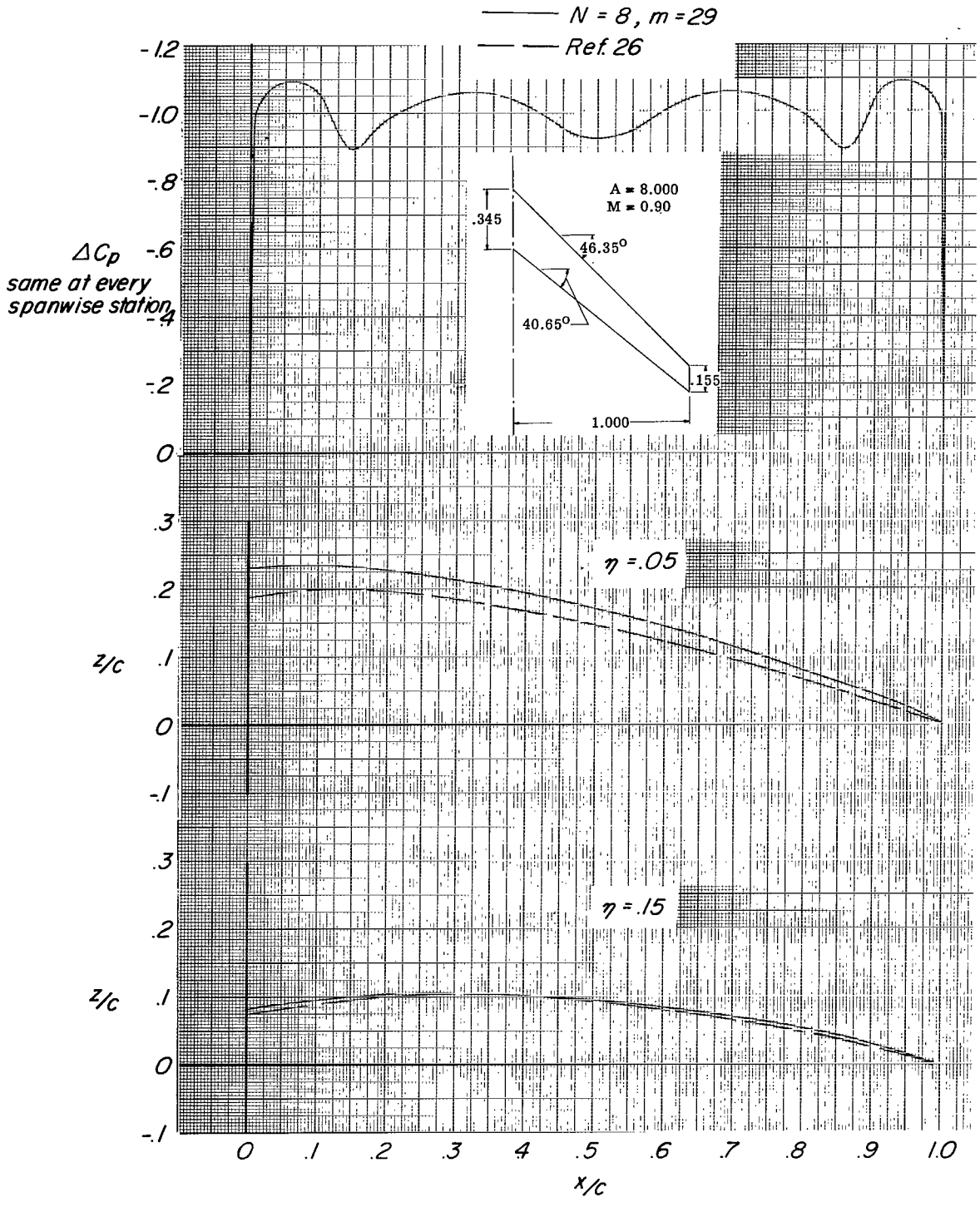

Figure 24.- Chord loading distributions and comparison of mean camber shapes resulting from present and another method for A = 8 sweptback and tapered planform at M = 0.9 for a uniform area loading at C_L = 1.0.

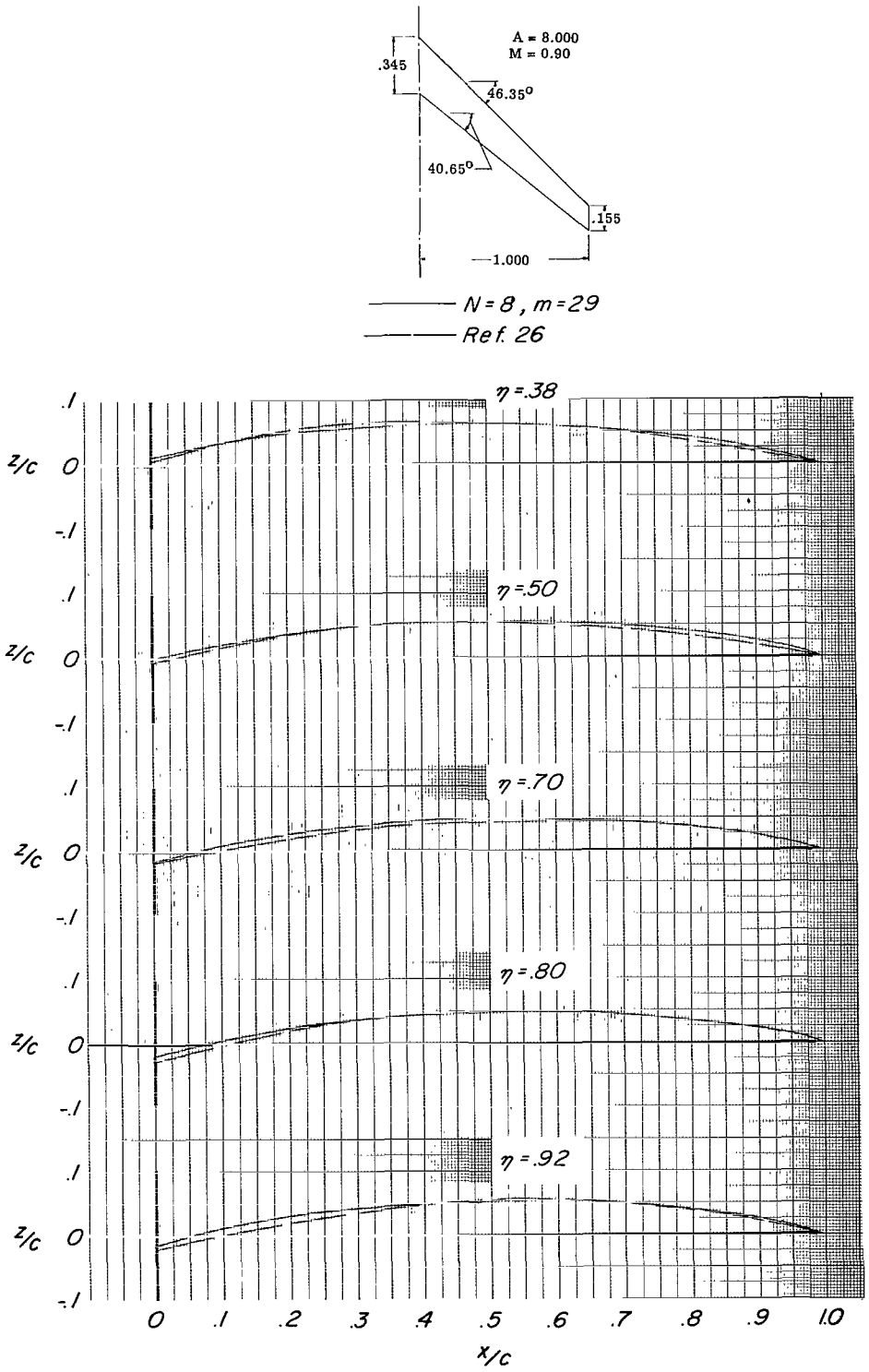

Figure 24.- Concluded.

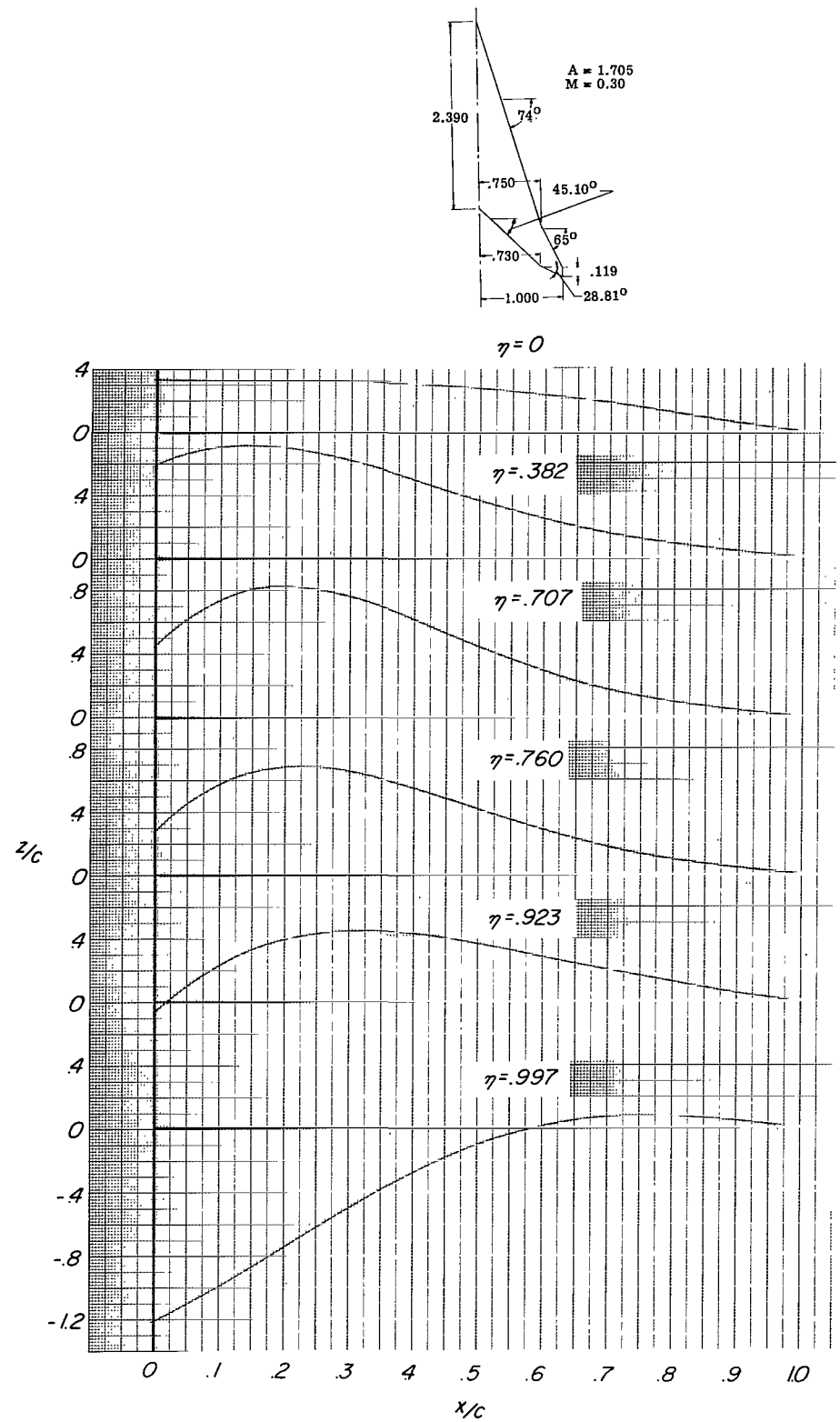

Figure 25.- Predicted mean camber shapes for A = 1.705 highly sweptback and tapered planform at M = 0.30 when N = 4 and m = 39.

NATIONAL AERONAUTICS AND SPACE ADMINISTRATION
WASHINGTON, D. C. 20546
OFFICIAL BUSINESS

FIRST CLASS MAIL

POSTAGE AND FEES PAID
NATIONAL AERONAUTICS AI
SPACE ADMINISTRATION

010 001 2, 51 3DS 68194 00903
AIR FORCE WEAPONS LABORATORY/AFWL/
KIRTLAND AIR FORCE BASE, NEW MEXICO 87117

ATT MISS MADELINE F. CANOVA, CHIEF TECHNI
LIBRARY /WLIL/

POSTMASTER: If Undeliverable (Section 15
Postal Manual) Do Not Ret

"The aeronautical and space activities of the United States shall be conducted so as to contribute . . . to the expansion of human knowledge of phenomena in the atmosphere and space. The Administration shall provide for the widest practicable and appropriate dissemination of information concerning its activities and the results thereof."

—NATIONAL AERONAUTICS AND SPACE ACT OF 1958

NASA SCIENTIFIC AND TECHNICAL PUBLICATIONS

TECHNICAL REPORTS: Scientific and technical information considered important, complete, and a lasting contribution to existing knowledge.

TECHNICAL NOTES: Information less broad in scope but nevertheless of importance as a contribution to existing knowledge.

TECHNICAL MEMORANDUMS: Information receiving limited distribution because of preliminary data, security classification, or other reasons.

CONTRACTOR REPORTS: Scientific and technical information generated under a NASA contract or grant and considered an important contribution to existing knowledge.

TECHNICAL TRANSLATIONS: Information published in a foreign language considered to merit NASA distribution in English.

SPECIAL PUBLICATIONS: Information derived from or of value to NASA activities. Publications include conference proceedings, monographs, data compilations, handbooks, sourcebooks, and special bibliographies.

TECHNOLOGY UTILIZATION PUBLICATIONS: Information on technology used by NASA that may be of particular interest in commercial and other non-aerospace applications. Publications include Tech Briefs, Technology Utilization Reports and Notes, and Technology Surveys.

Details on the availability of these publications may be obtained from:

SCIENTIFIC AND TECHNICAL INFORMATION DIVISION

NATIONAL AERONAUTICS AND SPACE ADMINISTRATION

Washington, D.C. 20546